A UNIQUE PATTERN OF PMN-MDSC MIGRATION IN CANCER

Sima N. Patel

A DISSERTATION

in

Pharmacology

Presented to the Faculties of the University of Pennsylvania

in

Partial Fulfillment of the Requirements for the

Degree of Doctor of Philosophy

2017

Supervisor of Dissertation

_____

Dmitry I. Gabrilovich, MD, PhD, Christopher M. David Professor of Cancer Research

Graduate Group Chairperson

_____

Julie A. Blendy, PhD, Professor of Pharmacology

Dissertation Committee

Margaret M. Chou, PhD, Associate Professor of Pathology and Laboratory Medicine

Jose Conejo-Garcia, PhD, Professor of Tumor Microenvironment and Metastasis

Serge Y. Fuchs, MD, PhD, Professor of Cell Biology

Marcelo G. Kazanietz, PhD, Professor of Pharmacology

DEDICATION

To my parents, who were my first teachers, gave me every opportunity, and have been my support system through it all.

&

To all of my school teachers, and especially Candace Sullivan Scott and the teachers of the Webster Academy Visions in Education middle school program, who broadened my horizons, encouraged my creativity, and ingrained in me a strong sense of self.

ACKNOWLEDGMENT

First, I want to thank my advisor Dr. Dmitry Gabrilovich for taking a chance on me and guiding me through these past few years. His support has been invaluable, and while he has molded me into the scientist I am today, he has also taught me how to lead with compassion; I am ever grateful. I also want to thank Dr. Thomas Condamine for reviving my passion for science and helping me get my bearings in a new field. I want to thank Dr. George Dominguez, Dr. Vinit Kumar, and Dr. Filippo Veglia for their friendship and scientific guidance. I want to thank Kevin Alicea-Torres, Dr. Cigdem Atay, Dr. Debora Barbosa, Dr. Ayumi Hashimoto, Dr. Sarah Herlihy, Dr. Cindy Lin, Dr. Jerome Mastio, Sridevi Mony, Dr. Michela Perego, and Dr. Evgenii Tcyganov for their friendship and support. I also want to thank other members of the lab, past and present, for creating a fun, supportive, and productive work environment.

I want to thank my thesis committee, Dr. Margaret Chou, Dr. Jose Conejo-Garcia, Dr. Serge Fuchs, and Dr. Marcelo Kazanietz, for their advice and support. I also want to thank Dr. Cecilia Caino, Dr. Lucia Languino, Dr. Robert Vonderheide, and Dr. Zachary Schug for their help in moving my project forward. I want to thank the Pharmacology Graduate Group, especially Dr. Julie Blendy and Sarah Squire, for this opportunity.

I want to thank Jeffrey Faust, Dr. Heather Steinman, Dr. Colin Smith, and Dr. Gayle Burstein-Teitelbaum for offering a reprieve from lab and supporting my career goals.

I want to thank Dr. Marisa Bartolomei and Dr. Richard Schultz for hearing me and helping me when things seemed hopeless.

Next, I want to thank Theonie Anastassiadis, Rohan Keshwara, and Sara Small for their friendship and invaluable support. They have been my sounding board for experiments, my shoulders to cry on, and my inspiration to carry on. This dissertation would not have been possible without them and to say thank you is not enough.

I am grateful for the friendships I have made during graduate school. I want to thank Trisha Agrawal, Diana Avery, Claire Deken, Bridgin Lee, Jackie St. Louis, Kevin Patel, Mansi Shinde, and Abby Stonestrom for celebrating the good times with me and supporting me during the not-so-good times. I have also been fortunate enough to cultivate friendships that can survive the test of time. I want to thank Sofia Bengoa, Sujata Gidumal, Amy-Lee Goodman, Aparna Kumar, Manjula Raman, and Divya Yerramilli for making me laugh and filling me with joy.

I want to thank my older brother, Vishal Patel, for setting the bar impossibly high, but always giving me something to strive for. I must also thank my parents, Navinbhai Patel and Ansuyaben Patel, for their continuous love and support, even when I do not make it easy.

Finally, I must give credit where credit is due. This dissertation would not have been possible without the mice that sacrificed their lives for these studies. Forgive me.

ABSTRACT

A UNIQUE PATTERN OF PMN-MDSC MIGRATION IN CANCER

Sima N. Patel

Dmitry I. Gabrilovich, MD, PhD

Myeloid-derived suppressor cells (MDSC) are a heterogeneous population of pathologically activated immature myeloid cells that expand and accumulate in cancer, and are categorized as M-MDSC or PMN-MDSC. The role of MDSC to suppress T-cell activation and proliferation in the tumor microenvironment has been clarified over the past 15 years. Our lab has previously demonstrated that an inflammatory environment can lead to the expansion of "MDSC-like" cells that lack immunosuppressive capability. However, the role of these MDSC-like cells in cancer has not been elucidated. First, we hypothesized that PMN-MDSC-like cells will develop in relatively low inflammatory conditions, such as the early stages of tumor development. Next, we hypothesized that because bona fide PMN-MDSC must migrate into tissues to exert their immunosuppressive effects, PMN-MDSC-like cells that lack immunosuppressive capability will exhibit altered migratory behavior. Finally, because many immune cells undergo metabolic reprogramming to meet the energetic demands of their functionality, we hypothesized that PMN-MDSC-like cells would alter their metabolic profile compared to naïve PMN and bona fide PMN-MDSC. We have demonstrated that PMN-MDSC-like cells develop in the early stages of tumor development and in transgenic models, but not in the late stages of tumor development or in transplantable models. Moreover, we have found that PMN-MDSC-like cells

spontaneously migrate 2-3 fold more than naïve PMN, and that this motility is characterized by increased speed, persistence time, mean squared displacement and an overall increased random motility coefficient. We demonstrated that PMN-MDSC-like cell spontaneous migration is dependent upon pannexin-1 hemichannel-mediated ATP release, autocrine ATP signaling through the P2X1 purinergic receptor, and increased pMLC2 levels. Additionally, we have shown that PMN-MDSC-like cells increase cell surface expression of the glucose transporter Glut1. Finally, we have shown that, in comparison to naïve PMN and bona fide PMN-MDSC, PMN-MDSC-like cells increase their glycolytic rate to meet the energetic demands of their altered migratory behavior. Collectively, these studies have shed insight on the development of bona fide PMN-MDSC in cancer, and have suggested a role for PMN-MDSC-like cells in pre-metastatic niche development.

TABLE OF CONTENTS

LIST OF TABLES

LIST OF FIGURES

CHAPTER ONE: MYELOID-DERIVED SUPPRESSOR CELLS

Introduction

Cancer is the second leading cause of death in the United States and affects patients and families worldwide. In 2017 alone, it is estimated that approximately 600,000 Americans will die from cancer (Siegel, Miller, & Jemal, 2017). While conventional therapies, such as surgery, chemotherapy, and radiation therapy have proved successful at treating specific cancers, we are still struggling to achieve long-term success in patients, often because of disease recurrence. In fact, metastases are the cause of 90% of human cancer deaths (Mehlen & Puisieux, 2006). To address this impasse, on December 13, 2016, President Obama signed the 21st Century Cures Act, ensuring funding for initiatives from the Beau Biden Cancer Moonshot, which includes the development of immunotherapies (AACR, 2017). Immunotherapies are an attractive therapeutic approach as they activate the patient's own immune system to selectively target tumor cells. However, tumors have developed mechanisms to evade immune surveillance and the immunosuppressive tumor microenvironment presents a significant challenge to the efficacy of immunotherapies (Mellman, Coukos, & Dranoff, 2011).

Immune suppressive myeloid cells were observed in tumor-bearing hosts beginning in the early 1970s, and in 2007, these cells were termed myeloid-derived suppressor cells (MDSC) to reflect their origin and function (T. Condamine, Ramachandran, Youn, & Gabrilovich, 2015; D. I. Gabrilovich et al., 2007). MDSC accumulation has been reported in many cancers and studies have shown a correlation between levels of MDSC accumulation and stage, overall survival, and response to therapy. Several studies have also

found a correlation between MDSC and the development of metastases in patients (T. Condamine et al., 2015). Moreover, analysis of blood samples from patients that did not respond to immunotherapy indicated a correlation between MDSC level and lack of response (Kimura et al., 2013). Given the importance of these cells in cancer progression and their significance in the efficacy of immunotherapies, it is essential that we learn more about their biology and mechanism of action if we are to design therapies to effectively treat patients.

MDSC phenotype

MDSC are a heterogeneous population of pathologically activated immature myeloid cells that are phenotypically similar to myeloid cells in healthy individuals. These cells were described as $CD11b^{+}GR1^{+}$ cells in mice, and were found to accumulate in the spleen and bone-marrow of tumor-bearing mice (D. I. Gabrilovich, Velders, Sotomayor, & Kast, 2001; Kusmartsev, Li, & Chen, 2000). Based on their morphology and surface molecule expression, MDSC are divided into two subpopulations: mononuclear MDSC (M-MDSC) and polymorphonuclear MDSC (PMN-MDSC). M-MDSC, similar to monocytes, have a single-lobed nucleus and are defined in mice as $CD11b^{+}Ly6C^{hi}Ly6G^{-}$, and PMN-MDSC, similar to PMN, have a multi-lobed nucleus and are defined in mice as $CD11b^{+}Ly6C^{lo}Ly6G^{+}$ (Figure 1.1). With the isolation strategies currently available to us, it is impossible to differentiate between PMN and PMN-MDSC in mice. Therefore, it is an accepted convention in the field to assume that all $CD11b^{+}GR1^{+}$ cells from a mouse are MDSC. In human patients, however, we are able to distinguish between PMN and PMN-MDSC using density centrifugation. The high-density fraction of cells contain PMN, and

the low-density cells contain MDSC, though there is some controversy in the field, as it is believed that some activated PMN can also be present in the low density fraction (Moses & Brandau, 2016). From the low density fraction, PMN-MDSC are defined as $CD11b^{+}CD14^{-}CD15^{+}$ or $CD11b^{+}CD14^{-}CD66b^{+}$, and M-MDSC as $CD11b^{+}CD14^{+}HLA\text{-}DR^{-/lo}CD15^{-}$ (D. I. Gabrilovich, 2017).

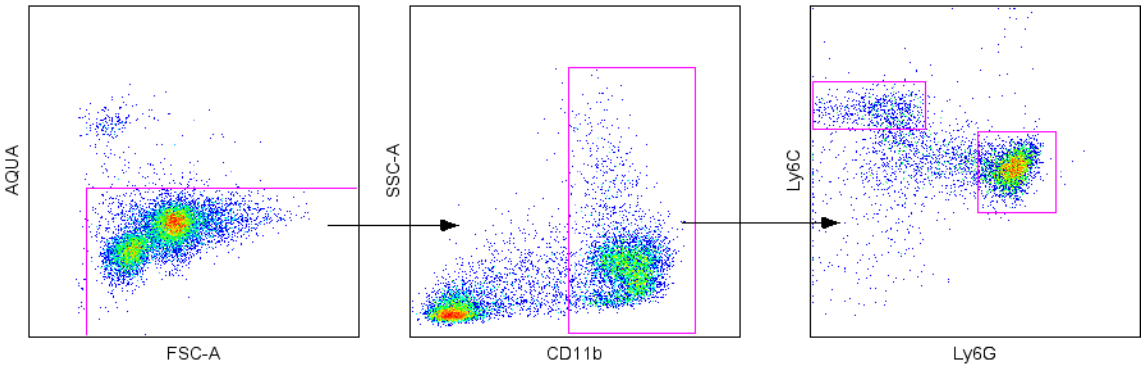

Figure 1.1 Phenotype of murine MDSC. $CD11b^{+}$ cells were gated from the live cell population (AQUA-negative). From the $Cd11b^{+}$ cells, M-MDSC are identified as $Ly6C^{hi}Ly6G^{-}$, and PMN-MDSC are identified as $Ly6C^{lo}Ly6G^{+}$.

MDSC and inflammation

Inflammation contributes to the development of cancer, and chronic inflammation can drive MDSC accumulation and suppressive function (Balkwill & Mantovani, 2001; K. H. Parker, Beury, & Ostrand-Rosenberg, 2015). Tumor-secreted factors such as VEGF, MMP9, GM-CSF, COX2, PGE_2, and HMGB1 have been implicated in the accumulation and function of MDSC (D. Gabrilovich et al., 1998; Melani, Sangaletti, Barazzetta, Werb, & Colombo, 2007; Morales, Kmieciak, Knutson, Bear, & Manjili, 2010; K. Parker et al., 2014; Serafini et al., 2004). In mice, there is some evidence to suggest that inflammation may lead to the accumulation of MDSC-like cells. For example, exposure to cigarette

smoke causes the accumulation of these cells in the lungs and spleen. However, they only acquired immunosuppressive function after the development of chemically-induced lung cancer (Ortiz, Lu, Ramachandran, & Gabrilovich, 2014). Additionally, in a skin carcinogenesis model, MDSC-like cells lacking immunosuppressive function accumulated in the skin and promoted tumor development (Ortiz et al., 2015). This suggests that a heterogeneous population of MDSC may exist, bona fide MDSC with suppressive capability, and MDSC-like cells that have yet to acquire immunosuppressive function. Only further studies will determine the purpose and function of this latter group of cells.

MDSC-mediated immune suppression

Importantly, MDSC are distinguished from their healthy-donor counterparts based off of their ability to suppress immune responses. There are several, often overlapping, mechanisms by which MDSC exert their immunomodulatory effects and they can be broadly separated into four categories 1) activation and expansion of the regulatory T-cell (T_{reg}) population, 2) amino acid deprivation, 3) generation of oxidative stress, and 4) interference of lymphocyte migration and viability, discussed in more detail below (Figure 1.2).

First, MDSC can promote the activation and expansion of the T_{reg} population. T_{reg} can protect tumors from antitumor immunity. MDSC induce and expand T_{reg} *in vitro* and *in vivo* in multiple tumor models (Adeegbe et al., 2011; B. Huang et al., 2006; MacDonald et al., 2005; Zoso et al., 2014). While the mechanisms are not completely understood, MDSC expression of CD40 and MDSC-mediated production of soluble factors such as IL-

10 and TGFβ have been shown to play a role in T_{reg} induction (Hoechst et al., 2008; B. Huang et al., 2006; Pan et al., 2010). Additionally, MDSC can activate T_{reg} by presenting tumor-specific antigens in an arginase (ARG1)-dependent manner (Serafini, Mgebroff, Noonan, & Borrello, 2008).

Second, MDSC can deplete amino acids in the extracellular space thereby depriving T-cells of amino acids they need to proliferate. For example, MDSC deplete L-arginine through ARG1-dependent consumption (Rodriguez et al., 2004). This results in the downregulation of the ζ-chain of the T-cell receptor (TCR), which is required for signal transduction, and also leads to T-cell arrest in G_0-G_1 (Rodriguez et al., 2010; Rodriguez et al., 2004; Rodriguez et al., 2002; Zea et al., 2004). Moreover, both MDSC and T-cells are unable to produce L-cystine. However, MDSC, but not naïve T-cells, express the cysteine transporter x_c^- and are able to scavenge L-cystine from the local environment. Naïve T-cells must rely on antigen presenting cells (APC) to acquire L-cystine. Therefore, large numbers of MDSC are able to quickly deplete the local environment of L-cystine and limit the ability of APC to provide it to T cells (Srivastava, Sinha, Clements, Rodriguez, & Ostrand-Rosenberg, 2010). Finally, some MDSC also express indoleamine-pyrrole 2,3-dioxygenase and can induce T-cell proliferative arrest by depleting the local environment of L-tryptophan (Munn et al., 2005; C. Smith et al., 2012).

Third, MDSC can generate oxidative stress by producing reactive oxygen species (ROS) and reactive nitrogen species such as nitric oxide (NO). MDSC upregulate activity of NADPH oxidase to generate superoxide and other forms of ROS which can suppress T-cell responses (Corzo et al., 2009). For example, H_2O_2 production in patients has been

shown to reduce the expression of the ζ-chain of the TCR (Schmielau & Finn, 2001). Additionally, different subsets of MDSC rely on different isoforms of inducible nitric oxide synthase to produce NO (Raber et al., 2014). NO can interfere with IL-2 receptor signaling, and lead to the nitration and desensitization of the TCR (Mazzoni et al., 2002; Nagaraj et al., 2007).

Fourth, MDSC can interfere with lymphocyte trafficking and viability. MDSC express ADAM17 on their plasma membrane, resulting in decreased CD62L expression on the surface of naïve T-cells, preventing their recirculation to lymph nodes (Hanson, Clements, Sinha, Ilkovitch, & Ostrand-Rosenberg, 2009). Additionally, MDSC-derived peroxynitrite can modify the chemoattractant CCL2 to prevent T-cell infiltration into tumors (Molon et al., 2011). Furthermore, in squamous cell carcinoma patients, NO produced by MDSC decreases E-selectin levels, preventing T-cell adhesion to tumor vessels and limiting T-cell access to the tumor (Gehad et al., 2012). MDSC also express galectin 9, which binds to T-cell immunoglobulin and mucin domain-containing protein 3 to induce T-cell apoptosis (Sakuishi, Jayaraman, Behar, Anderson, & Kuchroo, 2011). MDSC can also skew macrophages towards a pro-tumor M2 phenotype through an IL-10-dependent mechanism (Sinha, Clements, Bunt, Albelda, & Ostrand-Rosenberg, 2007). Finally, MDSC can impair NK cell-mediated cytotoxicity by producing TGFβ, which makes NK cells more difficult to activate by decreasing expression of NK cell activating receptors (Elkabets et al., 2010; Mao et al., 2014).

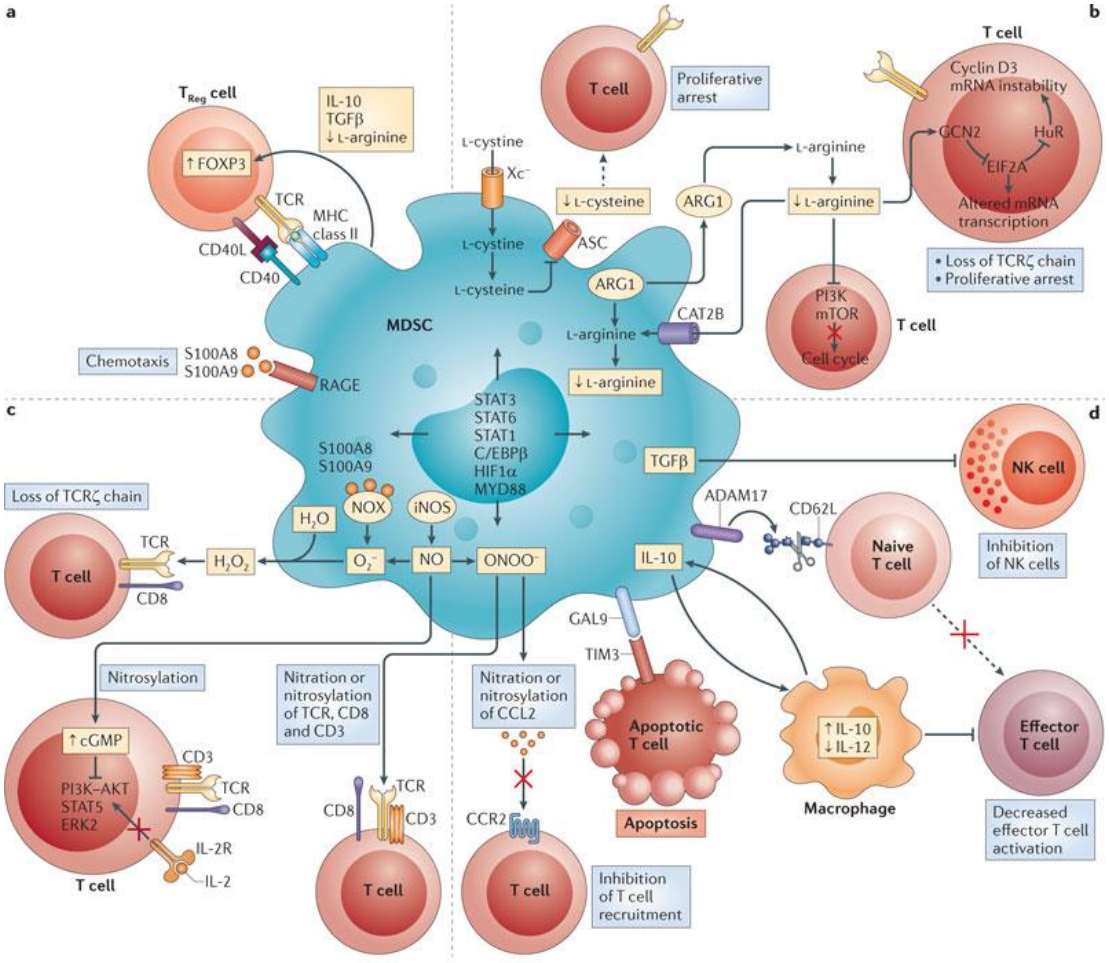

Figure 1.2 Mechanisms of MDSC-mediated immunomodulation. (a) MDSC can promote the induction and expansion of the T_{reg} population through mechanisms dependent on CD40, IL-10, TGFβ, and arginase. (b) MDSC affect T-cell activation and proliferation by depleting the local environment of amino acids, such as L-arginine and L-cystein, that T-cells cannot produce themselves. (c) MDSC generate oxidative stress in the form of iNOS-mediated NO and NOX-mediated superoxide that prevent the activation or IL-2-mediated signaling, of T-cells. (d) MDSC directly affect the trafficking and viability of T-cells through ADAM17 and galectin (GAL9) expression (D. I. Gabrilovich, Ostrand-Rosenberg, & Bronte, 2012).

MDSC metabolism

The metabolism and function of immune cells is linked. For example, effector T-cells rely primarily on glycolysis to produce ATP to support their rapid growth and proliferation, whereas memory T-cells switch to mitochondrial fatty acid oxidation (FAO) for their development and long term survival (Pearce & Pearce, 2013). Similarly, in *in vitro* generated MDSC, glycolysis increased concurrently with increased ARG1 activity. Interestingly, AMP-activated protein kinase was also activated, which can drive metabolism towards FAO (Hammami et al., 2012). These results were confirmed *in vivo* where, compared with splenic MDSC from a naïve or tumor-bearing mouse, both glycolytic and oxidative phosphorylation rates were increased in tumor-infiltrating MDSC. However, based on a comparison of the rates, tumor MDSC primarily used FAO and oxidative phosphorylation as their main metabolic pathway. In support of this finding, tumor-infiltrating MDSC increased fatty acid uptake and mitochondrial mass, and upregulated key FAO enzymes (Hossain et al., 2015).

MDSC and metastasis

In addition to their immunosuppressive function, MDSC also play a role in tumor metastasis. For example, in patients with non-small cell lung carcinoma, circulating M-MDSC correlated with extrathoracic metastases (A. Huang et al., 2013). In patients with melanoma, increases in circulating PMN-MDSC and M-MDSC both correlated with the development of metastases and poor survival (Achberger et al., 2014; Weide et al., 2014). There is significant crosstalk between the tumor and MDSC. For example, while tumor-

secreted factors can regulate the accumulation and expansion of MDSC, the tumor is also affected by chemokines, cytokines and enzymes produced by MDSC that can contribute to tumor cell invasion, proliferation, survival, adhesion and chemoattraction, and metastasis development (Figure 1.3) (Talmadge & Gabrilovich, 2013). For example, PMN-MDSC produce hepatocyte growth factor and TFGβ to induce epithelial-mesenchymal transition of primary melanoma cells in the RET-oncogene transgenic mouse model of spontaneous

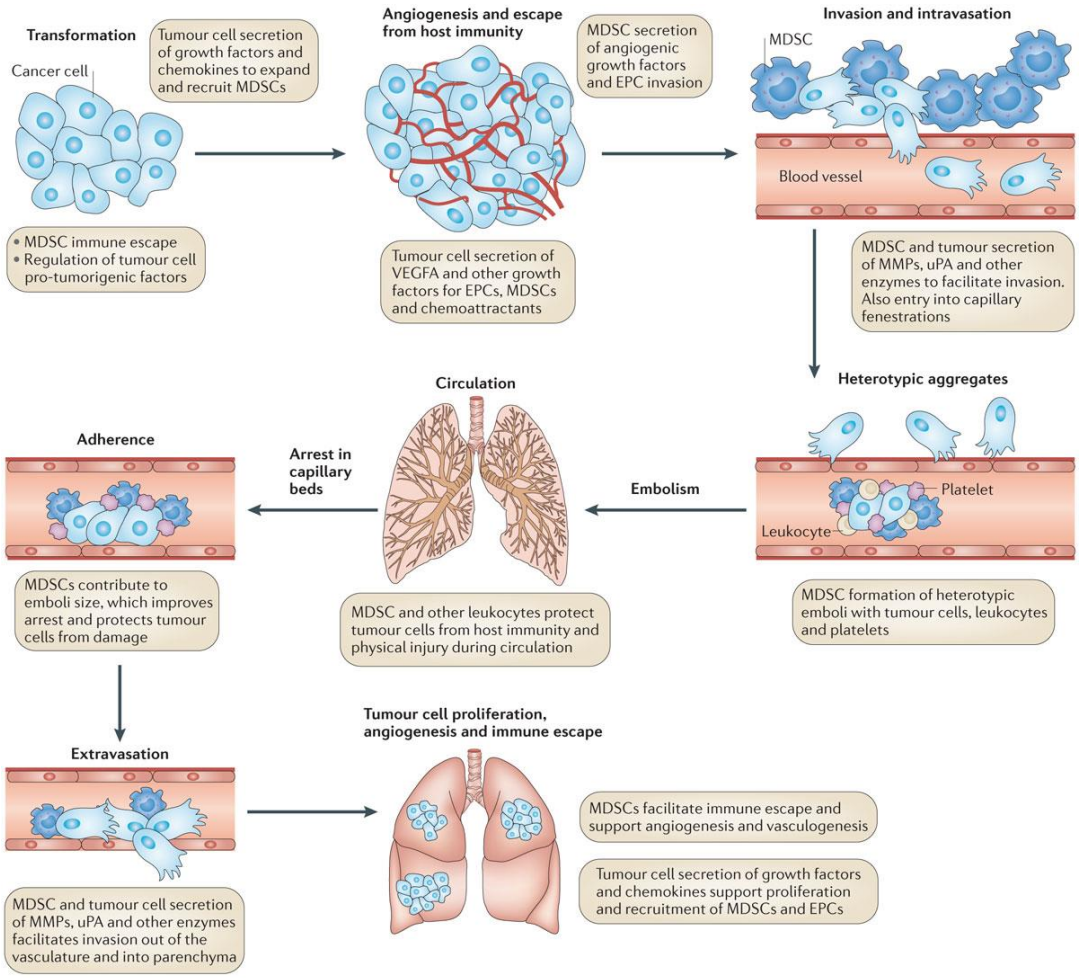

Figure 1.3 MDSC play a role in the development of metastases. Tumor cells release soluble factors that act systemically to affect the development of MDSC. In turn, MDSC can promote metastasis by promoting angiogenesis and invasion of tumor cells. MDSC can also protect these cells as they travel through the circulation. Finally, MDSC can facilitate formation of the pre-metastatic niche and extravasation of tumor cells into the tissue (Talmadge & Gabrilovich, 2013).

melanoma (Toh et al., 2011). Additionally, microRNA-494 induced by tumor-derived factors causes the increased production of matrix metalloproteinase 9 to facilitate tumor invasion (Yang Liu et al., 2012). MDSC have also been shown to facilitate tumor cell invasion and metastasis in mice with mammary carincomas lacking the TGFβ receptor through metalloproteinase activity (L. Yang et al., 2008). Moreover, MDSC contribute to the platelets and other myeloid cells that form heterotypic emboli to protect tumor cells during circulation and facilitate tumor cell arrest and extravasation (Talmadge & Gabrilovich, 2013).

MDSC and the pre-metastatic niche

MDSC have also been implicated to play a role in the development of the pre-metastatic niche. M-MDSC secreted versican in the lung of MMTV-PyMT spontaneous breast tumor-bearing mice to facilitate mesenchymal-epithelial transition and allow tumor cells to colonize the niche (Gao et al., 2012). In an orthotopic mammary tumor model, hypoxia in primary tumors promoted PMN-MDSC and NK cell infiltration of the lung and pre-metastatic niche formation (Sceneay et al., 2012). In a mouse model of hepatocellular carcinoma, large amounts of tissue inhibitor of metalloproteinases led to increased CXCL12 production, promoting CXCR4-mediated recruitment of PMN to sites for pre-metastatic niche formation (Seubert et al., 2015). In a xenograft model, CXCL8-mediated recruitment of PMN by human melanoma cells helped to tether the melanoma cells to the vascular endothelium and promoted lung metastasis (Huh, Liang, Sharma, Dong, & Robertson, 2010). S100A8 and S100A9 proteins also drive the recruitment of PMN and PMN-MDSC to pre-metastatic sites in colon cancer, and PMN, via production of S100

proteins, can create a positive feedback loop resulting in the accumulation of more PMN in the pre-metastatic lung (Ichikawa, Williams, Wang, Vogl, & Srikrishna, 2011; Kowanetz et al., 2010).

Strategies to target MDSC

It is clear that inhibiting the immunosuppressive capabilities of myeloid cells will be important to the success of immunotherapies. Given the many different roles of MDSC in cancer, there are several strategies to target MDSC. In general, they strive to 1) inhibit mechanisms that inhibit lymphocyte activation and proliferation, 2) inhibit the generation of MDSC or promote the apoptosis of circulating MDSC, 3) force MDSC to mature into APC that can stimulate T-cell responses, 4) prevent trafficking of MDSC from the bone marrow to peripheral organs and to the tumor site, and 5) repolarize macrophages towards an M1 phenotype (D. I. Gabrilovich et al., 2012). Because there many different mechanisms by which MDSC exert their effects, and because inflammatory conditions can create "MDSC-like" cells, the most effective therapeutic strategies will likely target common effector molecules over one specific pathway.

Scope of dissertation

While much is known about bona fide MDSC, there is still ambiguity in regards to MDSC-like cells and their role in cancer progression and the development of metastases. Therefore, the goals of this dissertation are to gain insight into the development MDSC-like cells and characterize their behavior. First, we determine if MDSC-like cell development correlates with tumor progression. Second, because the migration of MDSC

into peripheral tissues and the tumor site enables them to exert their immunosuppressive function, we determine if MDSC-like cells, which lack immunosuppressive ability, exhibit altered migratory behavior. Third, because many immune cells undergo metabolic reprogramming to facilitate their function, we investigate the metabolic profile of MDSC-like cells in comparison to naïve PMN and bona fide MDSC. Because PMN-MDSC are simple and affordable to isolate from the bone marrow, and can yield sufficient cell numbers, the present study will focus only on PMN-MDSC-like cells. The insight we gain from these studies will be especially important in the context of minimal residual disease, a state during which a low inflammatory environment could contribute to the generation of MDSC-like cells that could lead to disease recurrence.

CHAPTER TWO: MECHANISM OF PMN MIGRATION

Introduction

Historically, eukaryotic cell motility has been categorized into two major forms: amoeboid and mesenchymal. Amoeboid migration is characterized by low adhesion, independence from extracellular matrix proteolytic degradation, and a rounded cell morphology with a highly contractile rear uropod, whereas mesenchymal migration is characterized as adhesion- and proteolysis-dependent, with an elongated cell tail. Classically, amoeboid migration is used to define the rapid migration of PMN (Hind, Vincent, & Huttenlocher, 2016). As described in the previous chapter, MDSC can migrate to the tumor site and to secondary organs to aid in the development of the pre-metastatic niche. As one of the aims of this dissertation is to investigate the migratory behavior of PMN-MDSC-like cells, in this chapter, we explore what is known already about the mechanisms by which PMN and PMN-MDSC migrate.

Morphological polarization

In order to move, PMN must turn intracellularly generated forces into net cell body translocation by acquiring spatial asymmetry. This asymmetry, or polarized morphology which distinguishes the rear of the cell from the front, can be achieved even in the absence of a concentration gradient of stimuli (Lauffenburger & Horwitz, 1996). In this situation, it has been suggested that PMN break polarity by first forming the rear of the cell through actomyosin activity (Cramer, 2010). Interestingly, this polarization is stable, and in order to reverse directions PMN will make U-turns (Gerisch & Keller, 1981). The crosstalk

between the front and rear of the cell that maintain this polarization are poorly understood, but is believed to be maintained by coordinated Rho guanosine triphosphatase (GTPase) signaling between Rac, Cdc42 and RhoA (Hind et al., 2016). For example, Cdc42 and Rac are commonly thought to be restricted to the leading edge of the cell and RhoA to the rear (Meili & Firtel, 2003). The GTPases themselves are regulated by guanine nucleotide exchange factors (GEF) and GTPase-activating proteins (GAP) which maintain Rho GTPases in the active, GTP-bound form, or the inactive, GDP-bound form.

Chemoattractant-mediated PMN and PMN-MDSC recruitment

PMN are the first responders of the innate immune system and are recruited into tissues by chemoattractants. Chemotaxis is mediated by G-protein coupled receptors (GPCR), such as CXCR1, CXCR2, and formyl peptide receptors (FPR). In humans, CXCR1 predominantly interacts with CXCL8, whereas CXCR2 is more promiscuous and can interact with CXCL1, 2, 3, 5, 6 and 7 (Fan et al., 2007; Raghuwanshi et al., 2012). Homologs of these receptors have been found in mice (Swamydas et al., 2016). There are several chemokines that have been implicated in PMN and PMN-MDSC infiltration of tumors and are summarized in Table 2.1. Upon engagement of GPCR, $G_{\alpha i}$ proteins activate phospholipase C, resulting in the generation of diacylglycerol and inositol 1,4,5-triphosphate signaling molecules. The $G_{\beta\gamma}$ activates PI3K leading to the formation of PI (3,4,5)-triphosphate (PIP_3) (Raghuwanshi et al., 2012). PIP_3 can bind to the pleckstrin homology domain of GEF rendering them into the active conformation to activate Rho GTPases, ultimately resulting in migration (Hanna & El-Sibai, 2013).

Chemokine	Cancer	Reference
CXCL5	Non-small cell lung cancer	(Kowalczuk et al., 2014)
	Melanoma (mouse)	(Toh et al., 2011)
CXCL6	Gastrointestinal tumors	(Gijsbers et al., 2005)
	Tongue squamous cell carcinoma	(Wang et al., 2014)
CXCL8	Head and neck squamous cell carcinoma	(Trellakis et al., 2011)
	Gastric carcinoma	(Eck, Schmausser, Scheller, Brandlein, & Muller-Hermelink, 2003)
	Bronchoalveolar carcinoma	(Bellocq et al., 1998)
	Tongue squamous cell carcinoma	(Wang et al., 2014)
CCL15	Colorectal cancer	(Inamoto et al., 2016)

Table 2.1 Chemokines recruiting PMN and PMN-MDSC to the tumor. Adapted from (V. Kumar, Patel, Tcyganov, & Gabrilovich, 2016).

Formation of the leading edge

Rac GTPase activation at the leading edge of the cell induces actin polymerization and leading edge protrusion (lamellipod), and it is believed that Cdc42 GTPase-mediated signaling steers the direction of migration (Charest & Firtel, 2007; Lam & Huttenlocher, 2013; H. W. Yang, Collins, & Meyer, 2016). In migrating PMN, lamellipod formation is caused by the polymerization of monomeric globular actin (G-actin) into filamentous actin (F-actin). This process relies on actin nucleation factors such as Arp2/3, and nucleation promoting factors (NPF) such as WASP/N-WASP, WAVE, WASH, and WHAMM. Because the Arp2/3 complex is inherently inactive, NPF localization is critical for determining where polymerized actin forms. In motile cells, actin depolymerizing factor

(ADF)/cofilin promotes lamellipod extension by severing older actin filaments to provide new nucleation sites for Arp2/3, and by recycling G-actin (C. T. Skau & Waterman, 2015). In migrating PMN, there is an increase in the total number of actin filaments, but not the distribution of actin filament lengths suggesting that most increased polymerization occurs from new nucleation sites or that severing and uncapping of actin filaments occurs in a coordinated fashion (Cano, Lauffenburger, & Zigmond, 1991). Another class of actin nucleation factors, known as formins also contribute to the formation of the lamellipod, however, their exact mechanism remains to be elucidated (Block et al., 2012; Colleen T. Skau, Plotnikov, Doyle, & Waterman, 2015; C. Yang et al., 2007).

Contractile force generation in the uropod

The rear of the cell (uropod) generates the contractile force that is needed to overcome any cell adhesions and move the cell body forward. This process is primarily regulated by RhoA activity and myosin II. Activation of RhoA leads to the activation of RHO-associated coiled-coil-containing protein kinase (ROCK), that directly phosphorylates Ser19 on the regulatory light chain of myosin, also known as myosin light chain 2 (MLC2), and indirectly promotes myosin phosphorylation by phosphorylating and inhibiting myosin light chain phosphatase (Tybulewicz & Henderson, 2009). MLC2 phosphorylation promotes myosin ATPase activity and results in the proper positioning of the myosin heads to attach to actin filaments (J. L. Tan, Ravid, & Spudich, 1992). However, Rac and Cdc42 can also play a role in the rear of the cell. For example, Rac is necessary for tail retraction during chemotaxis (Gardiner et al., 2002). Additionally, Cdc42 controls the redistribution of WASP, which controls clustering of CD11b in the rear of the cell, and

affects myosin light chain phosphorylation by ROCK (S. Kumar et al., 2012; Szczur, Zheng, & Filippi, 2009). Several signaling molecules localize to the uropod to drive PMN polarization and migration (Hind et al., 2016). For example, PDZRhoGEF, a RhoA GEF, localizes to the rear of PMN and acts in a positive feedback loop with RhoA, ROCK, and myosin II to restrict contractility to the rear of the cell (Wong, Van Keymeulen, & Bourne, 2007). The activities of Rho GTPases and their downstream effectors are summarized in Figure 2.1.

Purinergic signaling amplifies chemotactic signals

The controlled release of ATP from cells was first demonstrated in neurons. This process has since been discovered in immune cells and plays an important role in their activation. For example, autocrine ATP signaling facilitates T-cell activation at the immune synapse (Woehrle et al., 2010). Recent studies have shown that PMN release ATP in response to engagement of chemotactic receptors, and that autocrine signaling serves to amplify the chemotactic signal (Chen et al., 2006). This process, described in detail below, involves the coordinated involvement of mechanisms that allow for the release of ATP, metabolism of ATP, and expression of purinergic receptors that can bind to ATP.

ATP release

During polarization, membrane perturbations, such as ruffling, can allow ATP to be released through mechanosensitive channels, such as pannexin-1 hemichannels (L. Bao, Locovei, & Dahl, 2004; W. G. Junger, 2008). Additionally, PMN activation results in ATP release through connexin and pannexin-1 hemichannels (Chen et al., 2010; Eltzschig et al.,

2006). Pannexin-1 and connexin hemichannels are regulated by post translational modifications such as glycosylation and phosphorylation, however the exact role of these modifications is not yet elucidated (Begandt et al., 2017; Penuela, Gehi, & Laird, 2013).

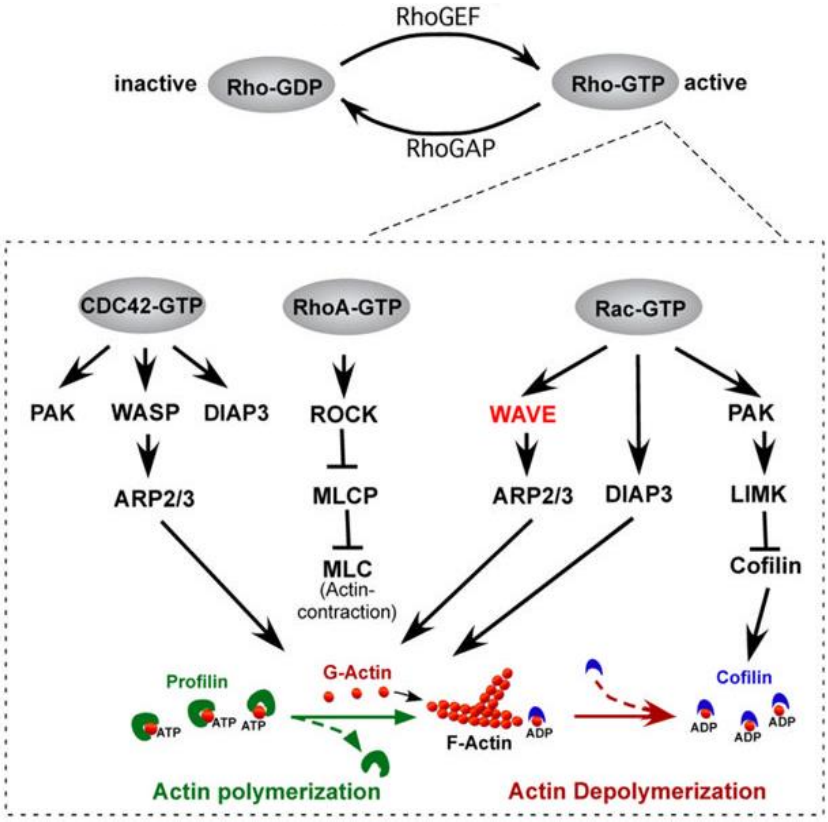

Figure 2.1 Intracellular signaling pathways mediated by Rho GTPase activation that result in PMN migration. Rho GTPases are regulated by guanine exchange factors (GEF) and GTPase activating proteins (GAP). Rac and Cd42 predominantly act at the leading edge of the cell. They regulate the proteins involved in the polymerization of F-actin and formation of the lamellipod, such as Arp2/3 and DIAP3, actin nucleating factors, and WASP/WAVE, nucleation promoting factors. RhoA predominantly functions in the rear of the cell to regulate Ser19 phosphorylation of MLC2, the regulatory light chain of myosin II, through the activation of RHO-associated coiled-coil-containing protein kinase (ROCK). ROCK can directly phosphorylate MLC2 or promote its phosphorylation by phosphorylating and inhibiting myosin light chain phosphatase (MLCP). Figure adapted from (Park, Chan, & Iritani, 2010).

ATP metabolism

Extracellular ATP can be recognized as a damage-associated molecular pattern and is quickly hydrolyzed by ectonucleotidases to ADP, AMP, and adenosine. There are four families of ectonucleotidases identified in mammalian cells. These include the ectonucleoside triphosphate diphosphohydrolase family (ENTPD), the ectonucleotide pyrophosphatase/phosphodiesterase family, the alkaline phosphatase family, and ecto-5'-nucleotidase (CD73). PMN express the ENTPD CD39 that converts ATP to ADP and AMP, as well as CD73 that converts AMP to adenosine (Bours, Swennen, Di Virgilio, Cronstein, & Dagnelie, 2006; W. G. Junger, 2008). Finally, extracellular adenosine can be converted to inosine by adenosine deaminase, or removed by cellular uptake facilitated by concentrative or equilibrative nucleoside transporters (Wolfgang G. Junger, 2011).

Purinergic receptors

There are three major families of purinergic receptors: 1) P1 receptors are GPCR that bind adenosine, 2) P2X receptors are ATP-gated ion channels that bind ATP, and 3) P2Y receptors are GPCR that bind ATP and ADP, as well as other nucleotides. Binding of ligand to these receptors can lead to receptor internalization and desensitization. Purinergic receptors that are expressed on PMN and their downstream effectors are summarized in Table 2.2 (Wolfgang G. Junger, 2011).

Studies have shown that engagement of FPR leads to the release of ATP through pannexin-1 hemichannels in human PMN (Chen et al., 2010). Additionally, mitochondria, which are not believed to have a role in PMN beyond redox maintenance, have been

implicated in the initial burst of ATP that is released upon FPR activation (Y. Bao et al., 2014). These studies have also demonstrated that P2Y2 and A3 are important mediators of

Receptor	Ligands	G-protein coupling	Main downstream signaling event
P2X ATP receptors			
P2X1	ATP	N/A	Ca^{2+} and Na^{+} influx
P2X4	ATP	N/A	Ca^{2+} influx
P2X5	ATP	N/A	Ion influx
P2X7	ATP	N/A	Cation influx and pore formation
P2Y nucleotide receptors			
P2Y1	ADP	$G_{q/11}$	PLCβ activation
P2Y2	ATP, UTP	$G_{q/11}$, $G_{i/o}$	PLCβ activation, cAMP inhibition
P2Y6	UDP, UTP	$G_{q/11}$	PLCβ activation
P2Y12	ADP	$G_{i/o}$	cAMP inhibition
P2Y13	ADP, ATP	$G_{i/o}$	cAMP inhibition
P2Y14	UDP-glucose	$G_{q/11}$	PLCβ activation
P1 adenosine receptors			
A1	Adenosine	$G_{i/o}$	cAMP inhibition
A2A	Adenosine	G_s	cAMP production
A2B	Adenosine	G_s	cAMP production
A3	Adenosine	$G_{i/o}$, $G_{q/11}$	cAMP inhibition, $InsP_3$ generation

Table 2.2 Downstream signaling of purinergic receptors found on PMN. N/A, not applicable; PLCβ, phospholipase C β; cAMP, cyclic AMP; $InsP_3$, inositol-1,4,5-triphosphate. Adapted from (Wolfgang G. Junger, 2011).

extracellular ATP, and with CD39, aid in the polarization of PMN by translocating to the leading edge of the cell (Figure 2.2) (Chen et al., 2006; Chen et al., 2010; Corriden et al., 2008). Moreover, P2X1-activation was shown to result in RhoA activation and phosphorylation of MLC2 in human and murine PMN (Lecut et al., 2009). The importance of purinergic signaling in chemotaxis has been confirmed using $P2Y2^{-/-}$, $A3^{-/-}$, $P2X1^{-/-}$ murine PMN that exhibit deficits in gradient sensing and speed (Chen et al., 2006; Lecut

et al., 2009). While signaling at the cell membrane through purinergic receptors affects chemotactic ability, the intracellular signaling events that link purinergic receptor activation to Rho GTPase activation or other factors has not yet been elucidated.

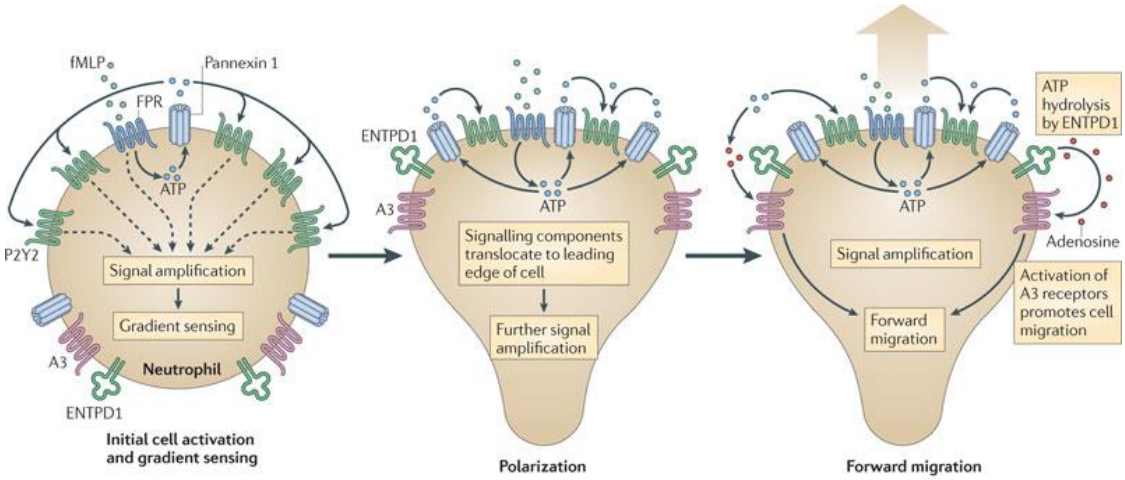

Figure 2.2 Purinergic signaling regulates PMN chemotaxis. Formyl peptide receptor (FPR) activation by formyl-methionine-leucine-phenylalanine (fMLP) induces the release of ATP through pannexin-1 hemichannels. This results in the activation of P2Y2 receptors, which provide signal amplification and facilitate the sensing of the chemotactic gradient (left). These signaling mechanisms lead to cell polarization (center) and translocation of pannexin-1 hemichannels, ectonucleoside triphosphate diphosphohydrolase 1 (ENTPD1, also known as CD39) and A3 receptors to the leading edge of the cell. Autocrine activation of A3 receptors promotes cell migration through an unknown mechanism (right) (Wolfgang G. Junger, 2011).

CHAPTER THREE: PMN-MDSC-LIKE CELLS RELY ON AUTOCRINE ATP SIGNALING TO SPONTANEOUSLY MIGRATE

Introduction

The roles of MDSC in tumor progression and metastasis are well understood. However, we currently know very little about MDSC-like cells. Our lab has previously described the expansion of MDSC-like cells, cells that lack immunosuppressive capability, in inflammatory conditions before cancer onset (Ortiz et al., 2014). We have also described their accumulation in the skin of a skin carcinogenesis model (Ortiz et al., 2014). In the present study, we aim to gain further insight into the characteristics of these cells. First, we hypothesize that PMN-MDSC-like cells develop in the context of cancer, specifically, during the early stages of tumor development when inflammatory conditions may support their development. Next, because the immunosuppressive behavior of PMN-MDSC is intrinsically linked to their physical migration into peripheral tissues or the tumor site to exert their effects, we hypothesize that PMN-MDSC-like cells exhibit altered migratory behavior (T. Condamine et al., 2015). Finally, because other immune cells such as T-cells, tumor-associated dendritic cells, and tumor-associated macrophages, and even tumor-infiltrating MDSC, undergo metabolic reprogramming to meet the energetic demands of their functionality, we hypothesize that PMN-MDSC-like cells will exhibit an altered metabolic profile compared to naïve PMN and bona fide PMN-MDSC (Hossain et al., 2015; V. Kumar et al., 2016; Pearce & Pearce, 2013). MDSC-like cells may represent an independent subset of MDSC or they may represent a stage of development that leads to

bona fide MDSC. By addressing these hypotheses, we hope to gain insight into the identity of PMN-MDSC-like cells and learn about the role of these cells in cancer to guide potential therapeutic interventions.

Results

PMN-MDSC-L develop in the early stages of tumor development and in transgenic models and are characterized by increased spontaneous migratory ability

We isolated PMN-MDSC from the bone marrow of mice sacrificed one week after intravenous LL2 injection, when 0-1 tumors were visible on the lungs, and directly tested their immunosuppressive capability. We co-cultured them with transgenic T-cells and their cognate ligand, and found that they are only able to weakly suppress T-cell proliferation (Figure 3.1).

Interestingly, when we tested the ability of these cells to chemotax in a 0.3um transwell assay for one hour in the presence of CXCL1 and fMLP, we found that the total number of PMN-MDSC migrated was greater than the total number of PMN at all concentrations of CXCL1 and fMLP (Figure 3.2A). However, we found that there was no difference in the fold change of PMN and PMN-MDSC to respond to CXCL1 and fMLP, suggesting that both PMN and PMN-MDSC are equally capable of responding to stimulation (Figure 3.2B). Moreover, we observed that PMN-MDSC randomly, spontaneously migrated more than PMN, and that this baseline level of increased motility accounted for enhanced PMN-MDSC chemotaxis (Figure 3.2C). We confirmed the presence of these cells that exhibit altered migratory behavior in the RET melanoma, KPC

pancreatic, and TRAMP prostate transgenic mouse models, using age-matched and PC mice as controls for the RET and TRAMP models and KPC model, respectively. We hypothesized that the slow development of tumors in transgenic models would create an inflammatory environment that would support their development (Figure 3.3A-C, Figure 3.4A-C, Figure3.5A-C). We also measured the levels of chemokine receptor expression in the transgenic models. We found that, contrary to reports in the literature of CXCR1 expression on murine neutrophils (Swamydas et al., 2016), PMN and PMN-MDSC from murine bone marrow do not express CXCR1 (Figure 3.3D, Figure 3.4D, Figure 3.5D). Consistent with our finding that PMN and PMN-MDSC are equally capable of responding to stimulation, PMN-MDSC from the RET and TRAMP model do not express increased levels of CXCR2 (Figure 3.3D, Figure 3.5D). While we did observe a significant increase in CXCR2 expression on KPC PMN-MDSC, this does not account for the increased ability of PMN-MDSC to spontaneously migrate (Figure 3.4D). Based on these results, we believe we have captured PMN-MDSC-like cell development in the early stages of tumor development and in transgenic models, where there is a relatively low inflammatory environment. These cells are characterized by weak immunosuppressive activity and enhanced spontaneous migration, and moving forward, we will refer to them as "PMN-MDSC-like cells" (PMN-MDSC-L).

Increased spontaneous migration is not observed in PMN-MDSC from the bone marrow of transplantable models or mice in the late stages of tumor development

Our lab has previously shown that PMN-MDSC from the bone marrow of mice inoculated subcutaneously with EL4, LLC, or CT26 cells exhibit immunosuppressive

activity by inhibiting T-cell proliferation (data not shown). We tested the migratory behavior of cells from these transplantable models in a transwell assay and found that they spontaneously migrate at levels comparable to naïve PMN (Figure 3.6A-C). Similarly, in the orthotopic model, we found that PMN-MDSC from the bone marrow of mice sacrificed three weeks after intravenous LL2 injection, when the lungs had three or more visible tumors, that PMN-MDSC no longer spontaneously migrated more than PMN (Figure 3.6D). These results suggest a correlation between migratory behavior and immunosuppressive function.

PMN-MDSC-L spontaneous migration is characterized by increased speed, persistence time, mean squared displacement and an overall greater random motility coefficient compared to PMN

To characterize the altered migratory behavior of PMN-MDSC-L cells, we tracked the movement of individual naïve PMN and RET PMN-MDSC-L by microscopy and ImageJ, and plotted the trajectory of each path, transposing the initial position of each path to the origin (Figure 3.7A). From these tracks, we observed that neither PMN nor PMN-MDSC-L demonstrate a preference for directional movement, confirming that in the absence of stimulation, both PMN and PMN-MDSC-L move randomly. We also observed that PMN tracks cluster towards the origin, whereas PMN-MDSC-L spread far from the origin, and found that PMN-MDSC-L have a greater mean squared displacement than PMN (Figure 3.7B). Next, we determined that PMN-MDSC-L migrate with greater speed and an increased persistence time compared to PMN (Figure 3.7C,D). Finally, we calculated the likelihood of a cell moving randomly as defined by the random motility coefficient,

$$\text{Random motility coefficient} = (1/2) \times (\text{speed})^2 \times (\text{persistence time})$$

and determined that PMN-MDSC-L have an approximately 15-fold higher random motility coefficient compared to PMN. Collectively, these quantitative measurements support our findings that PMN-MDSC-L spontaneously migrate more than PMN (Figure 3.7E).

PMN-MDSC-L utilize ATP released from the cell via pannexin-1 hemichannels to spontaneously migrate

We wanted to understand the mechanism by which PMN-MDSC-L spontaneously migrate. Studies in human neutrophils have shown that upon engagement of formyl-peptide receptors by fMLP, ATP is released through pannexin-1 hemichannels. Engagement of the receptor also results in rearrangement of pannexin-1 hemichannels and purinergic receptors to the leading edge of the cell. This promotes ATP-mediated autocrine signaling that enhances gradient sensing and chemotaxis (Chen et al., 2006). We hypothesized that PMN-MDSC-L may use ATP-mediated autocrine signaling as a mechanism to spontaneously migrate. To test this hypothesis, we first examined the effect of disrupting ATP release from the cell on the ability of cells to spontaneously migrate. We inhibited pannexin-1 hemichannels using ^{10}Panx (panx), a pannexin-1 mimetic inhibitory small peptide, and observed that the ability of PMN-MDSC-L from RET bone marrow to spontaneously migrate was abrogated (Figure 3.8A). We confirmed this finding in a second model, using PMN-MDSC-L from the bone marrow of mice sacrificed one week after intravenous injection of LL2 cells (Figure 3.8B). Furthermore, we confirmed that PMN-MDSC-L spontaneous migration was dependent upon pannexin-1 hemichannel-mediated ATP

release by treating cells with scrambled ^{10}Panx, (scr; Figure 3.8A,B). We did not observe an effect on the ability of PMN to spontaneously migrate in response to pannexin-1 hemichannel inhibition.

To confirm that spontaneous migration is truly dependent upon ATP, we treated PMN-MDSC-L from the orthotopic model and PMN from naïve mice with apyrase, an enzyme that catalyzes the hydrolysis of ATP to yield AMP and inorganic phosphate, before migrating cells in a transwell assay. We found that both PMN and PMN-MDSC-L migration was completely abrogated (Figure 3.8C).

PMN-MDSC-L utilize P2X1-mediated signaling to spontaneously migrate

There are several families of ectonucleotidases expressed on the cell surface of mammalian cells that can hydrolyze ATP to ADP, AMP, and adenosine, and each of these metabolites can signal through a distinct set of purinergic receptors (Wolfgang G. Junger, 2011). Human neutrophils have been reported to use the purinergic receptors P2X1, which binds ATP, and A3, which binds adenosine, to amplify chemotactic signals (Chen et al., 2006; Lecut et al., 2009). To determine if these receptors are involved in the spontaneous migration of PMN-MDSC-L, we first treated cells with suramin, a pan-P2 receptor (pan-P2R) inhibitor, and observed that only the spontaneous migration of PMN-MDSC-L was abrogated in transwell assays (Figure 3.9A). Next, we treated cells with NF449, a P2X1-specific inhibitor, and found that only the ability of PMN-MDSC-L to spontaneously migrate was inhibited (Figure 3.9B). However, while treatment with suramin resulted in an approximately 75% decrease in PMN-MDSC-L spontaneous migration, treatment with

NF449, only resulted in an approximately 50% decrease. These results suggest that another P2X receptor or a P2Y receptor plays a role in the spontaneous migration of PMN-MDSC-L mediated by ATP or its metabolites.

Finally, we treated cells with MRS 1191, an inhibitor of A3, and did not observe a decrease in the total number of PMN or PMN-MDSC-L that migrated through the transwell, suggesting that adenosine signaling though this receptor is not required for PMN-MDSC-L to spontaneously migrate (Figure 3.9C). While we observed a dramatic decrease in spontaneous migration at the 100μM dose, a concentration that does not compromise the viability of the cells (data not shown), in the absence of a titrated response to MRS 1191, we conclude that this is likely a result of off-target effects.

Increased PMN-MDSC-L spontaneous migration correlates with increased metabolic rates

Because PMN-MDSC-L rely on extracellular ATP to spontaneously migrate, we hypothesized that they alter flux through their metabolic pathways to increase ATP production to satisfy this energetic demand. To test this hypothesis, we utilized a Seahorse XF Analyzer to measure the glycolytic and oxidative phosphorylation rates of PMN and PMN-MDSC-L from RET mice and mice sacrificed one week after intravenous injection of LL2 cells. In this assay, the glycolytic rate is measured by lactic acid production, and is thus represented as the extracellular acidification rate, and the oxidative phosphorylation rate is measure by the consumption of oxygen, and is thus represented as the oxygen consumption rate (OCR). We found that the basal level of glycolysis was significantly

increased in both models (Figure 3.10A). Moreover, we found that the basal level of oxidative phosphorylation was significantly increased only in PMN-MDSC-L isolated from the orthotopic LL2 model (Figure 3.10B).

We tested the ability of these cells to respond to mitochondrial stress by inhibiting components of the electron transport chain. By combining inhibition of the electron transport chain complex V, ATP synthase, using oligomycin, and disrupting the proton gradient using the protonophore FCCP, we forced metabolic flux through oxidative phosphorylation and measured the ability of cells to maximally respire (Figure 3.10C). The spare respiratory capacity of cells is a measure of the ability of cells to increase metabolic flux through oxidative phosphorylation in the case of a sudden increase in energy demand. It is calculated as:

Spare Respiratory Capacity = Maximal respiration rate - Basal respiration rate

We found that PMN-MDSC-L from both models have an increased spare respiratory capacity compared to PMN (Figure 3.10D).

Next, we isolated PMN-MDSC from the bone marrow of mice that were sacrificed three weeks after intravenous injection of LL2 cells, PMN-MDSC that, as we have shown previously, do not exhibit increased spontaneous migratory behavior compared to naïve PMN, and measured the basal metabolic rates, maximal respiration, and the spare respiratory capacity. We found that PMN-MDSC do not have increased basal glycolytic or oxidative phosphorylation rates compared to PMN (Figure 3.11A-C). We also found that the spare respiratory capacity was reduced to levels exhibited by PMN (Figure 3.11D).

These results lend further support to the idea that PMN-MDSC-L metabolic reprogramming matches the energetic need that their altered migratory behavior demands.

PMN-MDSC-L have increased cell surface expression of the glucose transporter Glut1

PMN have few mitochondria, whose main function in these cells is to maintain redox balance, and thus, primarily use glycolysis to generate ATP (Biswas, 2015). We have observed increased basal glycolytic rates in PMN-MDSC-L from two different models. We hypothesized three possibilities to account for these increased metabolic rates: 1) PMN-MDSC-L increase the expression of glycolytic enzymes, 2) PMN-MDSC-L increase the cell surface expression of glucose transporters, or 3) PMN-MDSC-L increase glucose uptake. To address the first possibility, we investigated the expression of several glycolytic enzymes and HIF-1α, the master regulator of glycolysis, using real-time quantitative PCR (Iyer et al., 1998). We did not observe any differences in the expression of HIF-1α or any of the glycolytic enzymes investigated (Figure 3.12).

To address the second possibility, we investigated the expression of Glut1, Glut3 and Glut4 on PMN-MDSC-L. Glut1 expression on PMN is important for PMN function and is modulated by the activation state of the cells (A. S. Tan, Ahmed, & Berridge, 1998). For example, Glut1 levels increase on PMN stimulated with phorbol myristate acetate to form extracellular traps (Rodríguez-Espinosa, Rojas-Espinosa, Moreno-Altamirano, López-Villegas, & Sánchez-García, 2015). Glut3 and Glut4 are primarily expressed on monocytes, but are of interest to us because PMN-MDSC, and potentially PMN-MDSC-L,

can differentiate from M-MDSC (Maratou et al., 2007; Youn et al., 2013). First, we measured the gene expression of Glut1 and Glut3 using real-time quantitative PCR, but did not observe any differences in gene expression between PMN and PMN-MDSC-L (Figure 3.13A). Next, we measured the cell surface expression of these transporters using flow cytometry, and found that PMN-MDSC-L have significantly increased expression of Glut1 compared to PMN (Figure 3.13B).

Because we found increased expression of Glut1 on PMN-MDSC-L, we expected to also observe an increase in glucose uptake. Finally, to test the third possibility, we cultured cells in the presence of 2-NBDG, a fluorescent analog of glucose, and used flow cytometry to measure the uptake of glucose. Surprisingly, PMN-MDSC-L did not increase glucose uptake in comparison to PMN by this method (Figure 3.14).

PMN-MDSC-L do not have an increased total pool of ATP compared to PMN

Because we observed an increase in the basal glycolytic rates in PMN-MDSC-L, and an increased basal oxidative phosphorylation rate in PMN-MDSC-L in at least one model, we hypothesized that the total ATP pool in PMN-MDSC-L would be increased compared to PMN. Primarily, we hypothesized that we would be able to capture an increase in the amount of ATP available extracellularly. We used a luciferase-based assay to determine if the intracellular pool of ATP or if the amount of ATP released into the supernatant of cultured cells was greater in PMN-MDSC-L compared to PMN. While we did not observe a difference in the concentration of ATP released by PMN or PMN-MDSC-L, we also observed great variability in the measurements (Figure 3.15A). We rationalized

that even small differences in the availability of ATP could contribute to spontaneous migration, and so we sought a more quantitative approach and used liquid chromatography-mass spectrometry. ATP is an easily diffusive molecule that can serve as a danger signal in the extracellular space, and so its levels are tightly regulated by ectonucleotidases (Carola Ledderose et al., 2016). To increase our chances of capturing changes in free ATP released into the supernatant of cultured cells, we cultured the cells in the presence of the ectonucleotidase inhibitor ARL 67156. As an alternative approach, we also blocked ATP release from pannexin-1 hemichannels by treating cells with ^{10}Panx to try to capture differences in intracellular ATP levels. However, using either of these approaches, we were unable to detect differences in the total pool of ATP available for PMN-MDSC-l (Figure 3.15B).

PMN-MDSC-L have increased levels of MLC2 and pMLC2

Finally, we investigated the intracellular signaling events that ultimately result in movement of PMN-MDSC. Classically, PMN migration is initiated by chemokine receptor or integrin receptor engagement, and results in the activation of the Rho GTPases, RhoA, Cdc42, and Rac, which are, themselves, regulated by RhoGAP and RhoGEF. Cdc42 and Rac activation initiates downstream signaling that predominantly results in the formation of the lamellipod, and RhoA activation initiates downstream signaling that predominantly affects the uropod, though there can be crossover in these functions (Park et al., 2010). We hypothesized that aberrant activation of the Rho GTPases may account for the increased ability of PMN-MDSC-L to spontaneously migrate. To test this hypothesis, we measured the activation state of RhoA and Cdc42 in PMN and RET PMN-MDSC-L using a G-LISA.

This colorimetric assay uses the binding domain of a Rho-family effector protein to capture RhoA and Cdc42 only in the active, GTP-bound, form. We did not observe significant activation of RhoA or Cdc42 in PMN-MDSC-L compared to PMN (Figure 3.16A,B).

Classically, GTPase activation results in the activation of kinases, such as PAK or ROCK, and further signal amplification through the activation of downstream kinases. We hypothesized that aberrant activation of these kinases would bypass the need for GTPase activation and could explain how PMN-MDSC-L are able to spontaneously migrate. Instead of determining the activation state of individual kinases, we sought to observe changes in the terminal effects of these signaling pathways, such as the polymerization of F-actin or actomyosin contraction. Therefore, we first measured levels of F-actin in cells using phalloidin, a phallotoxin derived from the death cap mushroom that tightly binds to and stabilizes F-actin. We found that both PMN and PMN-MDSC-L were equally stimulated by CXCL1 and fMLP and that in the absence of stimulation, PMN and PMN-MDSC-L generated similar amounts of F-actin (Figure 3.17A,B).

Based on these results, we hypothesized that PMN-MDSC-L and PMN are equivalently primed to spontaneously migrate, however, aberrant action in the uropod, such as increased actomyosin contraction, could explain the increased motility of PMN-MDSC-L. The preceding event to actomyosin contraction is the phosphorylation of myosin light chain 2 (MLC2) on Ser19 (pMLC2), an event that allows for the proper arrangement of myosin heads to facilitate contraction. To investigate this possibility, we measured pMLC2 by western blot, and interestingly, we found that not only were pMLC2 levels increased in PMN-MDSC-L, but total MLC2 levels were also increased (Figure 3.18).

Collectively, these experiments have demonstrated that relatively low inflammatory conditions in cancer results in the production of PMN-MDSC-L that exhibit enhanced spontaneous migratory behavior. Furthermore, we have identified pannexin-1 hemichannel-mediated ATP release and P2X1 engagement as the mechanism by which PMN-MDSC-L spontaneously migrate. We have also shown that PMN-MDSC-L alter their metabolic profile to meet the energetic demands of their altered migratory behavior by increasing cell surface expression of Glut1 and flux through glycolytic pathways (Figure 3.19). We discuss the implications of these findings in the next chapter.

Figures

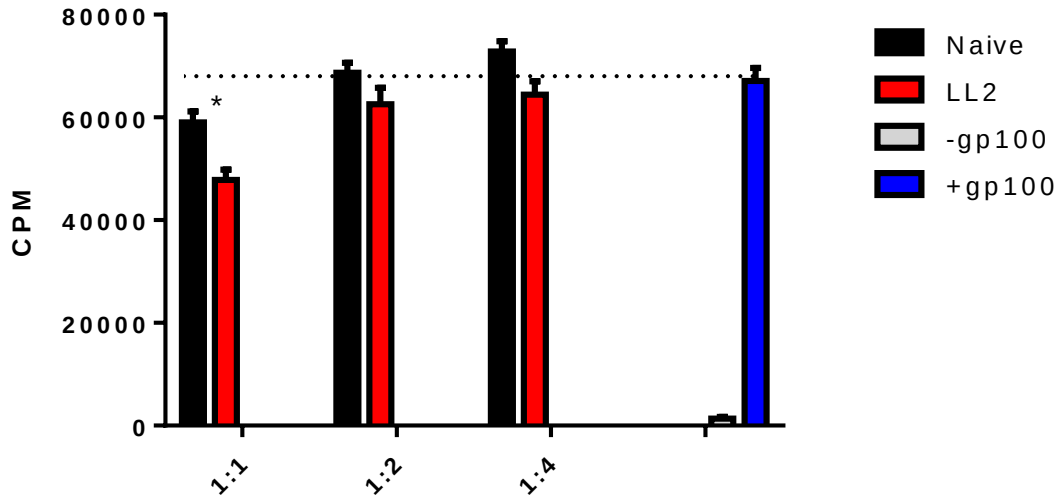

Figure 3.1

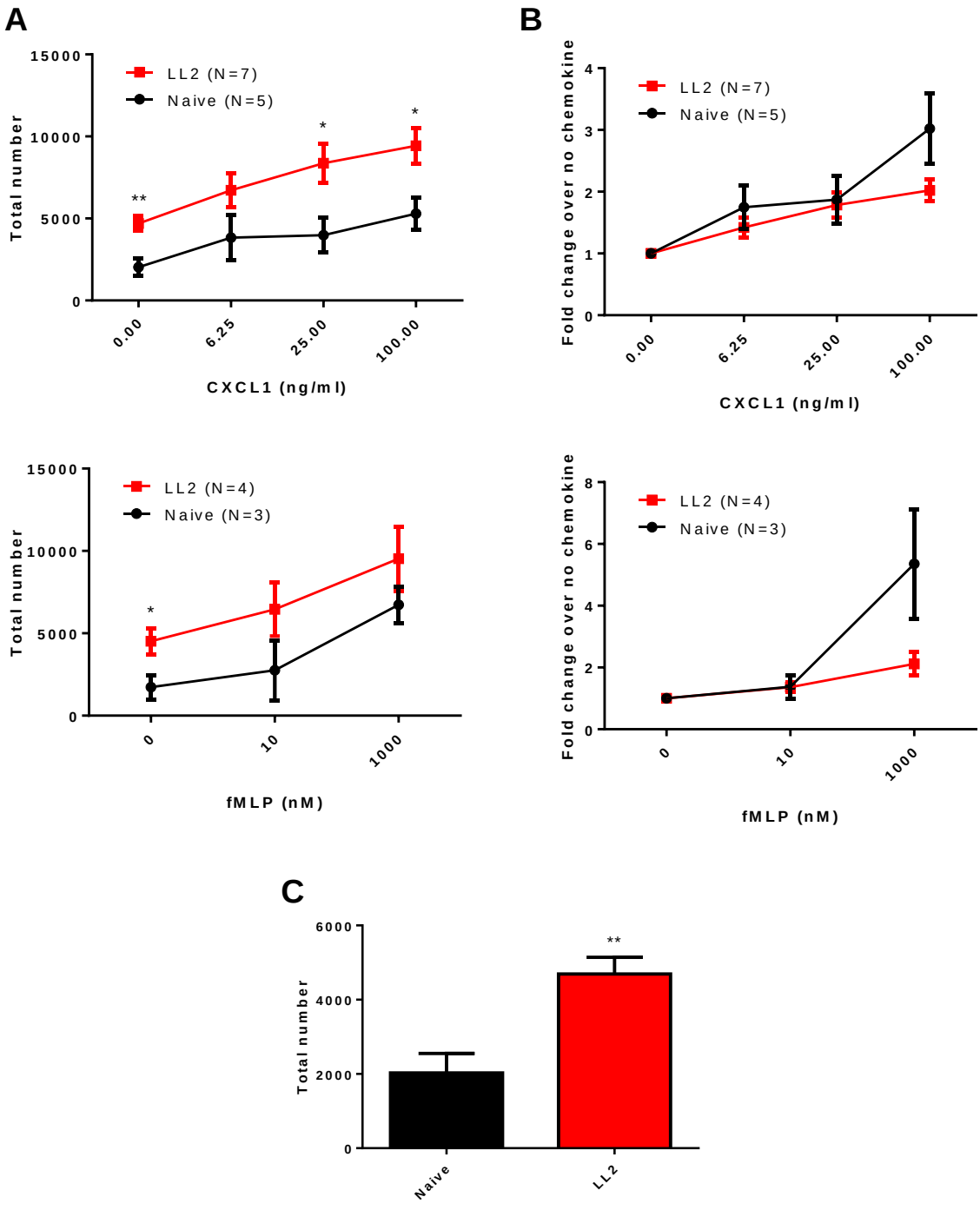
A
15000
10000
5000
0
Total number
LL2 (N=7)
Naive (N=5)
**
*
*
0.00
6.25
25.00
100.00
CXCL1 (ng/ml)
B
4
3
2
1
0
Fold change over no chemokine
LL2 (N=7)
Naive (N=5)
0.00
6.25
25.00
100.00
CXCL1 (ng/ml)
15000
10000
5000
0
Total number
LL2 (N=4)
Naive (N=3)
*
0
10
1000
fMLP (nM)
8
6
4
2
0
Fold change over no chemokine
LL2 (N=4)
Naive (N=3)
0
10
1000
fMLP (nM)
C
6000
4000
2000
0
Total number
**
Naive
LL2

Figure 3.2

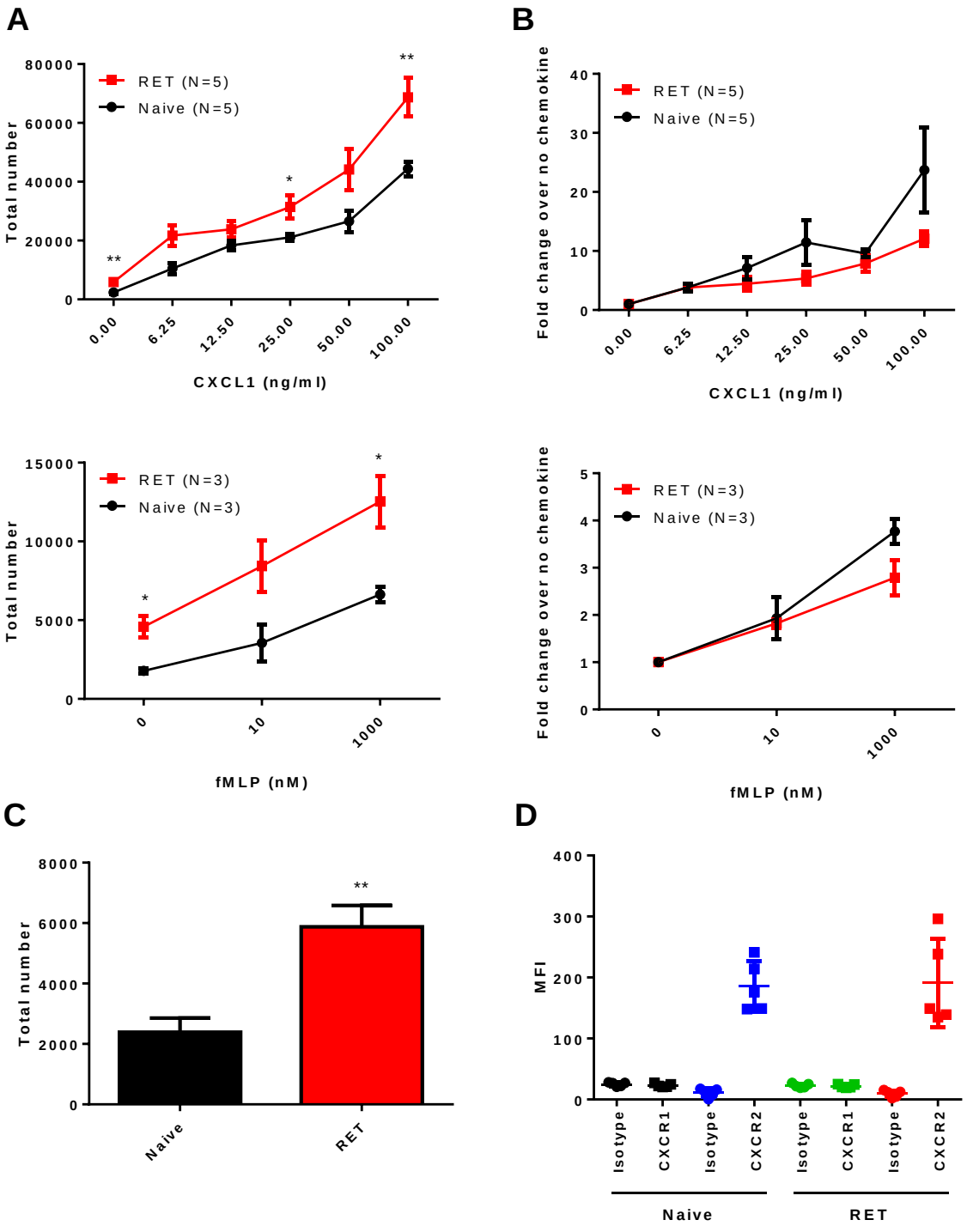
A
RET (N=5)
Naive (N=5)
Total number
CXCL1 (ng/ml)
B
Fold change over no chemokine
RET (N=3)
Naive (N=3)
fMLP (nM)
C
Naive
RET
D
MFI
Isotype
CXCR1
CXCR2
Naive
RET

Figure 3.3

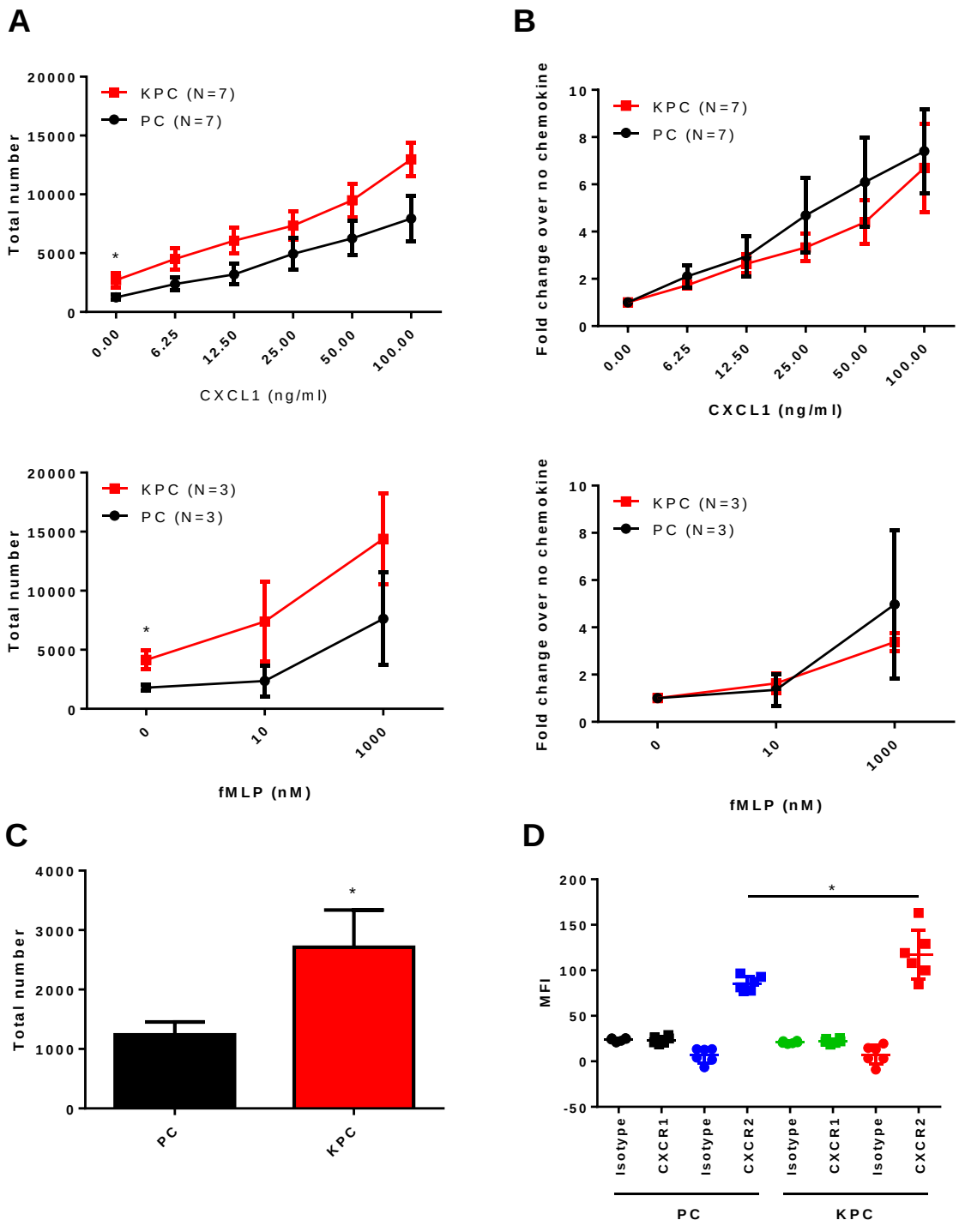
A
B
C
D
KPC (N=7)
PC (N=7)
Total number
CXCL1 (ng/ml)
Fold change over no chemokine
KPC (N=3)
PC (N=3)
fMLP (nM)
0.00
6.25
12.50
25.00
50.00
100.00
0
10
1000
PC
KPC
MFI
Isotype
CXCR1
CXCR2

Figure 3.4

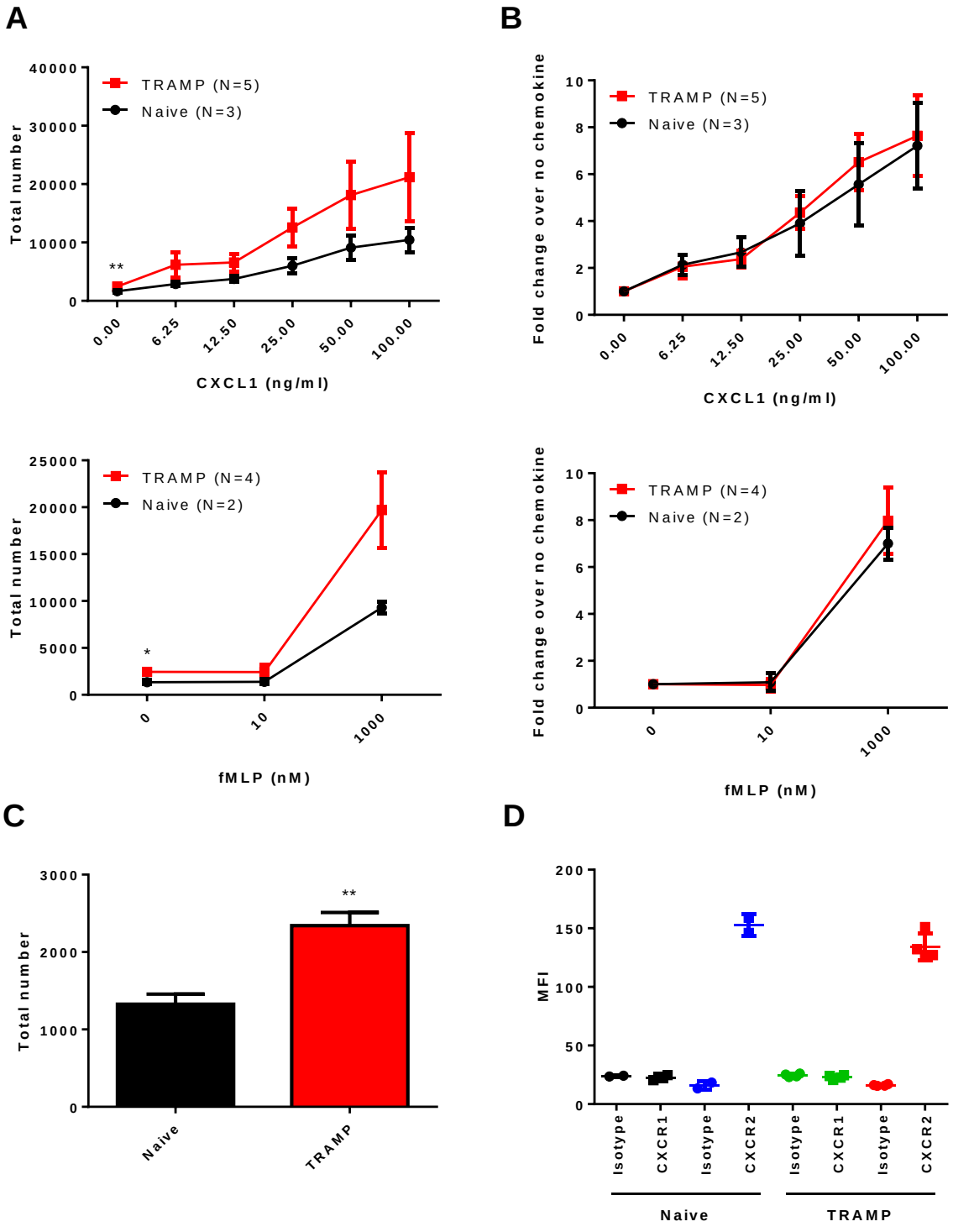
A
B
TRAMP (N=5)
Naive (N=3)
Total number
Fold change over no chemokine
CXCL1 (ng/ml)
0.00
6.25
12.50
25.00
50.00
100.00
**
TRAMP (N=4)
Naive (N=2)
fMLP (nM)
0
10
1000
*
C
D
Total number
Naive
TRAMP
MFI
Isotype
CXCR1
CXCR2

Figure 3.5

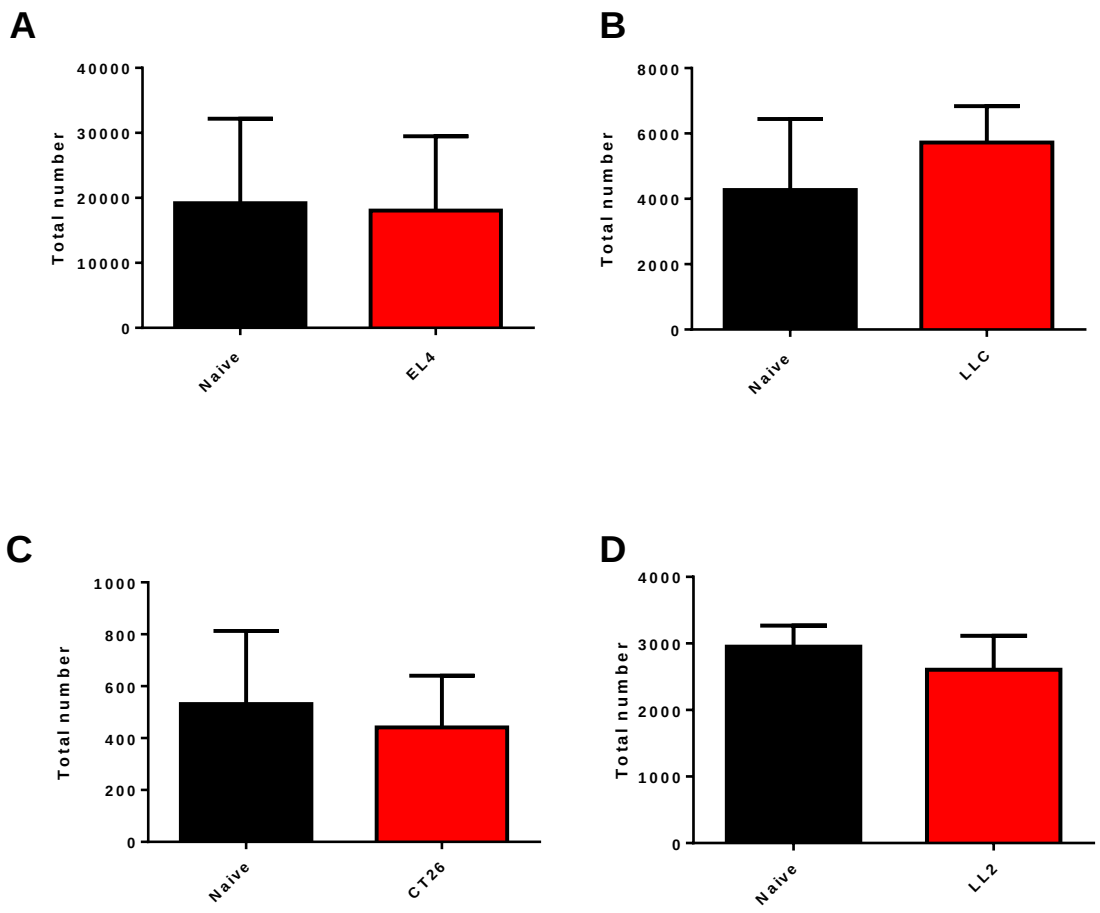
A
40000
30000
20000
10000
0
Total number
Naive
EL4
B
8000
6000
4000
2000
0
Total number
Naive
LLC
C
1000
800
600
400
200
0
Total number
Naive
CT26
D
4000
3000
2000
1000
0
Total number
Naive
LL2

Figure 3.6

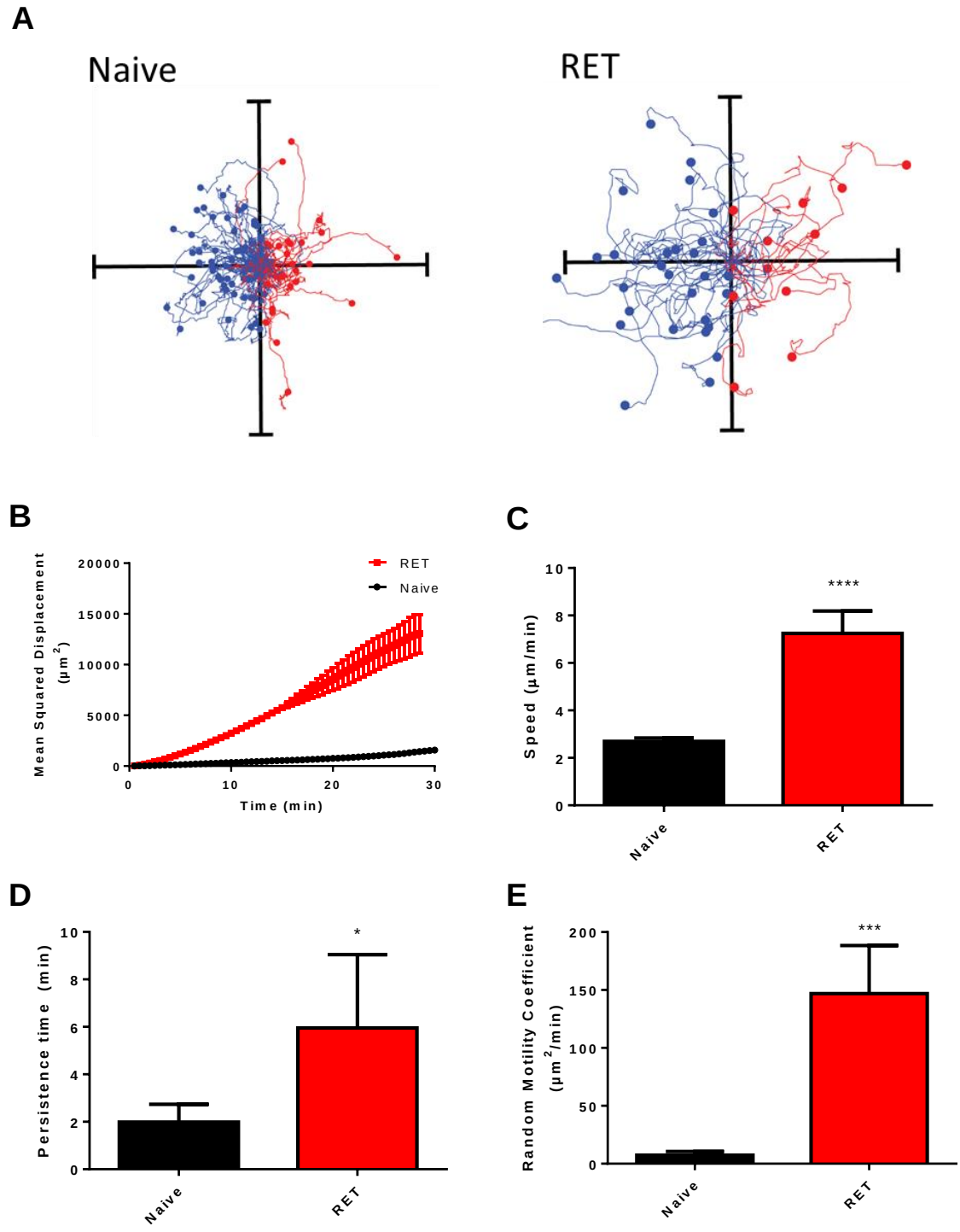
A
Naive
RET
B
Mean Squared Displacement (µm²)
20000
15000
10000
5000
0
0
10
20
30
Time (min)
RET
Naive
C
Speed (µm/min)
10
8
6
4
2
0
****
Naive
RET
D
Persistence time (min)
10
8
6
4
2
0
*
Naive
RET
E
Random Motility Coefficient (µm²/min)
200
150
100
50
0
***
Naive
RET

Figure 3.7

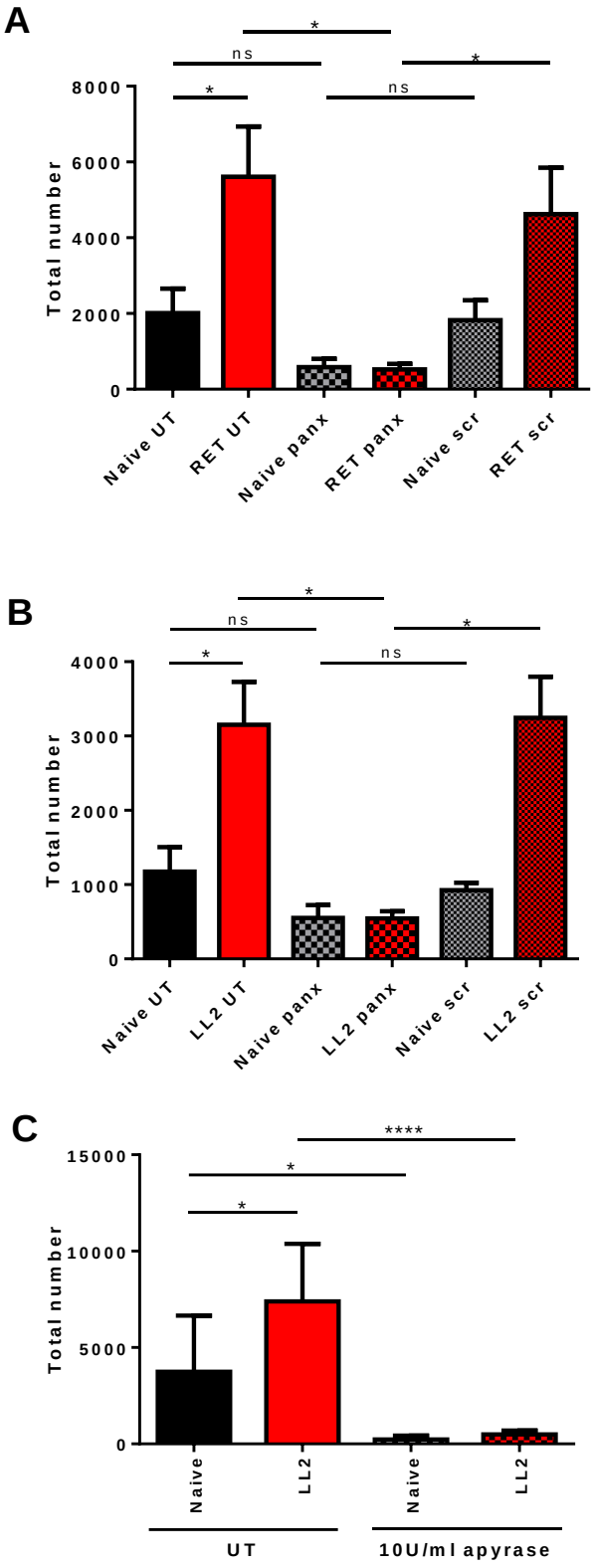
A
*
ns
*
*
ns
8000
6000
4000
2000
0
Total number
Naive UT
RET UT
Naive panx
RET panx
Naive scr
RET scr
B
*
ns
*
*
ns
4000
3000
2000
1000
0
Total number
Naive UT
LL2 UT
Naive panx
LL2 panx
Naive scr
LL2 scr
C
****
*
*
15000
10000
5000
0
Total number
Naive
LL2
Naive
LL2
UT
10U/ml apyrase

Figure 3.8

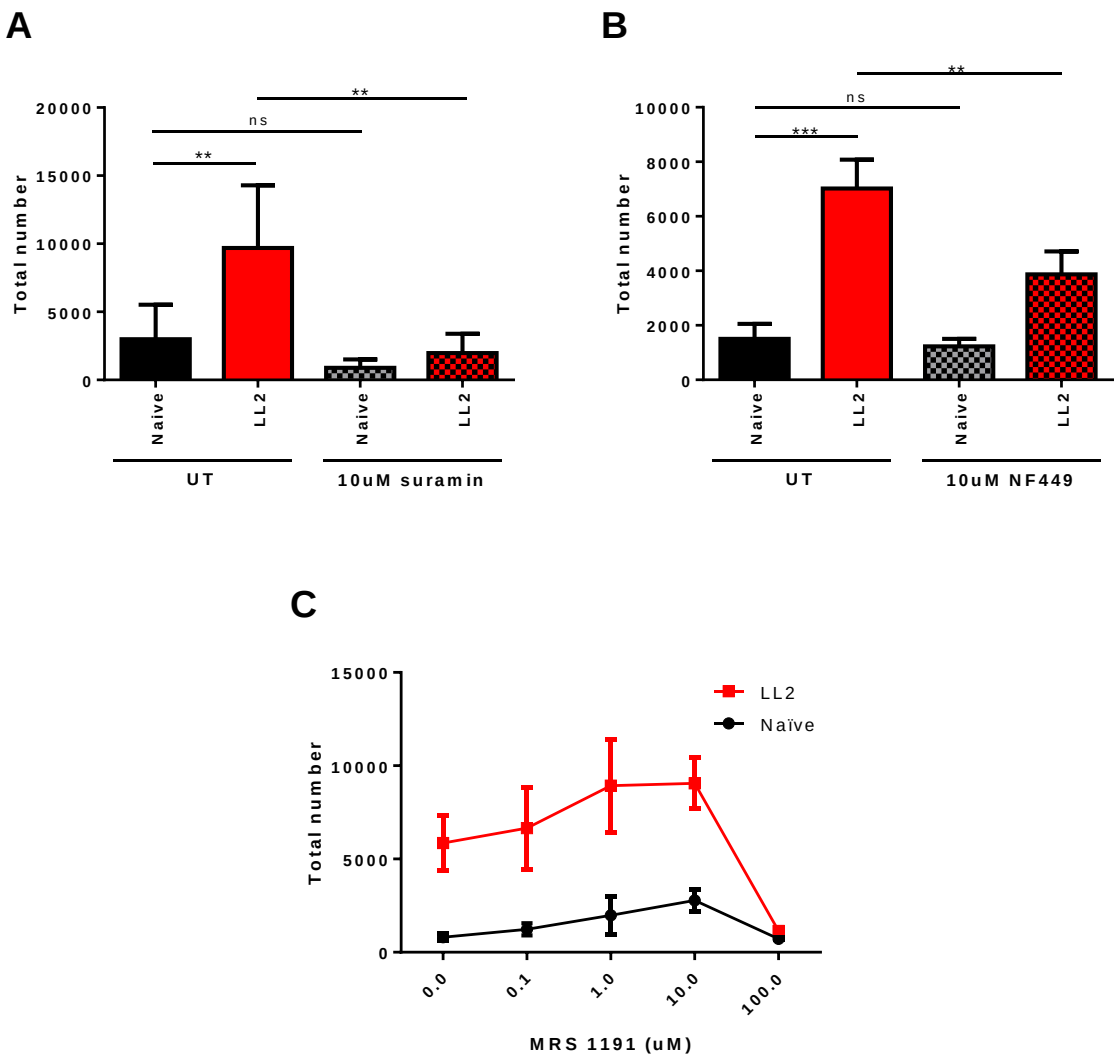
A
B
C
Total number
20000
15000
10000
5000
0
**
ns
**
Naive
LL2
Naive
LL2
UT
10uM suramin
10000
8000
6000
4000
2000
0
**
ns
***
Naive
LL2
Naive
LL2
UT
10uM NF449
15000
10000
5000
0
LL2
Naïve
0.0
0.1
1.0
10.0
100.0
MRS 1191 (uM)

Figure 3.9

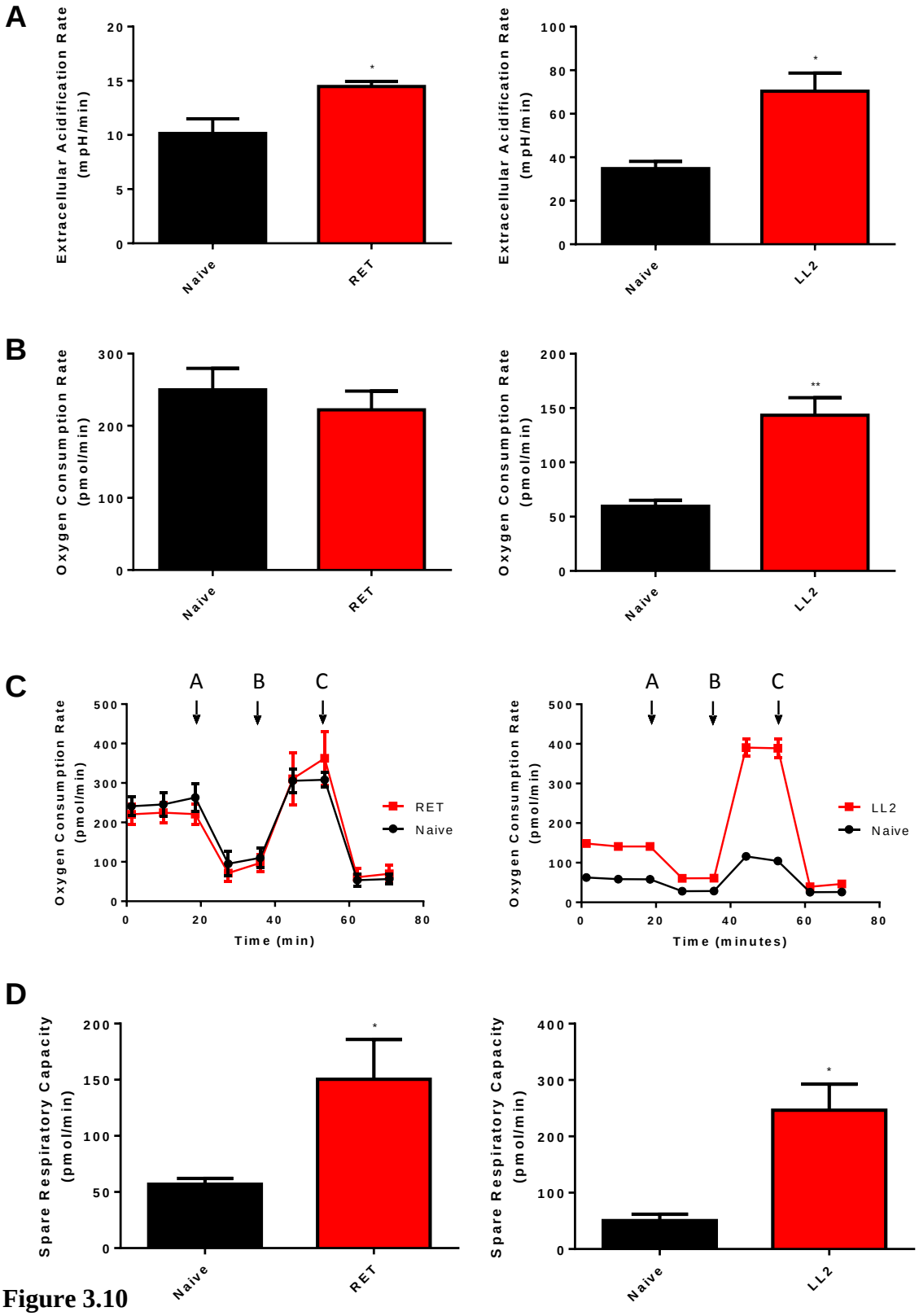
A
Extracellular Acidification Rate (mpH/min)
Naive
RET
LL2
B
Oxygen Consumption Rate (pmol/min)
C
A
B
C
RET
Naive
LL2
Time (min)
Time (minutes)
D
Spare Respiratory Capacity (pmol/min)

Figure 3.10

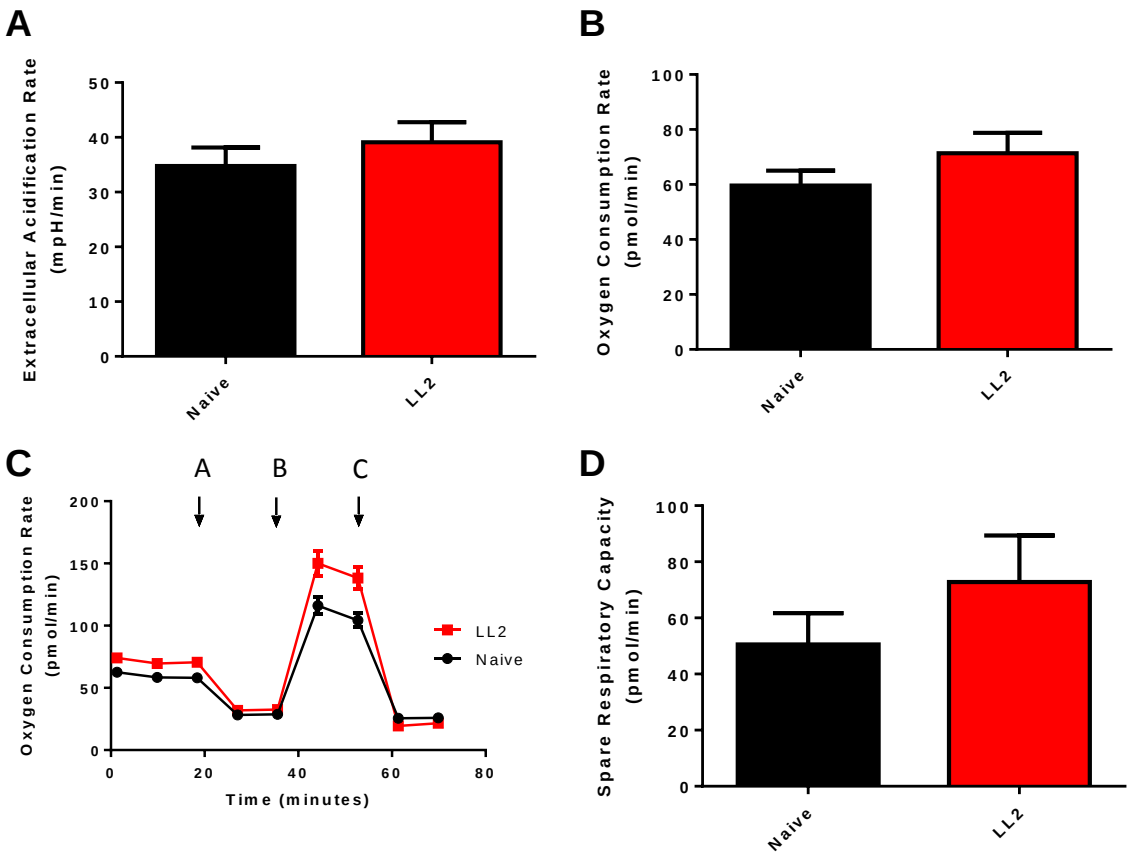
A
Extracellular Acidification Rate (mpH/min)
50
40
30
20
10
0
Naive
LL2
B
Oxygen Consumption Rate (pmol/min)
100
80
60
40
20
0
Naive
LL2
C
A
B
C
Oxygen Consumption Rate (pmol/min)
200
150
100
50
0
0
20
40
60
80
Time (minutes)
LL2
Naive
D
Spare Respiratory Capacity (pmol/min)
100
80
60
40
20
0
Naive
LL2

Figure 3.11

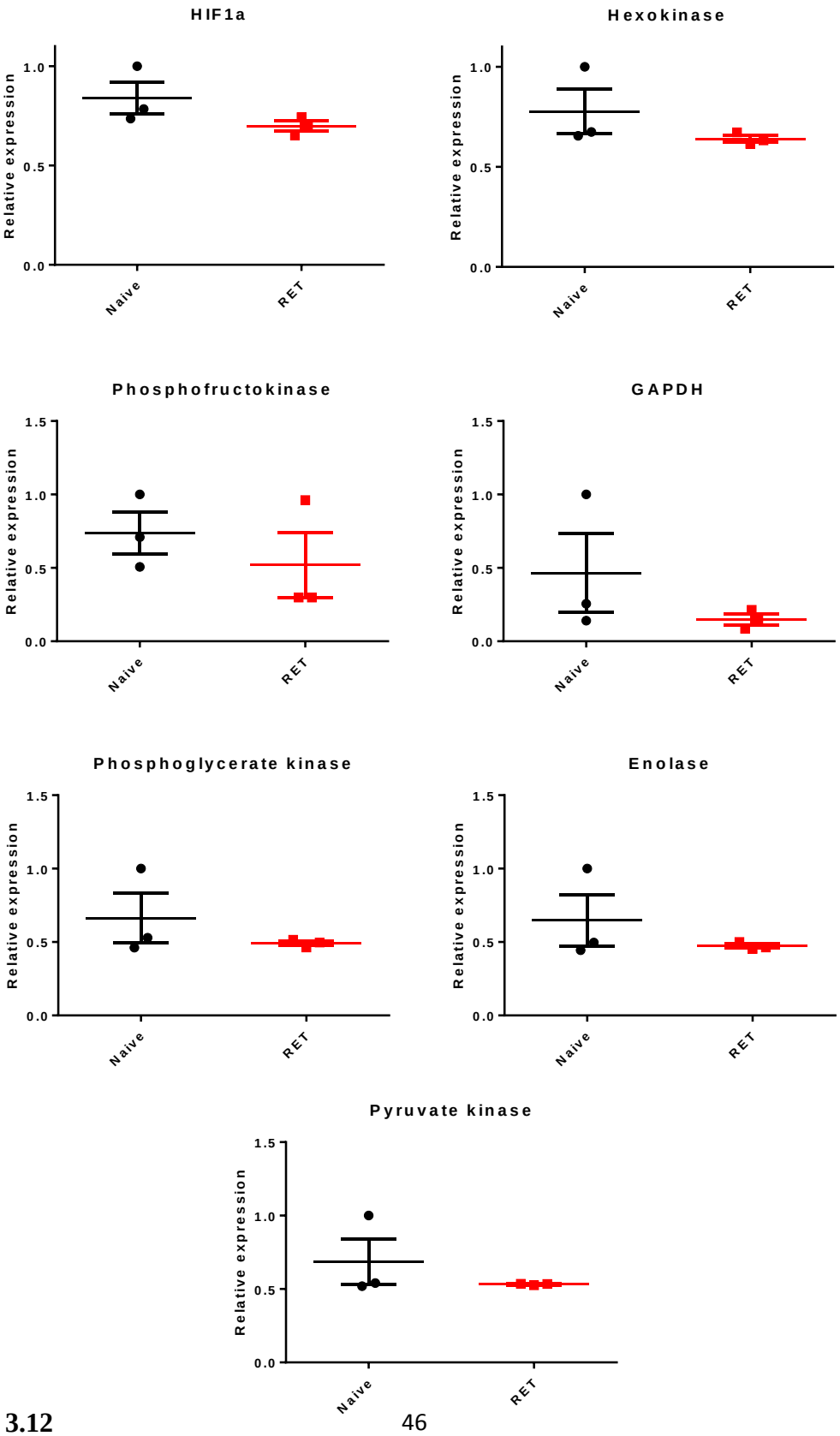
HIF1a
Hexokinase
Phosphofructokinase
GAPDH
Phosphoglycerate kinase
Enolase
Pyruvate kinase
Relative expression
0.0
0.5
1.0
1.5
Naive
RET

Figure 3.12

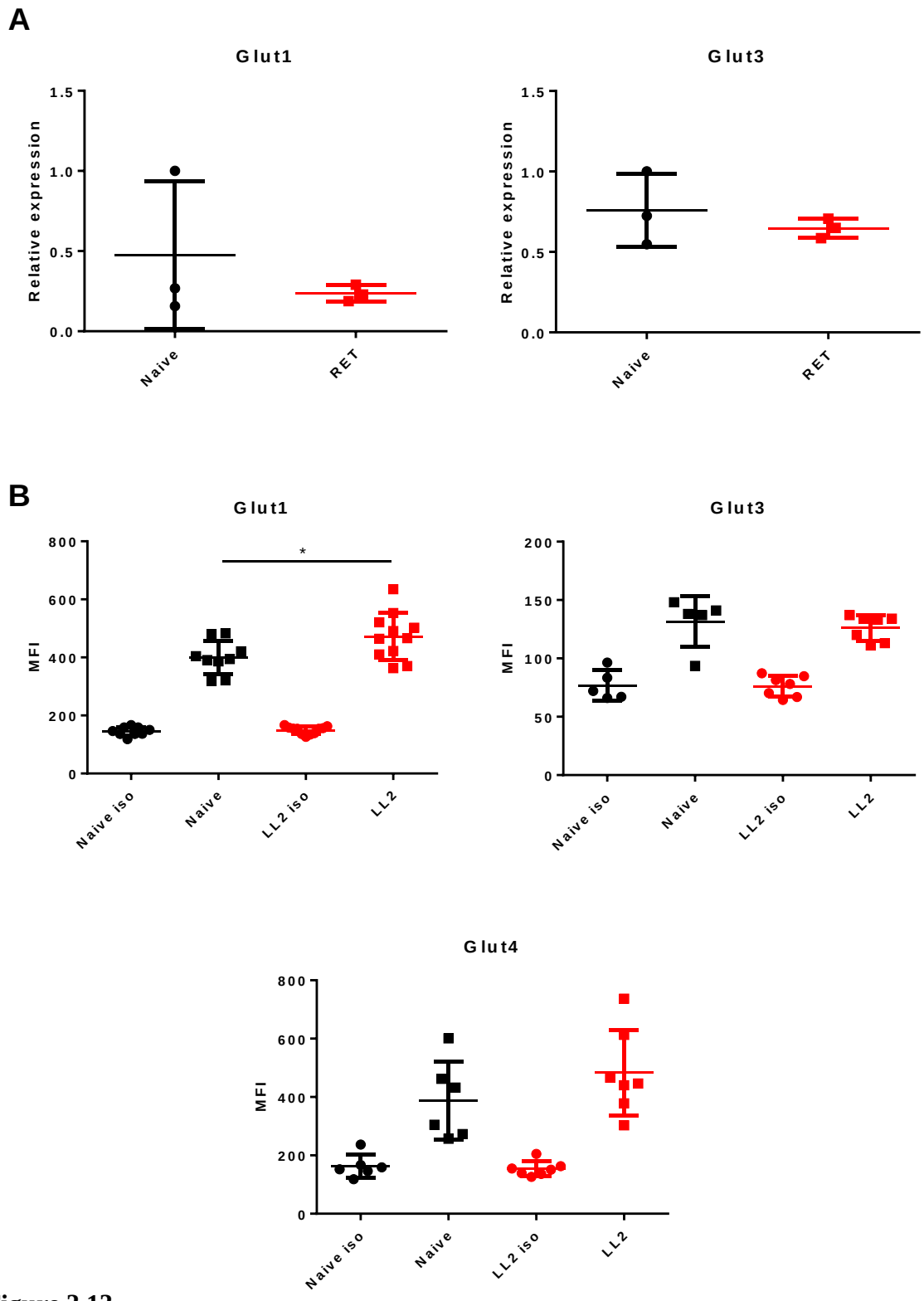
A
Glut1
Relative expression
1.5
1.0
0.5
0.0
Naive
RET
Glut3
Relative expression
1.5
1.0
0.5
0.0
Naive
RET
B
Glut1
MFI
800
600
400
200
0
*
Naive iso
Naive
LL2 iso
LL2
Glut3
MFI
200
150
100
50
0
Naive iso
Naive
LL2 iso
LL2
Glut4
MFI
800
600
400
200
0
Naive iso
Naive
LL2 iso
LL2

Figure 3.13

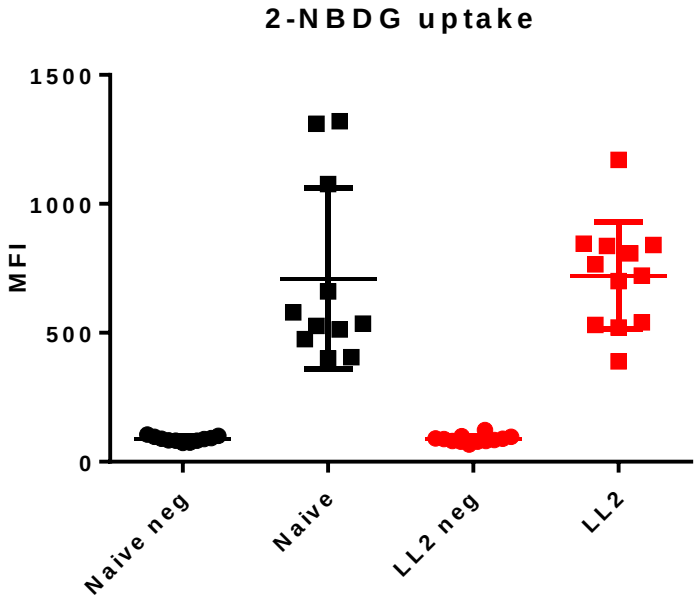

Figure 3.14

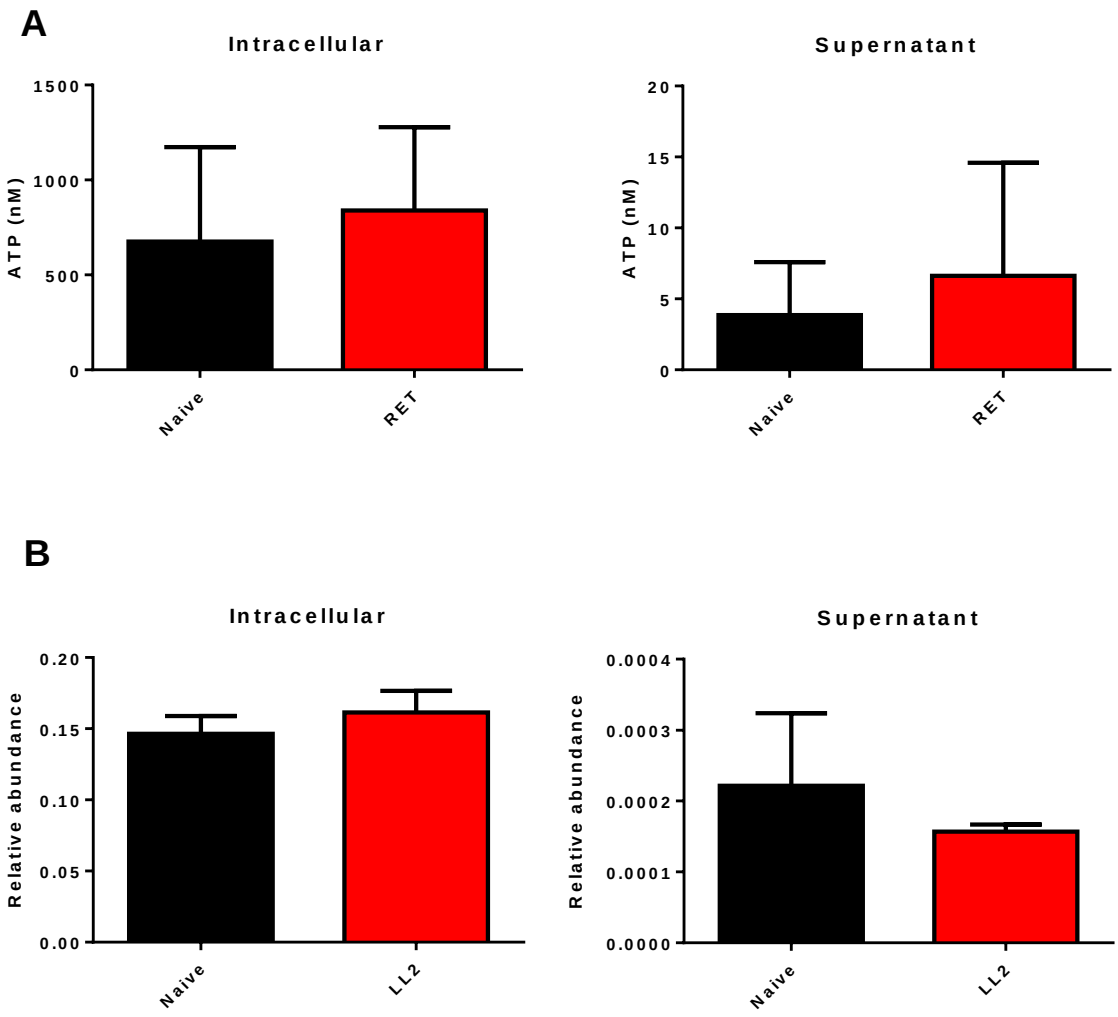
A
Intracellular
ATP (nM)
1500
1000
500
0
Naive
RET
Supernatant
ATP (nM)
20
15
10
5
0
Naive
RET
B
Intracellular
Relative abundance
0.20
0.15
0.10
0.05
0.00
Naive
LL2
Supernatant
Relative abundance
0.0004
0.0003
0.0002
0.0001
0.0000
Naive
LL2

Figure 3.15

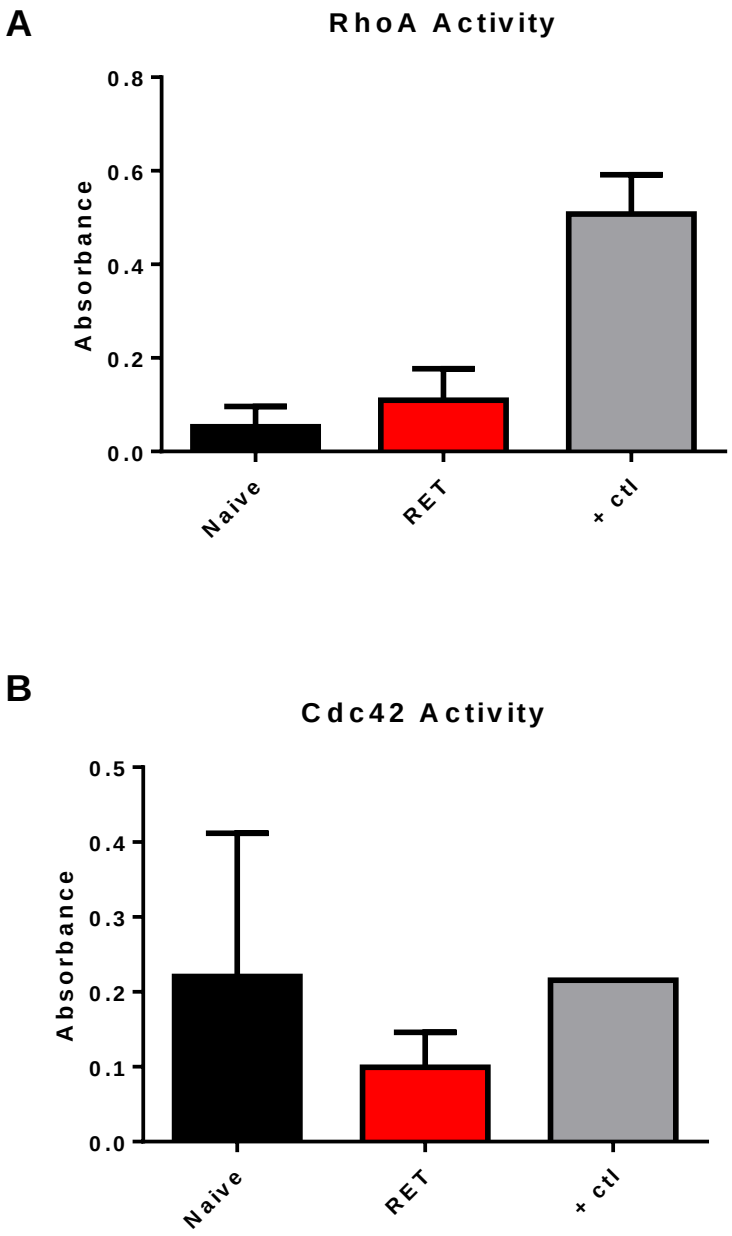
A
RhoA Activity
Absorbance
0.8
0.6
0.4
0.2
0.0
Naive
RET
+ ctl
B
Cdc42 Activity
Absorbance
0.5
0.4
0.3
0.2
0.1
0.0
Naive
RET
+ ctl

Figure 3.16

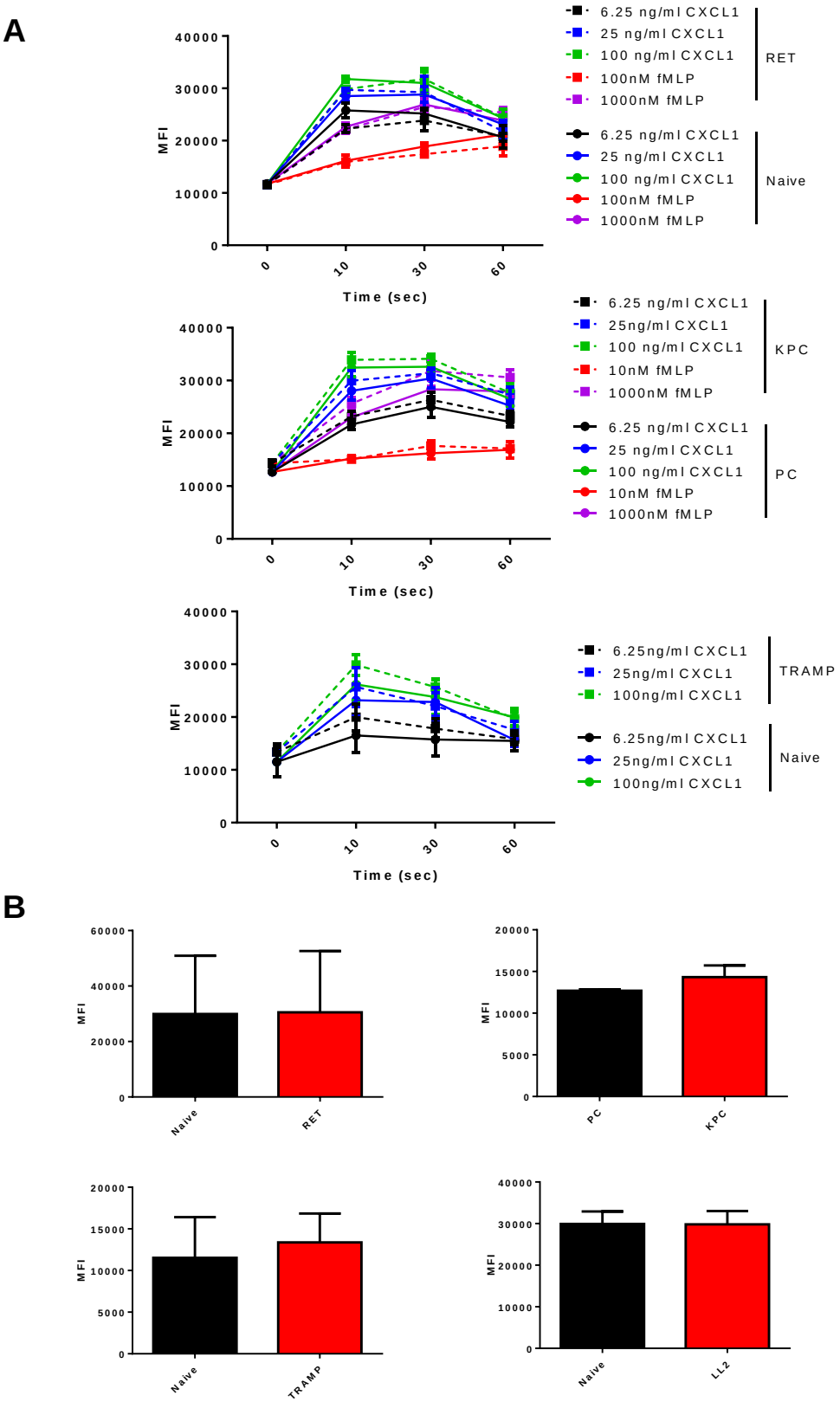
A
MFI
Time (sec)
6.25 ng/ml CXCL1
25 ng/ml CXCL1
100 ng/ml CXCL1
100nM fMLP
1000nM fMLP
RET
Naive
6.25 ng/ml CXCL1
25ng/ml CXCL1
100 ng/ml CXCL1
10nM fMLP
1000nM fMLP
KPC
6.25 ng/ml CXCL1
25 ng/ml CXCL1
100 ng/ml CXCL1
10nM fMLP
1000nM fMLP
PC
6.25ng/ml CXCL1
25ng/ml CXCL1
100ng/ml CXCL1
TRAMP
Naive
B
MFI
Naive
RET
PC
KPC
TRAMP
LL2

Figure 3.17

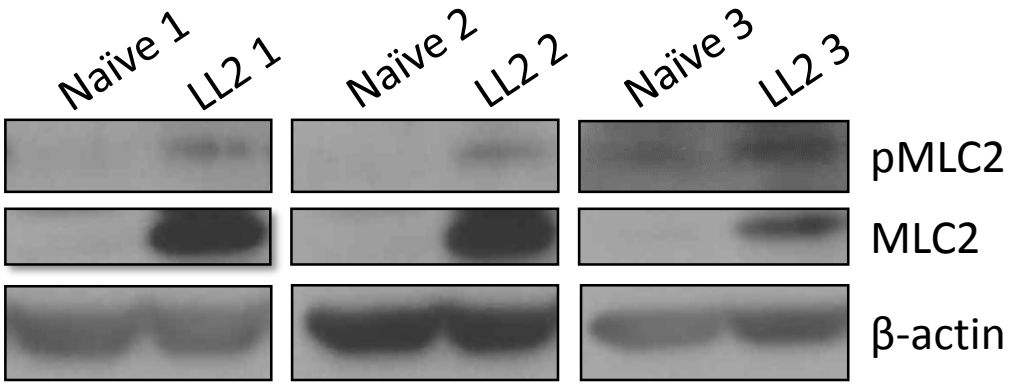

Figure 3.18

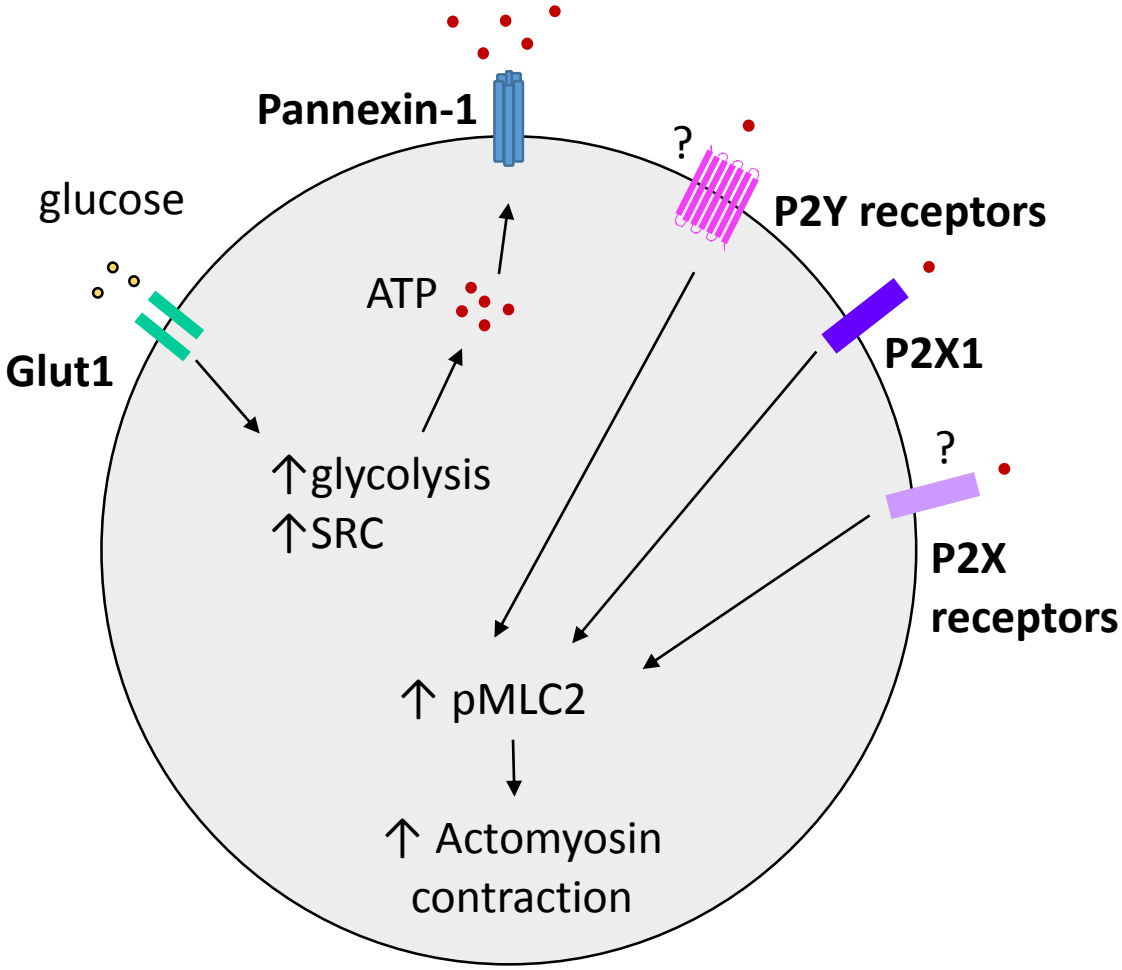
Pannexin-1
?
P2Y receptors
glucose
ATP
Glut1
P2X1
?
↑glycolysis
↑SRC
P2X
receptors
↑ pMLC2
↑ Actomyosin
contraction

Figure 3.19

Figure legends

Figure 3.1 PMN-MDSC-like cells from an orthotopic model in the early stage of tumor development are weakly immunosuppressive. Naïve PMN and PMN-MDSC from mice sacrificed one week after intravenous injection of LL2 cells were co-cultured with PMEL splenocytes and gp100 for 48h and spiked with ^{3}H-thymidine for 8h to measure T-cell proliferation (N=6). Control wells were plated with only PMEL splenocytes +/- gp100. Data are represented as counts per million (CPM) and the dashed line indicates the proliferation of the positive control.

Figure 3.2 PMN-MDSC-like cells from an orthotopic model in the early stage of tumor development spontaneously migrate more than PMN. (A) PMN-MSDC were isolated from the bone marrow of mice sacrificed one week after intravenous injection of LL2 cells. Total number of PMN and PMN-MDSC that migrated in transwell assay for 1h, 37°C, 5% CO_2 with varying doses of CXCL1 and fMLP. (B) Fold change in response to CXCL1 and fMLP. (C) Total number of cells that spontaneously migrate (Naïve N=5, LL2=7).

Figure 3.3 RET PMN-MDSC-like cells spontaneously migrate more than PMN. (A) Total number of PMN and PMN-MDSC that migrated in transwell assay for 1h, 37°C, 5% CO_2 with varying doses of CXCL1 and fMLP. (B) Fold change in response to CXCL1 and fMLP. (C) Total number of cells that spontaneously migrate (N=5). (D) Cell surface expression of CXCR1 and CXCR2 (N=5).

Figure 3.4 KPC PMN-MDSC-like cells spontaneously migrate more than PMN. (A) Total number of PMN and PMN-MDSC that migrated in transwell assay for 1h, 37°C, 5% CO_2 with varying doses of CXCL1 and fMLP. (B) Fold change in response to CXCL1 and fMLP. (C) Total number of cells that spontaneously migrate (N=7). (D) Cell surface expression of CXCR1 and CXCR2 (N=6).

Figure 3.5 TRAMP PMN-MDSC-like cells spontaneously migrate more than PMN. (A) Total number of PMN and PMN-MDSC that migrated in transwell assay for 1h, 37°C, 5% CO_2 with varying doses of CXCL1 and fMLP. (B) Fold change in response to CXCL1 and fMLP. (C) Total number of cells that spontaneously migrate (Naïve N=3, TRAMP N=5). (D) Cell surface expression of CXCR1 and CXCR2 (Naïve N=2, TRAMP N=4).

Figure 3.6 PMN-MDSC from transplantable models or from an orthotopic model in the late stage of tumor development do not spontaneously migrate more than PMN. Total number of PMN-MDSC from (A) EL4 tumor-bearing mice, (B) LLC tumor-bearing mice, (C) CT26 tumor-bearing mice, and (D) from mice sacrificed three weeks after intravenous injection of LL2 cells and naïve PMN were spontaneously migrated in a transwell assay for 1h, 37°C. For transplantable models, mice were sacrificed when the tumor diameter reached between 1.5-2.0cm.

Figure 3.7 Characteristics of PMN-MDSC-L spontaneous migration. (A) Trajectories of individual PMN and RET PMN-MDSC-L were plotted with the starting point transposed to the origin. The (B) mean squared displacement, (C) speed, (D) persistence time, and (E) random motility coefficient were calculated from at least 80 cells.

Figure 3.8 Extracellular ATP is required for PMN-MDSC-L spontaneous migration. PMN-MDSC-L from (A) RET mice (N=5) and (B) mice sacrificed one week after intravenous injection of LL2 cells (N=4) and naïve PMN were pre-treated with 100μM ^{10}Panx (panx) or scrambled ^{10}Panx (scr) prior to migration in a transwell assay for 1h, 37°C, 5% CO_2. (C) PMN-MDSC-L (N=10) from mice sacrificed one week after intravenous injection of LL2 cells and naïve PMN (N=8) were pretreated with 10units/ml apyrase prior to migration in a transwell assay for 1h, 37°C, 5% CO_2.

Figure 3.9 PMN-MDSC-L utilize the P2X1 receptor to spontaneously migrate. PMN-MDSC-L from mice sacrificed one week after intravenous injection of LL2 cells and naïve PMN were pre-treated with (A) 10μM suramin (pan-P2R inhibitor) (Naïve N=6, LL2 N=7), (B) NF449 (P2X1-specific inhibitor) (Naïve N=7, LL2 N=8), or (C) various doses of MRS 1191 (A3R inhibitor) (N=5) prior to migration in a transwell assay for 1h, 37°C, 5% CO_2.

Figure 3.10 PMN-MSDC-L from transgenic mice or from an orthotopic model in the early stage of tumor development have increased metabolic rates compared to PMN. PMN-MDSC-L from RET mice and mice sacrificed one week after intravenous injection of LL2 cells and naïve mice were analyzed on a Seahorse XF Analyzer. The (A) glycolytic rate and (B) oxidative phosphorylation rates were determined. (C) The changes in oxidative phosphorylation rates upon treatment with mitochondrial inhibitors A, 5μM oligomycin, B, 1μM FCCP, and C, a combination of 0.75μM Rotenone and 1μM Antimycin A were measured, and the (D) spare respiratory capacity was determined (N=3).

Figure 3.11 PMN-MDSC from an orthotopic model in the late stage of tumor development do not have altered metabolic rates compared to PMN. PMN-MDSC from mice sacrificed three weeks after intravenous injection of LL2 cells and naïve mice were analyzed on a Seahorse XF Analyzer. The (A) glycolytic rate and (B) oxidative phosphorylation rates were determined. (C) The changes in oxidative phosphorylation rates upon treatment with mitochondrial inhibitors A, 5μM oligomycin, B, 1μM FCCP, and C, a combination of 0.75μM Rotenone and 1μM Antimycin A were measured, and the (D) spare respiratory capacity was determined (N=3).

Figure 3.12 PMN-MDSC-L do not exhibit transcriptional changes HIF-1α or enzymes in the glycolytic pathway. Real-time quantitative PCR was conducted on naïve PMN and RET PMN-MDSC-L to investigate expression of proteins involved in glycolysis Gene expression was normalized to β-actin (N=3).

Figure 3.13 PMN-MDSC-L have increased cell surface expression of Glut1. (A) Real-time quantitative PCR was conducted on naïve PMN and RET PMN-MDSC-L to investigate Glut1 and Glut3 gene expression (N=3). (B) The cell surface expression of Glut1 (Naïve N=9, LL2 N=11), Glut3 (Naïve N=5, LL2 N= 7), and Glut4 (Naïve N=6, LL2 N=7) on naïve PMN and PMN-MDSC-L from mice sacrificed one week after intravenous injection of LL2 cells was determined.

Figure 3.14 PMN-MDSC-L do not increase glucose uptake. Naïve PMN (N=11) and PMN-MDSC-L (N=12) from mice sacrificed one week after intravenous injection of LL2

cells were incubated with 250μM 2-NBDG for 1h at 37°C, 5% CO_2, after which glucose uptake was determined by flow cytometry.

Figure 3.15 PMN-MDSC-L do not increase total ATP production. (A) Intracellular ATP levels (left) and levels of ATP released into the supernatant of naïve PMN and RET PMN-MDSC-L cultured for 1h, 37°C, 5% CO_2 (right), were determined using a luciferase-based assay (N=7). (B) Intracellular ATP levels of naïve PMN and PMN-MDSC-L from mice sacrificed one week after intravenous injection of LL2 cells treated with 100μM ^{10}Panx (left) and levels of ATP released into the supernatant of cells cultured with 100μM ARL 67156 for 1h, 37°C, 5% CO_2 (right), were determined by LC-MS/MS analysis (N=3).

Figure 3.16 PMN-MDSC-L do not have increased GTPase activation. The activation of (A) RhoA (N=4) and (B) Cdc42 (N=2) in naïve PMN and RET PMN-MDSC-L were determined by G-LISA.

Figure 3.17 PMN-MDSC-L do not have increased F-actin levels. (A) The amount of polymerized F-actin in naïve PMN and RET (top, N=3), KPC (middle, PC N=3, KPC N=4), and TRAMP (bottom, Naïve N=3, TRAMP N=5) PMN-MDSC-L was measured in response to stimulation with various doses of CXCL1 and fMLP by phalloidin and flow cytometry. (B) The unstimulated levels of F-actin from the experiments in (A) and from naïve PMN and PMN-MDSC-L from mice sacrificed one week after intravenous injection of LL2 cells were determined (N=4).

Figure 3.18 PMN-MDSC-L have increased levels of pMLC2. Naïve PMN and PMN-MDSC-L from mice sacrificed one week after intravenous injection of LL2 cells were

isolated and immediately snap frozen. The levels of pMLC2, total MLC2 and β-actin were determined by western blot analysis (N=3).

Figure 3.19 Model of PMN-MDSC-L spontaneous migration. PMN-MDSC-L increase the expression of the Glut1 glucose transporter on the cell surface and have an increased glycolytic rate and spare respiratory capacity (SRC). PMN-MDSC-L rely on pannexin-1 hemichannel-mediated release of ATP to spontaneously migrate. Autocrine ATP signaling occurs at least partially through the P2X1 purinergic receptor, suggesting a role for other P2Y or P2X receptors in this process. Finally, PMN-MDSC-L increase phosphorylation of MLC2 at Ser19 (pMLC2) to drive actomyosin contraction and motility.

Methods

Transgenic mouse models. WT C57BL/6 or Balb/c female 6-8 week old mice were obtained from the National Cancer Institute or Charles River Laboratory. TRAMP transgenic and age-matched control mice were provided by Dr. Lucia Languino, Thomas Jefferson University. KPC and PC mice were provided by Dr. Robert Vonderheide, University of Pennsylvania. RET mice were obtained from Dr. Viktor Umansky, German Cancer Research Center, and the colony maintained in-house.

Transplantable and orthotopic mouse models. EL4 lymphoma, Lewis lung carcinoma (LLC), and CT26 colon carcinoma cells were obtained from ATCC. LL2 cells were obtained from Moffitt Cancer Center. For transplantable models, $0.5x10^6$ tumor cells were injected in 100µl PBS subcutaneously in the flank of mice. For the orthotopic model, $0.1x10^6$ LL2 cells were injected in 100µl PBS intravenously through the tail vein. Tumors developed three weeks.

Murine bone marrow, PMN, and PMN-MDSC isolation. The muscle and connective tissue was removed from the femurs and tibia of euthanized mice. Bone marrow was flushed from the bones with PBS using a 25-gauge needle (Fisher Scientific, Cat#: 14-826AA), and red blood cells were lysed using Ammonium-Chloride-Potassium (ACK) lysing buffer. Cells were filtered through 70µm cell strainer (Fisher Scientific, Cat#: 087712) and resuspended in MACS buffer (0.5% heat-inactivated FBS and 2mM EDTA in PBS, filtered) for further use. PMN were isolated from the bone marrow of naïve mice and PMN-MDSC were isolated from the bone marrow of tumor-bearing mice: Bone marrow cells were incubated with $Ly6G^+$-biotin beads (Miltenyi Biotec, Cat#: 130-101-

884), anti-streptavidin beads (Miltenyi Biotec, Cat#: 130-048-101), and isolated following the manufacturer's protocol.

Transwell assays for migration and chemotaxis. Unstimulated migration and chemotaxis was measured using a 3μm pore transwell system (Neuro Probe Inc, Cat#: 101-3 or Sigma-Aldrich, Cat#: CLS3415). Advanced RPMI with CXCL1 (BioLegend, Cat#: 573702) or fMLP (Sigma-Aldrich, Cat#: F3506) was placed in the bottom of the transwell, as indicated. Cells were incubated with pannexin inhibitor (^{10}Panx; Tocris, Cat#: 3348), scrambled ^{10}Panx (Tocris, Cat#: 3708), pan-P2XR inhibitor suramin (R&D Systems, Cat#: 1472), P2X1 inhibitor NF 449 (Tocris, Cat#: 1391), A3R inhibitor MRS 1191 (Santa Cruz, Cat#: sc-253056), ectonucelotidase inhibitor ARL 67156 (Sigma-Aldrich, Cat#: A265), or apyrase (New England Biolabs, Cat#: M0398L) in Advanced RPMI for 10min prior to being plated on top of the filter, $0.1x10^6$ or $0.5x10^6$ cells for the Neuro Probe system or Sigma-Aldrich system, respectively, and placed at 37°C, 5% CO_2 for 1 hour. Cells that migrated through the transwell were counted by hemocytometer.

Chemokine receptor and glucose transporter measurement. Total bone marrow cells were stained with LIVE/DEAD Fixable Aqua Dead cell stain (AQUA; Thermo Fisher, Cat#: L34966), CD11b-BV421 (BioLegend, Cat#: 101236), Ly6G-APC (Becton-Dickinson, Cat#: 560599), and CXCR1-PE (R&D Systems, Cat#:FAB8628P), CXCR2-PE (R&D Systems, Cat#: FAB2164P), Glut1 (Novus Biologicals, Cat#: NB110-39113), Glut3 (Abcam, Cat#: ab136180), or Glut4 (Novus Biologicals, Cat#: NBP1-49533), washed in PBS, run on a flow cytometer (LSR II 14-color, Becton-Dickinson), and analyzed using FlowJo.

T-cell suppression assay. PMN and PMN-MDSC were co-cultured with splenocytes from transgenic PMEL mice at the indicated dilutions and T-cells were stimulated to proliferate using PMEL-specific peptide gp100 for 48 hours. Cells were pulsed with ^{3}H-Thymidine (PerkinElmer, 1μCi/well) for 8 hours, and ^{3}H-Thymidine uptake was measured using a liquid scintillation counter and expressed as counts per million (CPM).

Live-cell imaging. The wells of a 6-well plate were coated with 50μg/ml fibronectin (Sigma-Aldrich, Cat#: F1141) and washed with PBS. 0.5 x 10^6 cells were plated per well in Advanced RPMI (Thermo Fisher, Cat#: 12633-012) and placed in a 37°C, 5% CO_2 incubator for 15 minutes to allow the cells to attach. The wells were gently washed with PBS one time to remove non-adherent cells and Advanced RPMI was added to the wells. Cells were placed onto a motorized stage and observed using a Nikon Eclipse TE_{300} fluorescence microscope maintained in an environment of 37°C and 5% CO_2. Images were captured every 30 seconds over the course of 15 minutes from at least four different fields.

Measurement of cell trajectories and mean-squared displacements. Cell movement was tracked using the ImageJ plugin Manual Tracking. ImageJ and the plugin are both freely available through the NIH website (http://rsbweb.nih.gov/ij/). The centroid of the cell was considered to represent the cell position. Time lapse microscopy was used and images were taken every 30 seconds over a total of 15 minutes. The result was a series of (x,y) positions with time for each cell. The net displacement during the *i*th 30 second increment, D_i, was calculated as the difference of the position from the beginning to the end of that time step. The mean-squared displacement, $\langle D^2(t) \rangle$, over time was calculated using the method of non-overlapping intervals (Dickinson & Tranquillo, 1993). Speed, S,

can be considered as the total path length over time and persistence time, P, is the time a cell remains moving without changing direction. S and P were obtained by fitting these to the persistent random walk equation $\langle D^2(t)\rangle = 2S^2\left[t - P\left(1 - e^{-t/P}\right)\right]$ where *t* is the time interval, using a non-linear least squares regression analysis (Dunn, 1983). The random motility coefficient (μ) is then calculated as $\mu = \frac{1}{2}S^2P$ (Ford & Lauffenburger, 1991).

Seahorse assay. Metabolic rates were determined using the Seahorse XF24 and XF96 Flux Analyzers (Seahorse Biosciences) following the manufacturer's protocol. Briefly, the microplate was coated with 22.4μg/ml Cell-Tak (Fisher, Cat#: 354240) using 200mM sodium bicarbonate. $1.2x10^6$ or $0.4x10^6$ cells were seeded per well immediately after isolation in 50μl and 80μl of unbuffered RPMI (Sigma-Aldrich, Cat#: R1383) for the XF24 and XF96 analyzers, respectively. The plate was incubated for 30min at 37°C to allow the cells to settle into a monolayer. Unbuffered RPMI was gently added to the wells without disturbing the monolayer to bring the assay volume to 675μl and 180μl for the XF24 and XF96 analyzer, respectively. The basal oxygen consumption rate (OCR) and extracellular acidification rate (ECAR) was measured, in addition to rate changes upon treatment with 5μM oligomycin (Sigma-Aldrich, Cat#: 75351), 1μM FCCP (Sigma-Aldrich, Cat#: C2920), and 0.75μM Rotenone and 1μM Antimycin A (Sigma-Aldrich, Cat#: R8875 and A8674, respectively).

Real-time quantitative PCR. Cells were lysed and RNA was isolated using the E.Z.N.A. total RNA purification kit (Omega Bio-Tek, Cat#: R6834-02). Reverse transcription was performed using the High Capacity cDNA Reverse Transcription Kit (Applied Biosystems

Inc. #4368813). Quantitative PCR was then performed using Sybr Green PCR Master Mix (Applied Biosystems Inc. #4368706) on an ABI 7500 Fast instrument, using the following primers:

Glut1	Fwd: AGCCCTGCTACAGTGTAT
	Rev: AGGTCTCGGGTCACATC
Glut3	Fwd: ATGGGGACAACGAAGGTGAC
	Rev: CAGGTGCATTGATGACTCCAG
HIF1α	Fwd: TCTCGGCGAAGCAAAGAGTC
	Rev: AGCCATCTAGGGCTTTCAGATAA
Hexokinase	Fwd: ATGATCGCCTGCTTATTCACG
	Rev: CGCCTAGAAATCTCCAGAAGGG
Phosphofructokinase	Fwd: CATCGCCGTGTTGACCTCT
	Rev: CCCGTGAAGATACCAACTCGG
GAPDH	Fwd: CCCTTAAGAGGGATGCTGCC
	Rev: ACTGTGCCGTTGAATTTGCC
Phosphoglycerate kinase	Fwd: CCCAGAAGTCGAGAATGCCTG
	Rev: CTCGGTGTGCAGTCCCAAA
Enolase	Fwd: AGTACGGGAAGGACGCCACCA
	Rev: GCGGCCACATCCATGCCGAT

Pyruvate kinase	Fwd: GCCGCCTGGACATTGACTC
	Rev: CCATGAGAGAAATTCAGCCGAG
β-actin	Fwd: CCTTCTTGGGTATGGAATCCTGT
	Rev: GGCATAGAGGTCTTTACGGATGT

Glucose uptake assay. PMN and PMN-MDSC ($1x10^6$ cells) were stained with AQUA, washed in PBS, and cultured in MACS buffer with 250μM 2-(*N*-(7-Nitrobenz-2-oxa-1,3-diazol-4-yl)Amino)-2-Deoxyglucose (2-NBDG; Thermo Fisher, Cat#: N13195) for 1 hour at 37°C, 5% CO_2. Cells were washed in PBS and fixed with 4% paraformaldehyde in PBS before flow cytometry and FlowJo analysis.

ATP measurement. The total pool of intracellular ATP and the levels of ATP released into the supernatant of cultured cells ($1x10^6$ cells/ml, 1h, 37°C) was measured by ATP Determination Kit (Thermo Fisher, Cat#: A22066) following the manufacturer's protocol. Intracellular ATP was measured by centrifuging the cells at 1500rpm, 5min, removing the supernatant and permeabilizing the cells in 1% TritonX-100 in PBS, supplemented with protease inhibitors. A second approach to measuring ATP levels utilized LC-MS/MS. In this method, cells were incubated in the presence of ^{10}Panx to measure levels of intracellular ATP, and cells were incubated in the presence of ARL 67156 to measure levels of ATP released into the supernatant of cultured cells. Nucleotides were extracted from the supernatant and cell pellet as described (Kochanowski et al., 2006). Briefly, nucleotides were precipitated from the supernatant and cell pellet using 1M and 0.5M perchloric acid, respectively. The supernatants containing ATP were neutralized with 2.5M potassium

hydroxide in 1.5M potassium phosphate, centrifuged to remove the potassium perchlorate precipitate, filtered, and stored at -80°C before analysis. LC-MS/MS analysis was carried out using a Q-trap5500 coupled to a Shimadzu UHPLC system by the Wistar Institute Proteomics and Metabolomics Core Facility. Metabolites were normalized to heavy internal standards added to the samples and peak identification was confirmed by injecting a solution of pure ATP.

GTPase activation assay. RhoA and Cdc42 activity was determined using G-LISA™ activation Assay Kits (Cytoskeleton Inc., Cat#: BK124 and BK127, respectively) following the manufacturer's protocol. Briefly, samples were added to the wells of a G-LISA plate coated with Rho/Cdc42-GTP-binding protein. The plate was washed and incubated with anti-RhoA/Cdc42 primary antibody, incubated with HRP-conjugated secondary antibody and detected by a microplate spectrophotometer reader at 490nm.

F-actin measurement. Total bone marrow cells were stained with AQUA, CD11b-BV421, and Ly6G-APC. Cells were washed and stimulated with doses of CXCL1 and fMLP in Advanced RPMI for the time points indicated. Cells were immediately fixed and permeabilized using Cytofix/Cytoperm Solution (Becton-Dickinson, Cat#: 554722) and washed in Perm/Wash Buffer (Becton-Dickinson, Cat#: 554723) following the manufacturer's protocol. Cells were stained with 1 unit of Phalloidin-AF488 (Thermo Fisher, Cat#: A12379) for 20min at 4°C, washed in Perm/Wash Buffer, run on a flow cytometer, and analyzed using FlowJo.

Western blot. Cells were lysed in RIPA buffer (Sigma-Aldrich, Cat#: R0278) supplemented with protease inhibitors (Sigma-Aldrich, Cat#: P8340), phosphatase inhibitors (Sigma-Aldrich, Cat#: P5726 and P0044) and 1mM PMSF, and cleared by centrifugation. Protein concentration was determined by Bio-Rad Protein Assay Dye Reagent (Bio-Rad, Cat#: 500-0006) following the manufacturer's protocol. Lysates were diluted in reducing Laemmli buffer (Fisher Scientific, Cat#: NC9566545), denatured at 95°C, run on 12% polyacrylamide gels, transferred to PVDF membrane, blocked in 5% milk, and incubated with primary antibodies for pMLC2, MLC2, and β-actin (Cell Signaling Cat#: 3671S, 3672S, and 5125S, respectively) at 4°C, overnight. Immunoreactive bands were developed using horseradish peroxidase-conjugated secondary antibodies (Santa Cruz, Cat#: SC-2301) and enhanced chemiluminescent substrate (Thermo Scientific, Cat#: 32209, or GE Healthcare, Cat#: RPN2232).

Statistics. Unless otherwise indicated, data are presented as mean ± SEM. An unpaired, 2-tailed t-test was used to determine significance, and *p* values less than 0.05 were considered significant (*$p<0.05$, **$p<0.01$, ***$p<0.001$, ****$p<0.0001$). All modeling and analysis was performed using Graphpad Prism v 6.07.

CHAPTER 4: DISCUSSION AND FUTURE DIRECTIONS

Discussion

In the preceding chapter, we have demonstrated that MDSC-like cells, PMN-MDSC-L, develop in the early stages of tumor development and exhibit an enhanced ability to spontaneously migrate. We have characterized this altered migratory behavior and identified a mechanism by which PMN-MDSC-L are able to spontaneously migrate. Moreover, we have demonstrated that PMN-MDSC-L undergo metabolic reprogramming. These findings further our understanding of MDSC-like cells and MDSC development. The remainder of this chapter discusses the implications of these findings and provides ideas to expand on these observations.

Identification of characteristics of PMN-MDSC-L in cancer

We began our studies by demonstrating that PMN-MDSC-L are characterized by poor immunosuppressive capability and an enhanced ability to spontaneously migrate in the context of cancer. We found that while PMN and PMN-MDSC-L are both equally able to respond to stimulation with CXCL1 or fMLP, PMN-MDSC-L spontaneously migrated 2-3 fold times more than PMN. We have shown that PMN-MDSC-L motility is characterized by increased speed, persistence time, mean squared displacement and an overall increased random motility coefficient compared to PMN. Collectively, these findings demonstrate that PMN-MDSC-L are predisposed to random walk.

Significantly, we have shown that PMN-MDSC-L develop in the early stages of tumor development and in transgenic mouse models, but not in transplantable models or in

the late stages of tumor development. We believe that because transplantable models force a highly inflammatory environment in a short amount of time, we may quickly bypass the stage where we are able to capture PMN-MDSC-L. In comparison, transgenic models, which also generate an inflammatory environment, develop tumors relatively slowly, allowing us to capture this distinct cell population.

Mechanism of PMN and PMN-MDSC-L spontaneous migration

To investigate the mechanism by which PMN-MDSC-L spontaneously migrate, we focused on studies investigating neutrophil chemotaxis. Several studies have shown that upon engagement of the FPR, ATP can be released via pannexin-1 hemichannels to act in an autocrine fashion by engaging purinergic receptors such as P2X1, P2Y2, and A3 (Chen et al., 2006; Lecut et al., 2009). Moreover, autocrine purinergic signaling has been shown to be important in other immune cells suggesting this may be a pervasive phenomenon. For example, pannexin-1 hemichannel-mediated ATP release and signaling through P2X1 and P2X4 has also been shown to be important for T-cell activation at the immune synapse (Woehrle et al., 2010). We found that PMN-MDSC-L spontaneous migration is dependent upon pannexin-1 hemichannel-mediated ATP release and, at least partially, on P2X1-mediated signaling. However, though reported to be important for murine neutrophil chemotaxis, we did not find a role for A3 in PMN-MDSC-L spontaneous migration (Chen et al., 2006).

These studies identified some distinct characteristics by which PMN and PMN-MDSC-L spontaneously migrate. First, our data clearly show that the ability of naïve PMN to spontaneously migrate is significantly affected by apyrase treatment, but not affected by

pannexin-1 hemichannel inhibition. This suggests that PMN use a different mechanism to release ATP. In fact, a study had demonstrated that murine PMN can utilize connexin hemichannels to release ATP (Eltzschig et al., 2006). Second, we have observed that PMN spontaneous migration is unaffected by pan-P2R or P2X1 inhibition. This suggests that while PMN also rely on extracellular ATP to spontaneously migrate, they must utilize a different set of purinergic receptors for this function.

Stimulation of P2X1 with nonhydrolyzable ATP has been shown to selectively activate RhoA in both human and mouse neutrophils, resulting in phosphorylation of MLC2 (Lecut et al., 2009). Moreover, studies in mouse neutrophils have shown that fMLP-induced chemotaxis depends on Cdc42-mediated activation of mixed lineage kinase 3 (Polesskaya et al., 2014). However, our studies have shown that PMN-MDSC-L and PMN have similar levels of RhoA and Cdc42 activation. Interestingly, we found that PMN-MDSC-L express more total MLC2 and have increased levels of pMLC2. This suggests that 1) PMN-MDSC-L are fundamentally different than PMN, and 2) that an alternative signaling pathway downstream of P2X1 activation can result in pMLC2. Moreover, we found similar levels of F-actin in PMN and PMN-MDSC-L suggesting that PMN may be equivalently primed to spontaneously migrate, but activation of alternative signaling pathways that lead to pMLC2 in PMN-MDSC-L ultimately results in spontaneous migration. We speculate on a potential intracellular signaling connection between P2X1 and pMLC2 in the next section.

Metabolic reprogramming of PMN-MDSC-L

Several immune cells have been shown to alter their metabolism to support their function. For example, tumor-associated macrophages and tumor-associated dendritic cells both undergo metabolic changes due to the tumor microenvironment that enhance their pro-tumoral effects. Additionally, compared to effector T cells, memory T-cells undergo metabolic changes to sustain their longevity (V. Kumar et al., 2016; Pearce & Pearce, 2013). Similarly, in *in vitro* differentiated MDSC, increases in glycolysis correlated with increases in ARG1 expression (Hammami et al., 2012). In an *in vivo* study, compared to splenic MDSC, tumor-infiltrating MDSC were shown to switch to a metabolic pathway that preferred FAO and increased flux through oxidative phosphorylation (Hossain et al., 2015). Increased flux though the electron transport chain would result in the generation of ROS, supporting the immunosuppressive function of tumor-infiltrating MDSC (Yuanbin Liu, Fiskum, & Schubert, 2002). However, we found that PMN-MDSC-L have an increased basal glycolytic rate compared to naïve PMN, though we did observe an increase in oxidative phosphorylation in one of our models. We propose that increased flux through the glycolytic pathway would quickly generate ATP to support the rapid and dynamic process of spontaneous cell migration.

We found that the metabolic profile of PMN-MDSC from the bone marrow of mice sacrificed three weeks after intravenous injection of LL2 cells was similar to the metabolic profile of naïve PMN. These results are in contrast to the observations of Hossain, et al that showed that tumor-infiltrating MDSC utilize FAO. However, it is important to note that Hossain et al. investigated the metabolic profile of the total MDSC population, not

specifically of PMN-MDSC. Moreover, we studied the metabolic profile of PMN, PMN-MDSC-L, and PMN-MDSC coming from the bone marrow, not the tumor microenvironment or the spleen, which may account for the differences in our observations.

To investigate what drives the changes in the metabolic rates, we found that there were no differences in the gene expression of HIF-1α, glycolytic enzymes, or the glucose transporters Glut1 and Glut3. This was an interesting finding as HIF-1α has been shown to increase the expression of ARG1 and iNOS to increase the immunosuppressive activity of MDSC, and may explain why the PMN-MDSC-L were not strongly immunosuppressive (Corzo et al., 2010). However, PMN-MDSC-L did increase cell surface expression of the glucose transporter Glut1 compared to PMN. Inconsistent with these results, however, is the observation that PMN-MDSC-L do not increase their glucose uptake. We believe this is due to limitations associated with the probe used to make these measurements. 2-NBDG is a fluorescent analog of glucose, however, upon uptake can be phosphorylated by hexokinase, and degraded to non-fluorescent products (Jung, Ha, Zheng, Chang, & Williams, 2011). We are exploring an alternative approach to investigate this discrepancy, discussed further in the next section.

We also found that PMN-MDSC-L have an increased spare respiratory capacity compared to PMN. This means that means that under stressful conditions, PMN-MDSC-L are able to increase flux through the oxidative phosphorylation pathway to meet energetic demands. However, PMN have been shown to rely primarily on glycolysis as their main method of ATP production (Borregaard & Herlin, 1982). Consistent with this report, previous experiments in our lab using electron microscopy showed that the murine PMN

have only approximately seven mitochondria per cell compared to other mammalian cells which can average between 100-1000 mitochondria per cell (data not shown; (Arthur Kornberg, 2005). Recent studies have demonstrated a metabolic role for mitochondria in PMN chemotaxis. They have shown that in response to FPR engagement, mitochondria generate the first burst of ATP that is released from the cell and that positive feedback through P2Y2 leads to increased mitochondrial activity near the leading edge of a polarized cell (Y. Bao et al., 2015; Y. Bao et al., 2014). The present study provides further evidence that beyond regulating apoptotic mechanisms, mitochondrial metabolism may play a significant role in PMN-MDSC-L function.

In spite of increased metabolic rates, we were unable to confirm that the total pool of ATP was increased in PMN-MDSC-L. However, there are several limitations to these experiments. First, we currently do not know the rate at which ATP is released by pannexin-1 hemichannels. If the number of ATP molecules released is greater than the number produced, the intracellular pool of ATP would appear unchanged compared to levels in PMN. Second, while we inhibited ectonucleotidases to try to measure ATP levels in the supernatant of cultured cells, binding of ATP to purinergic receptors would prevent us from detecting the total pool of ATP that is released. Taken together, these caveats suggest that instead of using endpoint assays to capture a potential buildup of ATP, in order to capture this dynamic process, we must use a kinetic assay, discussed further in the next section.

Significance

In this dissertation, we have shown that enhanced spontaneous migration is only observed in PMN-MDSC-L from transgenic models and mice in the early stages of tumor development, but not in transplantable models or mice in the late stages of tumor development, and that these results are linked to the metabolic profile and immunosuppressive capability of the cells. These observations raise the obvious next question: What is the role of these cells in cancer?

In 1889, Steven Paget proposed the seed-and-soil hypothesis to explain how metastases develop. He proposed that factors secreted during primary tumor progression act systemically at distant secondary sites, modifying the local tissue environment (soil), and recruiting immune cells to further condition these sites for the successful colonization by tumor cells (seed) (Paget, 1989). In 2005, Rosandra Kaplan coined the term "pre-metastatic niche" by showing that $VEGFR1^{+}$ hematopoietic progenitor cells home to specific tissue sites prior to the arrival of tumor cells, and that metastasis development was dependent on these cells (Kaplan et al., 2005). Since this study, several papers have implicated immune cells in the development of the pre-metastatic niche and there are many studies suggesting a role for PMN-MDSC in this process (T. Condamine et al., 2015; Huh et al., 2010; Ichikawa et al., 2011; Kowanetz et al., 2010; Sceneay et al., 2012; Seubert et al., 2015; Q. Yang et al., 2017). It is important to note that these studies all provide evidence of chemoattractant-mediated recruitment of PMN-MDSC to these secondary organs, often the result of signaling induced by the primary tumor. We propose that the enhanced spontaneous migratory, possibly invasive, behavior of PMN-MDSC-L uniquely poises

these cells to aid in the development of the pre-metastatic niche, even in the absence of chemoattractant-mediated recruitment. Because these cells develop under relatively low inflammatory conditions, we predict that they will develop either in the very early stages of tumor development or in patients in remission where few tumor cells evade the effects of therapies. Therefore, they could contribute to the early dissemination and seeding of cancer cells in secondary organs, or facilitate disease recurrence. It is unclear if these cells persist during tumor progression when bona fide PMN-MDSC develop, but are present at such a small percentage of the population that they are overlooked, or if persistent inflammatory signaling forces these cells to develop into bona fide immunosuppressive PMN-MDSC.

Finally, the field of MDSC research has taken off in the past 10 years, with over 2500 articles published, lending significant insight into immunosuppressive mechanisms of MDSC in mice and humans (D. I. Gabrilovich, 2017). However, while we have been able to distinguish PMN from PMN-MDSC using density centrifugation and have recently identified LOX1 as a marker for PMN-MDSC in humans, we have not made any advances in separating murine PMN from PMN-MDSC (Thomas Condamine et al., 2016). Currently, we assume that all the $CD11b^{+}GR1^{+}$ cells in a tumor-bearing mouse are MDSC. Our studies have identified a potential novel stage in the development of PMN-MDSC, one that is characterized by metabolic changes, altered migratory behavior, and weak immunosuppressive ability. These findings may shift our understanding of the PMN-MDSC population in mouse models.

Future Directions

As is the case with any scientific endeavor, these studies have raised more questions than they have answered. We have demonstrated some fundamental differences between naïve PMN, PMN-MDSC-L, PMN-MDSC. To explore our mechanistic insights further, it would be interesting to conduct a screen of the purinergic receptors expressed on the cell surface of these cells, and observe whether their expression changes over the course of tumor progression. Additionally, because pharmacologic inhibitors of purinergic receptors can often target more than one receptor, we could utilize genetic mouse models such as P2X1 or pannexin-1 hemichannel knockout mice to confirm our mechanistic findings. These genetic models may also help uncover any redundant purinergic signaling pathways. Finally, RNA-seq analysis on these three cell types would allow us to explore the transcriptional changes that occur in these cells, lend further insight into the functional changes we have observed, and help us understand the stages of bona fide PMN-MDSC development.

In this study, we have proposed that an alternative signaling pathway downstream of purinergic receptor signaling, one that is independent of RhoA activation, could lead to the phosphorylation of MLC2 and actomyosin contraction. In smooth muscle cells, engagement of purinergic receptors results in an influx of calcium and leads to MLCK-mediated phosphorylation of MLC2 (Kwon, Jung, Cho, Jeong, & Sohn, 2015). Several studies have demonstrated that ROCK and MLCK can phosphorylate Ser19 on MLC2 in various cell types (Aguilar, Tracey, Tsang, McGinnis, & Mitchell, 2011; Amano et al., 1996; Eikemo et al., 2016). In fact, both kinases have been shown to play a role in T-cell

migration (A. Smith, Bracke, Leitinger, Porter, & Hogg, 2003). Moreover, MLCK inhibitors have been shown to impair uropod retraction (Eddy, Pierini, Matsumura, & Maxfield, 2000). However, to our knowledge, while the ability of ROCK to phosphorylate MLC2 has been shown, direct evidence of MLCK-mediated phosphorylation of MLC2 in neutrophils has never been demonstrated (Niggli, 1999). To test if purinergic receptor-mediated calcium influx leads to the activation of MLCK and subsequent phosphorylation of MLC2, we could treat PMN-MDSC-L with the MLCK inhibitor ML-7 to see if this abolishes their ability to spontaneously migrate and confirm if this effect is mediated through phosphorylation of MLC2 by western blot.

Next, because we have shown that Glut1 cell surface expression is increased on PMN-MDSC-L and that this contributes to the metabolic changes in PMN-MDSC-L, we would like to understand more about the regulation of Glut1. Because we did not observe any transcriptional changes in Glut1 expression, we assume that Glut1 cell surface expression is regulated by Glut1 translocation from the cytoplasm to the cell surface. We could investigate this possibility by separating the plasma membrane from intracellular membranes using centrifugation and probe for Glut1 by western blot.

As discussed in the previous section, we could try an alternative approach to measure glucose uptake to confirm that Glut1-mediated increase of glucose uptake is what drives the increases in glycolytic rates that we have observed. To test this, we can culture cells in the presence of heavy-labeled ^{13}C-glucose and use mass spectrometry to measure glucose uptake. This strategy would also give us further insight into the metabolic pathways that were used and metabolites that were generated in PMN compared to PMN-MDSC-L. Additionally, to capture ATP released by the cells, we could utilize the new

fluorescent probe 2-2Zn(II) and microscopy. This probe has a polyethylene glycol linker that facilitates binding of 2-2Zn(II) to the cell surface of living cells, and would allow for real-time fluorescent visualization and quantitation of the amount of ATP that is released by PMN and PMN-MDSC-L (C. Ledderose, Bao, Zhang, & Junger, 2015).

To address our hypothesis that PMN-MDSC-L play a role in the development of the pre-metastatic niche, we need to determine if these cells that are highly motile in two dimensions are capable of invading tissues. To test this hypothesis, we could utilize two approaches. First, we could utilize an *in vitro* approach and evaluate the ability of PMN and PMN-MDSC-L to migrate through Matrigel-coated transwells. Second, we could utilize an *in vivo* approach and evaluate the ability of PMN and PMN-MDSC-L to directly invade tissues. For example, for these experiments, we could intravenously inject a mix of CD45.1 PMN and CD45.2 PMN-MDSC-L into a double positive recipient and evaluate the ability of these cells to invade various tissues by flow cytometry. Alternatively, we could utilize whole body GFP and RFP mice for these purposes, or any strategy that would allow us to differentiate injected PMN and PMN-MDSC-L from the host's PMN. As a next step, we would want to make the connection between extracellular ATP, purinergic receptor signaling and the development of metastases. We could treat a mouse model that is known to generate PMN-MDSC-L and develop metastases with apyrase, suramin, or NF449 and compare the development of metastases to untreated mice. We could then deplete $Ly6G^{+}$ cells to demonstrate the effect on metastasis development is truly dependent upon PMN-MDSC-L and not upon other cells that also utilize extracellular ATP and purinergic receptor signaling.

Finally, we must consider the implications of these findings on patient care. PMN-MDSC-L develop under low inflammatory conditions and can be distinguished from naïve PMN by their enhanced migratory behavior, increased Glut1 expression, and possibly by their purinergic receptor expression. If these findings are recapitulated in humans, screening for these cells and markers in the bone marrow biopsies of patients receiving treatment for leukemias using flow cytometry could serve as a surrogate or confirmatory marker of minimal residual disease, and guide treatment options.

REFERENCES

AACR. (2017). National Cancer Moonshot Initiative. Retrieved from http://www.aacr.org/AboutUs/Pages/national-cancer-moonshot-initiative.aspx#.WIPBpfkrI2w

Achberger, S., Aldrich, W., Tubbs, R., Crabb, J. W., Singh, A. D., & Triozzi, P. L. (2014). Circulating immune cell and microRNA in patients with uveal melanoma developing metastatic disease. *Molecular immunology, 58*(2), 182-186. doi:10.1016/j.molimm.2013.11.018

Adeegbe, D., Serafini, P., Bronte, V., Zoso, A., Ricordi, C., & Inverardi, L. (2011). In Vivo Induction of Myeloid Suppressor Cells and CD4+Foxp3+ T Regulatory Cells Prolongs Skin Allograft Survival in Mice. *Cell Transplantation, 20*(6), 941-954. doi:10.3727/096368910X540621

Aguilar, H. N., Tracey, C. N., Tsang, S. C., McGinnis, J. M., & Mitchell, B. F. (2011). Phos-tag-based analysis of myosin regulatory light chain phosphorylation in human uterine myocytes. *PLoS One, 6*(6), e20903. doi:10.1371/journal.pone.0020903

Amano, M., Ito, M., Kimura, K., Fukata, Y., Chihara, K., Nakano, T., . . . Kaibuchi, K. (1996). Phosphorylation and Activation of Myosin by Rho-associated Kinase (Rho-kinase). *Journal of Biological Chemistry, 271*(34), 20246-20249. doi:10.1074/jbc.271.34.20246

Arthur Kornberg, T. A. B. (2005). *DNA Replication* (Second ed.). Sausalito, California: University Science Books.

Balkwill, F., & Mantovani, A. (2001). Inflammation and cancer: back to Virchow? *The Lancet, 357*(9255), 539-545. doi:http://dx.doi.org/10.1016/S0140-6736(00)04046-0

Bao, L., Locovei, S., & Dahl, G. (2004). Pannexin membrane channels are mechanosensitive conduits for ATP. *FEBS Letters, 572*(1-3), 65-68. doi:10.1016/j.febslet.2004.07.009

Bao, Y., Ledderose, C., Graf, A. F., Brix, B., Birsak, T., Lee, A., . . . Junger, W. G. (2015). mTOR and differential activation of mitochondria orchestrate neutrophil chemotaxis. *The Journal of Cell Biology, 210*(7), 1153-1164. doi:10.1083/jcb.201503066

Bao, Y., Ledderose, C., Seier, T., Graf, A. F., Brix, B., Chong, E., & Junger, W. G. (2014). Mitochondria Regulate Neutrophil Activation by Generating ATP for Autocrine Purinergic Signaling. *The Journal of Biological Chemistry, 289*(39), 26794-26803. doi:10.1074/jbc.M114.572495

Begandt, D., Good, M. E., Keller, A. S., DeLalio, L. J., Rowley, C., Isakson, B. E., & Figueroa, X. F. (2017). Pannexin channel and connexin hemichannel expression in vascular function and inflammation. *BMC Cell Biology, 18*(Suppl 1), 2. doi:10.1186/s12860-016-0119-3

Bellocq, A., Antoine, M., Flahault, A., Philippe, C., Crestani, B., Bernaudin, J. F., . . . Cadranel, J. (1998). Neutrophil alveolitis in bronchioloalveolar carcinoma: induction by tumor-derived interleukin-8 and relation to clinical outcome. *Am J Pathol, 152*(1), 83-92.

Biswas, Subhra K. (2015). Metabolic Reprogramming of Immune Cells in Cancer Progression. *Immunity, 43*(3), 435-449. doi:http://dx.doi.org/10.1016/j.immuni.2015.09.001

Block, J., Breitsprecher, D., Kühn, S., Winterhoff, M., Kage, F., Geffers, R., . . . Rottner, K. (2012). FMNL2 Drives Actin-Based Protrusion and Migration Downstream of Cdc42. *Current Biology, 22*(11), 1005-1012. doi:10.1016/j.cub.2012.03.064

Borregaard, N., & Herlin, T. (1982). Energy Metabolism of Human Neutrophils during Phagocytosis. *Journal of Clinical Investigation, 70*(3), 550-557. Retrieved from http://www.ncbi.nlm.nih.gov/pmc/articles/PMC370256/

Bours, M. J. L., Swennen, E. L. R., Di Virgilio, F., Cronstein, B. N., & Dagnelie, P. C. (2006). Adenosine 5′-triphosphate and adenosine as endogenous signaling molecules in immunity and inflammation. *Pharmacology & Therapeutics, 112*(2), 358-404. doi:http://dx.doi.org/10.1016/j.pharmthera.2005.04.013

Cano, M. L., Lauffenburger, D. A., & Zigmond, S. H. (1991). Kinetic-Analysis of F-Actin Depolymerization in Polymorphonuclear Leukocyte Lysates Indicates That Chemoattractant Stimulation Increases Actin Filament Number without Altering the Filament Length Distribution. *Journal of Cell Biology, 115*(3), 677-687. doi:DOI 10.1083/jcb.115.3.677

Charest, Pascale G., & Firtel, Richard A. (2007). Big roles for small GTPases in the control of directed cell movement. *Biochemical Journal, 401*(Pt 2), 377-390. doi:10.1042/BJ20061432

Chen, Y., Corriden, R., Inoue, Y., Yip, L., Hashiguchi, N., Zinkernagel, A., . . . Junger, W. G. (2006). ATP Release Guides Neutrophil Chemotaxis via P2Y2 and A3 Receptors. *Science, 314*(5806), 1792-1795. doi:10.1126/science.1132559

Chen, Y., Yao, Y., Sumi, Y., Li, A., To, U. K., Elkhal, A., . . . Junger, W. G. (2010). Purinergic Signaling: A Fundamental Mechanism in Neutrophil Activation. *Science signaling, 3*(125), ra45-ra45. doi:10.1126/scisignal.2000549

Condamine, T., Dominguez, G. A., Youn, J.-I., Kossenkov, A. V., Mony, S., Alicea-Torres, K., . . . Gabrilovich, D. I. (2016). Lectin-type oxidized LDL receptor-1 distinguishes population of human polymorphonuclear myeloid-derived suppressor cells in cancer patients. *Science Immunology, 1*(2), aaf8943-aaf8943. doi:10.1126/sciimmunol.aaf8943

Condamine, T., Ramachandran, I., Youn, J. I., & Gabrilovich, D. I. (2015). Regulation of tumor metastasis by myeloid-derived suppressor cells. *Annu Rev Med, 66*, 97-110. doi:10.1146/annurev-med-051013-052304

Corriden, R., Chen, Y., Inoue, Y., Beldi, G., Robson, S. C., Insel, P. A., & Junger, W. G. (2008). Ecto-nucleoside Triphosphate Diphosphohydrolase 1 (E-NTPDase1/CD39) Regulates Neutrophil Chemotaxis by Hydrolyzing Released ATP to Adenosine. *The Journal of Biological Chemistry, 283*(42), 28480-28486. doi:10.1074/jbc.M800039200

Corzo, C. A., Condamine, T., Lu, L., Cotter, M. J., Youn, J.-I., Cheng, P., . . . Gabrilovich, D. I. (2010). HIF-1α regulates function and differentiation of myeloid-derived suppressor cells in the tumor microenvironment. *The Journal of Experimental Medicine, 207*(11), 2439-2453. doi:10.1084/jem.20100587

Corzo, C. A., Cotter, M. J., Cheng, P., Cheng, F., Kusmartsev, S., Sotomayor, E., . . . Gabrilovich, D. I. (2009). Mechanism regulating reactive oxygen species in tumor induced myeloid-derived suppressor cells: MDSC and ROS in cancer. *Journal of immunology (Baltimore, Md. : 1950), 182*(9), 5693-5701. doi:10.4049/jimmunol.0900092

Cramer, L. P. (2010). Forming the cell rear first: breaking cell symmetry to trigger directed cell migration. *Nat Cell Biol, 12*(7), 628-632. doi:http://www.nature.com/ncb/journal/v12/n7/suppinfo/ncb0710-628_S1.html

Dickinson, R. B., & Tranquillo, R. T. (1993). A stochastic model for adhesion-mediated cell random motility and haptotaxis. *J Math Biol, 31*(6), 563-600.

Dunn, G. A. (1983). Characterising a kinesis response: time averaged measures of cell speed and directional persistence. *Agents Actions Suppl, 12*, 14-33.

Eck, M., Schmausser, B., Scheller, K., Brandlein, S., & Muller-Hermelink, H. K. (2003). Pleiotropic effects of CXC chemokines in gastric carcinoma: differences in CXCL8 and CXCL1

expression between diffuse and intestinal types of gastric carcinoma. *Clin Exp Immunol, 134*(3), 508-515.

Eddy, R. J., Pierini, L. M., Matsumura, F., & Maxfield, F. R. (2000). Ca2+-dependent myosin II activation is required for uropod retraction during neutrophil migration. *J Cell Sci, 113 (Pt 7)*, 1287-1298.

Eikemo, H., Moltzau, L. R., Hussain, R. I., Nguyen, C. H., Qvigstad, E., Levy, F. O., . . . Osnes, J. B. (2016). CaMKII in addition to MLCK contributes to phosphorylation of regulatory light chain in cardiomyocytes. *Biochem Biophys Res Commun, 471*(1), 219-225. doi:10.1016/j.bbrc.2016.01.132

Elkabets, M., Ribeiro, V. S. G., Dinarello, C. A., Ostrand-Rosenberg, S., Di Santo, J. P., Apte, R. N., & Vosshenrich, C. A. J. (2010). IL-1β regulates a novel myeloid-derived suppressor cell subset that impairs NK cell development and function. *European Journal of Immunology, 40*(12), 3347-3357. doi:10.1002/eji.201041037

Eltzschig, H. K., Eckle, T., Mager, A., Küper, N., Karcher, C., Weissmüller, T., . . . Colgan, S. P. (2006). ATP Release From Activated Neutrophils Occurs via Connexin 43 and Modulates Adenosine-Dependent Endothelial Cell Function. *Circulation Research, 99*(10), 1100-1108. doi:10.1161/01.res.0000250174.31269.70

Fan, X., Patera, A. C., Pong-Kennedy, A., Deno, G., Gonsiorek, W., Manfra, D. J., . . . Hipkin, R. W. (2007). Murine CXCR1 Is a Functional Receptor for GCP-2/CXCL6 and Interleukin-8/CXCL8. *Journal of Biological Chemistry, 282*(16), 11658-11666. doi:10.1074/jbc.M607705200

Ford, R. M., & Lauffenburger, D. A. (1991). Measurement of bacterial random motility and chemotaxis coefficients: II. Application of single-cell-based mathematical model. *Biotechnol Bioeng, 37*(7), 661-672. doi:10.1002/bit.260370708

Gabrilovich, D., Ishida, T., Oyama, T., Ran, S., Kravtsov, V., Nadaf, S., & Carbone, D. P. (1998). Vascular Endothelial Growth Factor Inhibits the Development of Dendritic Cells and Dramatically Affects the Differentiation of Multiple Hematopoietic Lineages In Vivo. *Presented in part at the Keystone Symposium "Cellular and Molecular Biology of Dendritic Cells," Santa Fe, NM, March 3-9, 1998, and at the annual meeting of the American Association for Cancer Research, March 28-April 1, 1998., 92*(11), 4150-4166.

Gabrilovich, D. I. (2017). Myeloid-Derived Suppressor Cells. *Cancer Immunology Research, 5*(1), 3-8. doi:10.1158/2326-6066.cir-16-0297

Gabrilovich, D. I., Bronte, V., Chen, S.-H., Colombo, M. P., Ochoa, A., Ostrand-Rosenberg, S., & Schreiber, H. (2007). The Terminology Issue for Myeloid-Derived Suppressor Cells. *Cancer Research, 67*(1), 425-425. doi:10.1158/0008-5472.can-06-3037

Gabrilovich, D. I., Ostrand-Rosenberg, S., & Bronte, V. (2012). Coordinated regulation of myeloid cells by tumours. *Nature reviews. Immunology, 12*(4), 253-268. doi:10.1038/nri3175

Gabrilovich, D. I., Velders, M. P., Sotomayor, E. M., & Kast, W. M. (2001). Mechanism of Immune Dysfunction in Cancer Mediated by Immature Gr-1⁺ Myeloid Cells. *The Journal of Immunology, 166*(9), 5398-5406. doi:10.4049/jimmunol.166.9.5398

Gao, D., Joshi, N., Choi, H., Ryu, S., Hahn, M., Catena, R., . . . Mittal, V. (2012). Myeloid Progenitor Cells in the Premetastatic Lung Promote Metastases by Inducing Mesenchymal to Epithelial Transition. *Cancer Research, 72*(6), 1384-1394. doi:10.1158/0008-5472.can-11-2905

Gardiner, E. M., Pestonjamasp, K. N., Bohl, B. P., Chamberlain, C., Hahn, K. M., & Bokoch, G. M. (2002). Spatial and Temporal Analysis of Rac Activation during Live Neutrophil

Chemotaxis. *Current Biology, 12*(23), 2029-2034. doi:http://dx.doi.org/10.1016/S0960-9822(02)01334-9

Gehad, A. E., Lichtman, M. K., Schmults, C. D., Teague, J. E., Calarese, A. W., Jiang, Y., . . . Clark, R. A. (2012). Nitric Oxide–Producing Myeloid-Derived Suppressor Cells Inhibit Vascular E-Selectin Expression in Human Squamous Cell Carcinomas. *Journal of Investigative Dermatology, 132*(11), 2642-2651. doi:http://dx.doi.org/10.1038/jid.2012.190

Gerisch, G., & Keller, H. U. (1981). Chemotactic reorientation of granulocytes stimulated with micropipettes containing fMet-Leu-Phe. *Journal of Cell Science, 52*(1), 1-10.

Gijsbers, K., Gouwy, M., Struyf, S., Wuyts, A., Proost, P., Opdenakker, G., . . . Van Damme, J. (2005). GCP-2/CXCL6 synergizes with other endothelial cell-derived chemokines in neutrophil mobilization and is associated with angiogenesis in gastrointestinal tumors. *Exp Cell Res, 303*(2), 331-342. doi:10.1016/j.yexcr.2004.09.027

Hammami, I., Chen, J., Murschel, F., Bronte, V., De Crescenzo, G., & Jolicoeur, M. (2012). Immunosuppressive activity enhances central carbon metabolism and bioenergetics in myeloid-derived suppressor cells in vitro models. *BMC Cell Biology, 13*, 18-18. doi:10.1186/1471-2121-13-18

Hanna, S., & El-Sibai, M. (2013). Signaling networks of Rho GTPases in cell motility. *Cellular Signalling, 25*(10), 1955-1961. doi:http://dx.doi.org/10.1016/j.cellsig.2013.04.009

Hanson, E. M., Clements, V. K., Sinha, P., Ilkovitch, D., & Ostrand-Rosenberg, S. (2009). Myeloid-Derived Suppressor Cells Down-Regulate L-Selectin Expression on CD4(+) and CD8(+) T Cells. *Journal of immunology (Baltimore, Md. : 1950), 183*(2), 937-944. doi:10.4049/jimmunol.0804253

Hind, Laurel E., Vincent, William J. B., & Huttenlocher, A. (2016). Leading from the Back: The Role of the Uropod in Neutrophil Polarization and Migration. *Developmental Cell, 38*(2), 161-169. doi:http://dx.doi.org/10.1016/j.devcel.2016.06.031

Hoechst, B., Ormandy, L. A., Ballmaier, M., Lehner, F., Krüger, C., Manns, M. P., . . . Korangy, F. (2008). A New Population of Myeloid-Derived Suppressor Cells in Hepatocellular Carcinoma Patients Induces CD4+CD25+Foxp3+ T Cells. *Gastroenterology, 135*(1), 234-243. doi:http://dx.doi.org/10.1053/j.gastro.2008.03.020

Hossain, F., Al-Khami, A. A., Wyczechowska, D., Hernandez, C., Zheng, L., Reiss, K., . . . Ochoa, A. C. (2015). Inhibition of Fatty Acid Oxidation Modulates Immunosuppressive Functions of Myeloid-Derived Suppressor Cells and Enhances Cancer Therapies. *Cancer Immunology Research, 3*(11), 1236-1247. doi:10.1158/2326-6066.CIR-15-0036

Huang, A., Zhang, B., Wang, B., Zhang, F., Fan, K.-X., & Guo, Y.-J. (2013). Increased CD14+HLA-DR-/low myeloid-derived suppressor cells correlate with extrathoracic metastasis and poor response to chemotherapy in non-small cell lung cancer patients. *Cancer Immunology, Immunotherapy, 62*(9), 1439-1451. doi:10.1007/s00262-013-1450-6

Huang, B., Pan, P.-Y., Li, Q., Sato, A. I., Levy, D. E., Bromberg, J., . . . Chen, S.-H. (2006). Gr-1^{+}CD115^{+} Immature Myeloid Suppressor Cells Mediate the Development of Tumor-Induced T Regulatory Cells and T-Cell Anergy in Tumor-Bearing Host. *Cancer Research, 66*(2), 1123-1131. doi:10.1158/0008-5472.can-05-1299

Huh, S. J., Liang, S., Sharma, A., Dong, C., & Robertson, G. P. (2010). Transiently entrapped circulating tumor cells interact with neutrophils to facilitate lung metastasis development. *Cancer Research, 70*(14), 6071-6082. doi:10.1158/0008-5472.CAN-09-4442

Ichikawa, M., Williams, R., Wang, L., Vogl, T., & Srikrishna, G. (2011). S100A8/A9 activate key genes and pathways in colon tumor progression. *Molecular cancer research : MCR, 9*(2), 133-148. doi:10.1158/1541-7786.MCR-10-0394

Inamoto, S., Itatani, Y., Yamamoto, T., Minamiguchi, S., Hirai, H., Iwamoto, M., . . . Kawada, K. (2016). Loss of SMAD4 Promotes Colorectal Cancer Progression by Accumulation of Myeloid-Derived Suppressor Cells through the CCL15-CCR1 Chemokine Axis. *Clin Cancer Res, 22*(2), 492-501. doi:10.1158/1078-0432.ccr-15-0726

Iyer, N. V., Kotch, L. E., Agani, F., Leung, S. W., Laughner, E., Wenger, R. H., . . . Semenza, G. L. (1998). Cellular and developmental control of O(2) homeostasis by hypoxia-inducible factor 1α. *Genes & Development, 12*(2), 149-162. Retrieved from http://www.ncbi.nlm.nih.gov/pmc/articles/PMC316445/

Jung, D.-W., Ha, H.-H., Zheng, X., Chang, Y.-T., & Williams, D. R. (2011). Novel use of fluorescent glucose analogues to identify a new class of triazine-based insulin mimetics possessing useful secondary effects. *Molecular BioSystems, 7*(2), 346-358. doi:10.1039/C0MB00089B

Junger, W. G. (2008). Purinergic regulation of neutrophil chemotaxis. *Cellular and molecular life sciences : CMLS, 65*(16), 2528-2540. doi:10.1007/s00018-008-8095-1

Junger, W. G. (2011). Immune cell regulation by autocrine purinergic signalling. *Nature reviews. Immunology, 11*(3), 201-212. doi:10.1038/nri2938

Kaplan, R. N., Riba, R. D., Zacharoulis, S., Bramley, A. H., Vincent, L., Costa, C., . . . Lyden, D. (2005). VEGFR1-positive haematopoietic bone marrow progenitors initiate the pre-metastatic niche. *Nature, 438*(7069), 820-827. doi:10.1038/nature04186

Kimura, T., McKolanis, J. R., Dzubinski, L. A., Islam, K., Potter, D. M., Salazar, A. M., . . . Finn, O. J. (2013). MUC1 Vaccine for Individuals with Advanced Adenoma of the Colon: A Cancer Immunoprevention Feasibility Study. *Cancer Prevention Research, 6*(1), 18-26. doi:10.1158/1940-6207.capr-12-0275

Kochanowski, N., Blanchard, F., Cacan, R., Chirat, F., Guedon, E., Marc, A., & Goergen, J. L. (2006). Intracellular nucleotide and nucleotide sugar contents of cultured CHO cells determined by a fast, sensitive, and high-resolution ion-pair RP-HPLC. *Analytical Biochemistry, 348*(2), 243-251. doi:http://dx.doi.org/10.1016/j.ab.2005.10.027

Kowalczuk, O., Burzykowski, T., Niklinska, W. E., Kozlowski, M., Chyczewski, L., & Niklinski, J. (2014). CXCL5 as a potential novel prognostic factor in early stage non-small cell lung cancer: results of a study of expression levels of 23 genes. *Tumour Biol, 35*(5), 4619-4628. doi:10.1007/s13277-014-1605-x

Kowanetz, M., Wu, X., Lee, J., Tan, M., Hagenbeek, T., Qu, X., . . . Ferrara, N. (2010). Granulocyte-colony stimulating factor promotes lung metastasis through mobilization of Ly6G+Ly6C+ granulocytes. *Proceedings of the National Academy of Sciences of the United States of America, 107*(50), 21248-21255. doi:10.1073/pnas.1015855107

Kumar, S., Xu, J., Perkins, C., Guo, F., Snapper, S., Finkelman, F. D., . . . Filippi, M.-D. (2012). Cdc42 regulates neutrophil migration via crosstalk between WASp, CD11b, and microtubules. *Blood, 120*(17), 3563-3574. doi:10.1182/blood-2012-04-426981

Kumar, V., Patel, S., Tcyganov, E., & Gabrilovich, D. I. (2016). The Nature of Myeloid-Derived Suppressor Cells in the Tumor Microenvironment. *Trends in immunology, 37*(3), 208-220. doi:http://dx.doi.org/10.1016/j.it.2016.01.004

Kusmartsev, S. A., Li, Y., & Chen, S.-H. (2000). Gr-1^{+} Myeloid Cells Derived from Tumor-Bearing Mice Inhibit Primary T Cell Activation Induced Through CD3/CD28 Costimulation. *The Journal of Immunology, 165*(2), 779-785. doi:10.4049/jimmunol.165.2.779

Kwon, T. H., Jung, H., Cho, E. J., Jeong, J. H., & Sohn, U. D. (2015). The Signaling Mechanism of Contraction Induced by ATP and UTP in Feline Esophageal Smooth Muscle Cells. *Molecules and Cells, 38*(7), 616-623. doi:10.14348/molcells.2015.2357

Lam, P.-y., & Huttenlocher, A. (2013). Interstitial leukocyte migration in vivo. *Current opinion in cell biology, 25*(5), 650-658. doi:10.1016/j.ceb.2013.05.007

Lauffenburger, D. A., & Horwitz, A. F. (1996). Cell Migration: A Physically Integrated Molecular Process. *Cell, 84*(3), 359-369. doi:http://dx.doi.org/10.1016/S0092-8674(00)81280-5

Lecut, C., Frederix, K., Johnson, D. M., Deroanne, C., Thiry, M., Faccinetto, C., . . . Oury, C. (2009). $P2X_1$ Ion Channels Promote Neutrophil Chemotaxis through Rho Kinase Activation. *The Journal of Immunology, 183*(4), 2801-2809. doi:10.4049/jimmunol.0804007

Ledderose, C., Bao, Y., Kondo, Y., Fakhari, M., Slubowski, C., Zhang, J., & Junger, W. G. (2016). Purinergic Signaling and the Immune Response in Sepsis: A Review. *Clinical Therapeutics, 38*(5), 1054-1065. doi:http://dx.doi.org/10.1016/j.clinthera.2016.04.002

Ledderose, C., Bao, Y., Zhang, J., & Junger, W. G. (2015). Novel method for real-time monitoring of ATP release reveals multiple phases of autocrine purinergic signalling during immune cell activation. *Acta Physiol (Oxf), 213*(2), 334-345. doi:10.1111/apha.12435

Liu, Y., Fiskum, G., & Schubert, D. (2002). Generation of reactive oxygen species by the mitochondrial electron transport chain. *Journal of Neurochemistry, 80*(5), 780-787. doi:10.1046/j.0022-3042.2002.00744.x

Liu, Y., Lai, L., Chen, Q., Song, Y., Xu, S., Ma, F., . . . Wang, Q. (2012). MicroRNA-494 Is Required for the Accumulation and Functions of Tumor-Expanded Myeloid-Derived Suppressor Cells via Targeting of PTEN. *The Journal of Immunology, 188*(11), 5500-5510. doi:10.4049/jimmunol.1103505

MacDonald, K. P. A., Rowe, V., Clouston, A. D., Welply, J. K., Kuns, R. D., Ferrara, J. L. M., . . . Hill, G. R. (2005). Cytokine Expanded Myeloid Precursors Function as Regulatory Antigen-Presenting Cells and Promote Tolerance through IL-10-Producing Regulatory T Cells. *The Journal of Immunology, 174*(4), 1841-1850. doi:10.4049/jimmunol.174.4.1841

Mao, Y., Sarhan, D., Steven, A., Seliger, B., Kiessling, R., & Lundqvist, A. (2014). Inhibition of Tumor-Derived Prostaglandin-E2 Blocks the Induction of Myeloid-Derived Suppressor Cells and Recovers Natural Killer Cell Activity. *Clinical Cancer Research, 20*(15), 4096-4106. doi:10.1158/1078-0432.ccr-14-0635

Maratou, E., Dimitriadis, G., Kollias, A., Boutati, E., Lambadiari, V., Mitrou, P., & Raptis, S. A. (2007). Glucose transporter expression on the plasma membrane of resting and activated white blood cells. *European Journal of Clinical Investigation, 37*(4), 282-290. doi:10.1111/j.1365-2362.2007.01786.x

Mazzoni, A., Bronte, V., Visintin, A., Spitzer, J. H., Apolloni, E., Serafini, P., . . . Segal, D. M. (2002). Myeloid Suppressor Lines Inhibit T Cell Responses by an NO-Dependent Mechanism. *The Journal of Immunology, 168*(2), 689-695. doi:10.4049/jimmunol.168.2.689

Mehlen, P., & Puisieux, A. (2006). Metastasis: a question of life or death. *Nat Rev Cancer, 6*(6), 449-458. Retrieved from http://dx.doi.org/10.1038/nrc1886

Meili, R., & Firtel, R. A. (2003). Two Poles and a Compass. *Cell, 114*(2), 153-156. doi:http://dx.doi.org/10.1016/S0092-8674(03)00553-1

Melani, C., Sangaletti, S., Barazzetta, F. M., Werb, Z., & Colombo, M. P. (2007). Amino-Biphosphonate–Mediated MMP-9 Inhibition Breaks the Tumor-Bone Marrow Axis Responsible for Myeloid-Derived Suppressor Cell Expansion and Macrophage Infiltration in Tumor Stroma. *Cancer Research, 67*(23), 11438-11446. doi:10.1158/0008-5472.can-07-1882

Mellman, I., Coukos, G., & Dranoff, G. (2011). Cancer immunotherapy comes of age. *Nature, 480*(7378), 480-489. Retrieved from http://dx.doi.org/10.1038/nature10673

Molon, B., Ugel, S., Del Pozzo, F., Soldani, C., Zilio, S., Avella, D., . . . Viola, A. (2011). Chemokine nitration prevents intratumoral infiltration of antigen-specific T cells. *The Journal of Experimental Medicine, 208*(10), 1949-1962. doi:10.1084/jem.20101956

Morales, J. K., Kmieciak, M., Knutson, K. L., Bear, H. D., & Manjili, M. H. (2010). GM-CSF is one of the main breast tumor-derived soluble factors involved in the differentiation of CD11b−Gr1− bone marrow progenitor cells into myeloid-derived suppressor cells. *Breast cancer research and treatment, 123*(1), 39-49. doi:10.1007/s10549-009-0622-8

Moses, K., & Brandau, S. (2016). Human neutrophils: Their role in cancer and relation to myeloid-derived suppressor cells. *Seminars in Immunology, 28*(2), 187-196. doi:http://dx.doi.org/10.1016/j.smim.2016.03.018

Munn, D. H., Sharma, M. D., Baban, B., Harding, H. P., Zhang, Y., Ron, D., & Mellor, A. L. (2005). GCN2 Kinase in T Cells Mediates Proliferative Arrest and Anergy Induction in Response to Indoleamine 2,3-Dioxygenase. *Immunity, 22*(5), 633-642. doi:http://dx.doi.org/10.1016/j.immuni.2005.03.013

Nagaraj, S., Gupta, K., Pisarev, V., Kinarsky, L., Sherman, S., Kang, L., . . . Gabrilovich, D. I. (2007). Altered recognition of antigen is a mechanism of CD8+ T cell tolerance in cancer. *Nat Med, 13*(7), 828-835. doi:http://www.nature.com/nm/journal/v13/n7/suppinfo/nm1609_S1.html

Niggli, V. (1999). Rho-kinase in human neutrophils: a role in signalling for myosin light chain phosphorylation and cell migration. *FEBS Lett, 445*(1), 69-72.

Ortiz, M. L., Kumar, V., Martner, A., Mony, S., Donthireddy, L., Condamine, T., . . . Gabrilovich, D. (2015). Immature myeloid cells directly contribute to skin tumor development by recruiting IL-17–producing CD4⁺ T cells. *The Journal of Experimental Medicine, 212*(3), 351-367. doi:10.1084/jem.20140835

Ortiz, M. L., Lu, L., Ramachandran, I., & Gabrilovich, D. I. (2014). Myeloid-derived suppressor cells in the development of lung cancer. *Cancer Immunology Research, 2*(1), 50-58. doi:10.1158/2326-6066.CIR-13-0129

Paget, S. (1989). The distribution of secondary growths in cancer of the breast. 1889. *Cancer Metastasis Rev, 8*(2), 98-101.

Pan, P.-Y., Ma, G., Weber, K. J., Ozao-Choy, J., Wang, G., Yin, B., . . . Chen, S.-H. (2010). Immune Stimulatory Receptor CD40 Is Required for T-Cell Suppression and T Regulatory Cell Activation Mediated by Myeloid-Derived Suppressor Cells in Cancer. *Cancer Research, 70*(1), 99. doi:10.1158/0008-5472.CAN-09-1882

Park, H., Chan, M. M., & Iritani, B. M. (2010). Hem-1: Putting the “WAVE” into actin polymerization during an immune response. *FEBS Letters, 584*(24), 4923-4932. doi:10.1016/j.febslet.2010.10.018

Parker, K., Sinha, P., Horn, L. A., Clements, V. K., Yang, H., Li, J., . . . Ostrand-Rosenberg, S. (2014). HMGB1 enhances immune suppression by facilitating the differentiation and

suppressive activity of myeloid-derived suppressor cells. *Cancer Research, 74*(20), 5723-5733. doi:10.1158/0008-5472.CAN-13-2347

Parker, K. H., Beury, D. W., & Ostrand-Rosenberg, S. (2015). Chapter Three - Myeloid-Derived Suppressor Cells: Critical Cells Driving Immune Suppression in the Tumor Microenvironment. In W. Xiang-Yang & B. F. Paul (Eds.), *Advances in Cancer Research* (Vol. Volume 128, pp. 95-139): Academic Press.

Pearce, E. L., & Pearce, E. J. (2013). Metabolic Pathways In Immune Cell Activation And Quiescence. *Immunity, 38*(4), 633-643. doi:10.1016/j.immuni.2013.04.005

Penuela, S., Gehi, R., & Laird, D. W. (2013). The biochemistry and function of pannexin channels. *Biochimica et Biophysica Acta (BBA) - Biomembranes, 1828*(1), 15-22. doi:http://dx.doi.org/10.1016/j.bbamem.2012.01.017

Polesskaya, O., Wong, C., Lebron, L., Chamberlain, J. M., Gelbard, H. A., Goodfellow, V., . . . Dewhurst, S. (2014). MLK3 regulates fMLP-stimulated neutrophil motility. *Molecular immunology, 58*(2), 214-222. doi:10.1016/j.molimm.2013.11.016

Raber, P. L., Thevenot, P., Sierra, R., Wyczechowska, D., Halle, D., Ramirez, M. E., . . . Rodriguez, P. C. (2014). Subpopulations of Myeloid-Derived Suppressor Cells (MDSC) impair T cell responses through independent nitric oxide-related pathways. *International journal of cancer. Journal international du cancer, 134*(12), 2853-2864. doi:10.1002/ijc.28622

Raghuwanshi, S. K., Su, Y., Singh, V., Hayes, K., Richmond, A., & Richardson, R. M. (2012). The chemokine receptors CXCR1 and CXCR2 couple to distinct G protein-coupled receptor kinases to mediate and regulate leukocyte functions. *Journal of immunology (Baltimore, Md. : 1950), 189*(6), 2824-2832. doi:10.4049/jimmunol.1201114

Rodríguez-Espinosa, O., Rojas-Espinosa, O., Moreno-Altamirano, M. M. B., López-Villegas, E. O., & Sánchez-García, F. J. (2015). Metabolic requirements for neutrophil extracellular traps formation. *Immunology, 145*(2), 213-224. doi:10.1111/imm.12437

Rodriguez, P. C., Hernandez, C. P., Morrow, K., Sierra, R., Zabaleta, J., Wyczechowska, D. D., & Ochoa, A. C. (2010). l-Arginine Deprivation Regulates Cyclin D3 mRNA Stability in Human T Cells by Controlling HuR Expression. *Journal of immunology (Baltimore, Md. : 1950), 185*(9), 5198-5204. doi:10.4049/jimmunol.1001224

Rodriguez, P. C., Quiceno, D. G., Zabaleta, J., Ortiz, B., Zea, A. H., Piazuelo, M. B., . . . Ochoa, A. C. (2004). Arginase I Production in the Tumor Microenvironment by Mature Myeloid Cells Inhibits T-Cell Receptor Expression and Antigen-Specific T-Cell Responses. *Cancer Research, 64*(16), 5839-5849. doi:10.1158/0008-5472.can-04-0465

Rodriguez, P. C., Zea, A. H., Culotta, K. S., Zabaleta, J., Ochoa, J. B., & Ochoa, A. C. (2002). Regulation of T Cell Receptor CD3ζ Chain Expression byl-Arginine. *Journal of Biological Chemistry, 277*(24), 21123-21129. doi:10.1074/jbc.M110675200

Sakuishi, K., Jayaraman, P., Behar, S. M., Anderson, A. C., & Kuchroo, V. K. (2011). Emerging Tim-3 functions in anti-microbial and tumor immunity. *Trends in immunology, 32*(8), 345-349. doi:10.1016/j.it.2011.05.003

Sceneay, J., Chow, M. T., Chen, A., Halse, H. M., Wong, C. S. F., Andrews, D. M., . . . Möller, A. (2012). Primary Tumor Hypoxia Recruits $CD11b^{+}Ly6C^{med}Ly6G^{+}$ Immune Suppressor Cells and Compromises NK Cell Cytotoxicity in the Premetastatic Niche. *Cancer Research, 72*(16), 3906-3911. doi:10.1158/0008-5472.can-11-3873

Schmielau, J., & Finn, O. J. (2001). Activated Granulocytes and Granulocyte-derived Hydrogen Peroxide Are the Underlying Mechanism of Suppression of T-Cell Function in Advanced Cancer Patients. *Cancer Research, 61*(12), 4756-4760.

Serafini, P., Carbley, R., Noonan, K. A., Tan, G., Bronte, V., & Borrello, I. (2004). High-Dose Granulocyte-Macrophage Colony-Stimulating Factor-Producing Vaccines Impair the Immune Response through the Recruitment of Myeloid Suppressor Cells. *Cancer Research, 64*(17), 6337-6343. doi:10.1158/0008-5472.can-04-0757

Serafini, P., Mgebroff, S., Noonan, K., & Borrello, I. (2008). Myeloid derived suppressor cells promote cross-tolerance in B cell lymphoma by expanding regulatory T cells. *Cancer Research, 68*(13), 5439-5449. doi:10.1158/0008-5472.CAN-07-6621

Seubert, B., Grünwald, B., Kobuch, J., Cui, H., Schelter, F., Schaten, S., . . . Krüger, A. (2015). TIMP-1 creates a pre-metastatic niche in the liver through SDF-1/CXCR4-dependent neutrophil recruitment in mice. *Hepatology (Baltimore, Md.), 61*(1), 238-248. doi:10.1002/hep.27378

Siegel, R. L., Miller, K. D., & Jemal, A. (2017). Cancer statistics, 2017. *CA: A Cancer Journal for Clinicians, 67*(1), 7-30. doi:10.3322/caac.21387

Sinha, P., Clements, V. K., Bunt, S. K., Albelda, S. M., & Ostrand-Rosenberg, S. (2007). Cross-Talk between Myeloid-Derived Suppressor Cells and Macrophages Subverts Tumor Immunity toward a Type 2 Response. *The Journal of Immunology, 179*(2), 977-983. doi:10.4049/jimmunol.179.2.977

Skau, C. T., Plotnikov, S. V., Doyle, A. D., & Waterman, C. M. (2015). Inverted formin 2 in focal adhesions promotes dorsal stress fiber and fibrillar adhesion formation to drive extracellular matrix assembly. *Proceedings of the National Academy of Sciences of the United States of America, 112*(19), E2447-E2456. doi:10.1073/pnas.1505035112

Skau, C. T., & Waterman, C. M. (2015). Specification of Architecture and Function of Actin Structures by Actin Nucleation Factors. *Annu Rev Biophys, 44*, 285-310. doi:10.1146/annurev-biophys-060414-034308

Smith, A., Bracke, M., Leitinger, B., Porter, J. C., & Hogg, N. (2003). LFA-1-induced T cell migration on ICAM-1 involves regulation of MLCK-mediated attachment and ROCK-dependent detachment. *J Cell Sci, 116*(Pt 15), 3123-3133. doi:10.1242/jcs.00606

Smith, C., Chang, M.-Y., Parker, K., Beury, D., DuHadaway, J. B., Flick, H. E., . . . Muller, A. J. (2012). IDO is a nodal pathogenic driver of lung cancer and metastasis development. *Cancer discovery, 2*(8), 722-735. doi:10.1158/2159-8290.CD-12-0014

Srivastava, M. K., Sinha, P., Clements, V. K., Rodriguez, P., & Ostrand-Rosenberg, S. (2010). Myeloid-derived Suppressor Cells Inhibit T Cell Activation by Depleting Cystine and Cysteine. *Cancer Research, 70*(1), 68-77. doi:10.1158/0008-5472.CAN-09-2587

Swamydas, M., Gao, J.-L., Break, T. J., Johnson, M. D., Jaeger, M., Rodriguez, C. A., . . . Lionakis, M. S. (2016). CXCR1-mediated Neutrophil Degranulation and Fungal Killing Promotes Candida Clearance and Host Survival. *Science translational medicine, 8*(322), 322ra310-322ra310. doi:10.1126/scitranslmed.aac7718

Szczur, K., Zheng, Y., & Filippi, M.-D. (2009). The small Rho GTPase Cdc42 regulates neutrophil polarity via CD11b integrin signaling. *Blood, 114*(20), 4527-4537. doi:10.1182/blood-2008-12-195164

Talmadge, J. E., & Gabrilovich, D. I. (2013). History of myeloid derived suppressor cells (MDSCs) in the macro- and micro-environment of tumour-bearing hosts. *Nature reviews. Cancer, 13*(10), 739-752. doi:10.1038/nrc3581

Tan, A. S., Ahmed, N., & Berridge, M. V. (1998). Acute Regulation of Glucose Transport After Activation of Human Peripheral Blood Neutrophils by Phorbol Myristate Acetate, fMLP, and Granulocyte-Macrophage Colony-Stimulating Factor. *Blood, 91*(2), 649-655.

Tan, J. L., Ravid, S., & Spudich, J. A. (1992). Control of nonmuscle myosins by phosphorylation. *Annu Rev Biochem, 61*, 721-759. doi:10.1146/annurev.bi.61.070192.003445

Toh, B., Wang, X., Keeble, J., Sim, W. J., Khoo, K., Wong, W.-C., . . . Abastado, J.-P. (2011). Mesenchymal Transition and Dissemination of Cancer Cells Is Driven by Myeloid-Derived Suppressor Cells Infiltrating the Primary Tumor. *PLoS Biology, 9*(9), e1001162. doi:10.1371/journal.pbio.1001162

Trellakis, S., Bruderek, K., Dumitru, C. A., Gholaman, H., Gu, X., Bankfalvi, A., . . . Brandau, S. (2011). Polymorphonuclear granulocytes in human head and neck cancer: enhanced inflammatory activity, modulation by cancer cells and expansion in advanced disease. *Int J Cancer, 129*(9), 2183-2193. doi:10.1002/ijc.25892

Tybulewicz, V. L. J., & Henderson, R. B. (2009). Rho family GTPases and their regulators in lymphocytes. *Nature reviews. Immunology, 9*(9), 630-644. doi:10.1038/nri2606

Wang, N., Feng, Y., Wang, Q., Liu, S., Xiang, L., Sun, M., . . . Wei, F. (2014). Neutrophils infiltration in the tongue squamous cell carcinoma and its correlation with CEACAM1 expression on tumor cells. *PLoS One, 9*(2), e89991. doi:10.1371/journal.pone.0089991

Weide, B., Martens, A., Zelba, H., Stutz, C., Derhovanessian, E., Di Giacomo, A. M., . . . Pawelec, G. (2014). Myeloid-Derived Suppressor Cells Predict Survival of Patients with Advanced Melanoma: Comparison with Regulatory T Cells and NY-ESO-1- or Melan-A–Specific T Cells. *Clinical Cancer Research, 20*(6), 1601-1609. doi:10.1158/1078-0432.ccr-13-2508

Woehrle, T., Yip, L., Elkhal, A., Sumi, Y., Chen, Y., Yao, Y., . . . Junger, W. G. (2010). Pannexin-1 hemichannel–mediated ATP release together with P2X1 and P2X4 receptors regulate T-cell activation at the immune synapse. *Blood, 116*(18), 3475-3484. doi:10.1182/blood-2010-04-277707

Wong, K., Van Keymeulen, A., & Bourne, H. R. (2007). PDZRhoGEF and myosin II localize RhoA activity to the back of polarizing neutrophil-like cells. *The Journal of Cell Biology, 179*(6), 1141-1148. doi:10.1083/jcb.200706167

Yang, C., Czech, L., Gerboth, S., Kojima, S.-i., Scita, G., & Svitkina, T. (2007). Novel Roles of Formin mDia2 in Lamellipodia and Filopodia Formation in Motile Cells. *PLoS Biology, 5*(11), e317. doi:10.1371/journal.pbio.0050317

Yang, H. W., Collins, S., & Meyer, T. (2016). Locally excitable Cdc42 signals steer cells during chemotaxis. *Nature cell biology, 18*(2), 191-201. doi:10.1038/ncb3292

Yang, L., Huang, J., Ren, X., Gorska, A. E., Chytil, A., Aakre, M., . . . Moses, H. L. (2008). Abrogation of TGFβ signaling in mammary carcinomas recruits Gr-1+CD11b+ myeloid cells that promote metastasis. *Cancer cell, 13*(1), 23-35. doi:10.1016/j.ccr.2007.12.004

Yang, Q., Li, X., Chen, H., Cao, Y., Xiao, Q., He, Y., . . . Zhou, J. (2017). IRF7 regulates the development of granulocytic myeloid-derived suppressor cells through S100A9 transrepression in cancer. *Oncogene*. doi:10.1038/onc.2016.448

Youn, J.-I., Kumar, V., Collazo, M., Nefedova, Y., Condamine, T., Cheng, P., . . . Gabrilovich, D. I. (2013). Epigenetic silencing of retinoblastoma gene regulates pathologic differentiation of myeloid cells in cancer. *Nature immunology, 14*(3), 211-220. doi:10.1038/ni.2526

Zea, A. H., Rodriguez, P. C., Culotta, K. S., Hernandez, C. P., DeSalvo, J., Ochoa, J. B., . . . Ochoa, A. C. (2004). l-Arginine modulates CD3ζ expression and T cell function in activated human T lymphocytes. *Cellular Immunology, 232*(1–2), 21-31. doi:http://dx.doi.org/10.1016/j.cellimm.2005.01.004

Zoso, A., Mazza, E. M. C., Bicciato, S., Mandruzzato, S., Bronte, V., Serafini, P., & Inverardi, L. (2014). Human fibrocytic myeloid-derived suppressor cells express IDO and promote

tolerance via Treg-cell expansion. *European Journal of Immunology, 44*(11), 3307-3319. doi:10.1002/eji.201444522